UNIONE EUROPEA
Fondo Sociale Europeo

Ministero dell'Istruzione, dell'Università e della Ricerca

PON RICERCA E INNOVAZIONE 2014 - 2020


University of Naples Federico II
Polytechnic and Basic Science School
Department of Chemical Sciences


neapōlis

Ph.D. in Chemical Science

# Fungal and plant metabolites formulated into biopolymers, with anti-mold activity for food packaging

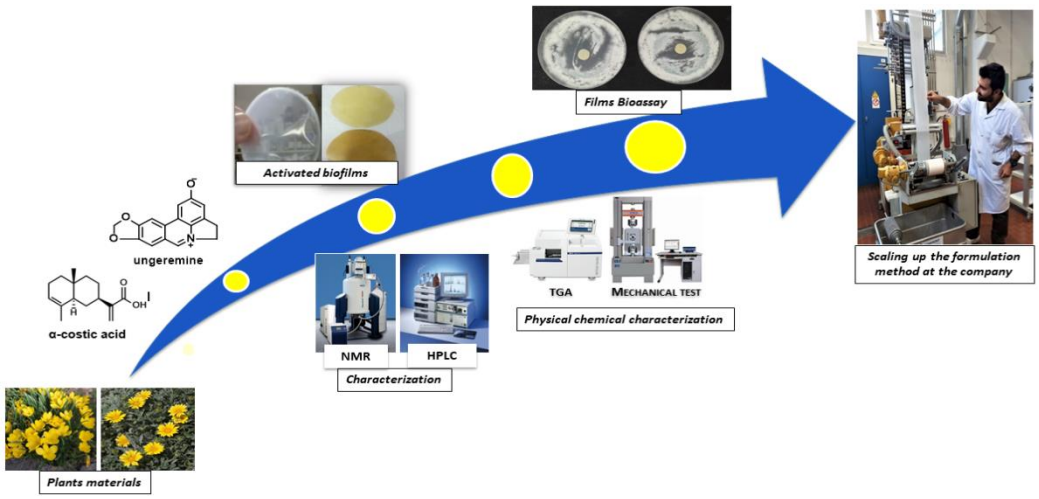



**Author:Arash Moeini**

***Advisors:***
***Prof. Antonio Evidente*** *(Federico II University)*
***Prof. Willem Van Otterlo*** *(Stellenbosch University)*
***Dr. Luigi Capuzzi*** *(Novamont Company)*

***Examiner:*** ***Prof. Martino Di Serio***

**Coordinator:** Prof. Angela Lombardi


**XXXII Cycle 2017 – 2020**

UNIONE EUROPEA
Fondo Sociale Europeo

Ministero dell'Istruzione, dell'Università e della Ricerca

PON RICERCA E INNOVAZIONE 2014 - 2020

# University of Naples Federico II

# Polytechnic and Basic Science School


## Department of Chemical Sciences

**PhD. in**
**Chemical Science**
**XXXII Cycle**

# Fungal and plant metabolites formulated into biopolymers, with anti-mold activity for food packaging


Ph.D. dissertation by
**Arash Moeini**

**Supervisor: Prof. Antonio Evidente** (Federico II University)
**Supervisor: Prof. Willem Van Otterlo** (Stellenbosch University)
**Supervisor: Dr. Luigi Capuzzi** (Novamont Company)
**Examiner: Prof. Martino Di Serio**

**Coordinator: Prof. Angela Lombardi**

**2017-2020**

La borsa di dottorato è stata cofinanziata con risorse del
Programma Operativo Nazionale Ricerca e Innovazione 2014-2020 (CCI 2014IT16M2OP005),
Fondo Sociale Europeo, Azione I.1 "Dottorati Innovativi con caratterizzazione Industriale"

UNIONE EUROPEA
Fondo Sociale Europeo

Ministero dell'Istruzione, dell'Università e della Ricerca

PON RICERCA E INNOVAZIONE

**Dedication,**

**This thesis and all other 17 scientific works (articles, reviews, chapters and conferences) during my PhD, are dedicated:**

To my best friend and wife who always sacrifice herself for my success by supporting and motivating me even in the hardest time, I never forget that. My darling Parisa, this is the nothing to show how much I love you.

To my Family BABA (my closest friend and real supporter), MAMAN (My secret keeper), Aida (the best sister) and Arta (all my best childhood memory), you all know how important role you played in my life I owe you a lot. I worked all three years almost without any rest and your memories every single second motivated me to go forward, I wanted to show you how precious you are and to give you feel proud and happiness, Thank you for everything.

این پایان نامه و تمام ۱۷ کار علمی (مقاله ها، ریوو ها، فصل ها و کنفرانس ها) تقدیم میشود به:

پریسای عزیزم که با از خودگذشتگی همیشه من را حمایت کرد اگر اینجا هستم بخاطر تو بوده عزیزم هرگز فراموش نمیکنم. عاشقتم.

خانواده عزیزم پدرم (صمیمی ترین دوستم و یک حامی واقعی)، مادرم (محرم اسرارم)، آیدا (بهترین خواهر دنیا) و برادر کلم آرتا جان (خاطرات خوب بچگیم) شما بهترین هستید و میدانید چه نقش مهمی در زندگی من داشتید. در سه سال گذشته بدون استراحت کار کردم و یاد شما انگیزه من برای حرکت به جلو بود، تا به شما نشان دهم چقدر با ارزش هستید و بهتون احساس افتخار و شادی بدهم. ممنونم از تون.

**Contents**..... **Page**


**1. INTRODUCTION**.....**1**
**1.1. Preliminary investigation**.....**2**
**1.1.1.** Cavoxin (CVX).....**4**
**1.1.2.** Ungeremine (UNG).....**4**
**1.1.3.** α-costic acid (α-CA).....**6**
**1.2. Active packaging**.....**8**
**1.3. Synthetic polymer drawbacks**.....**9**
**1.4. Biopolymers**.....**10**
**1.4.1. Chitosan (CH)**.....**12**
**1.4.1.1.** Synthesis and characterization.....**12**
**1.4.1.2.** Food packaging application.....**14**
**1.4.2. Polylactic acid (PLA)**.....**15**
**1.4.2.1.** Synthesis and characterization.....**15**
**1.4.2.2.** Food packaging application.....**18**
**1.4.3. Mater Bi (MBi)**.....**19**
**1.4.3.1.** Food packaging application.....**19**

**2. OBJECTIVES**.....**22**

**3. MATERIALS AND METHODS**.....**23**
**3.1. Natural metabolites**.....**23**
**3.1.1.** Fungi.....**23**
**3.1.2.** Plant materials.....**23**
**3.2. Biopolymers**.....**23**
**3.3. General procedures for natural metabolites characterization**.....**23**
**3.4. General procedures for formulated films, composites and particles characterization**.....**24**

**4. EXPERIMENTAL**.....**26**
**4.1. Antimould microbial and plant metabolites with potential application in intelligent food packaging (preliminary investigation)**.....**26**
**4.1.1. Biological assays**.....**26**
***Microbial strains and growth conditions***.....**26**
***Antifungal microdilution test***.....**26**
**4.2. Extraction and purification of cavoxin and cavoxon from *Phoma cava* culture filtrates**.....**27**
**4.2.1. HPLC method for the identification and quantification of cavoxin and cavoxone in *Phoma cava* culture filtrates**.....**28**

***Preparation of standard solution*** **28**
***Preparation of calibration graph*** **28**
***Method validation*** **29**
**4.3. Extraction and purification of lycorine from *Sternbergia lutea*** **29**
**4.3.1. Synthesis of ungeremine** **29**
**4.3.2. Formulation of ungeremine into the polymer matrices** **30**
**4.3.2.1. Encapsulation of ungeremine in chitosan/tripolyphosphate (CH/TPP) micro-beads** **30**
***Loading efficiency test of ungeremine in CH/TPP/UNG beads*** **31**
***Releasing kinetics*** **32**
**Biological assay** **32**
***Microbial strains and growth conditions*** **32**
***Antifungal assays against Penicillium roqueforti*** **33**
***Porosity test*** **33**
**4.3.2.2. Preparation of sub-micron particles of CH/TPP/UNG** **33**
**4.3.2.3. Formulation of sub-micron particles into the Mater Bi polymer matrix** **34**
***Microbial strains and growth conditions*** **35**
***Antifungal activity of films by disc diffusion method*** **35**
***Determination of residual ungeremine mass in biocomposites after antifungal tests by means of UV–Vis Spectroscopy*** **36**
***Differential scanning calorimetry (DSC)*** **36**
***Thermogravimetric analysis (TGA)*** **37**
***Permeability test*** **37**
***Scanning Electron Microscopy (SEM)*** **37**
***Tensile test*** **38**
**4.3.2.4. Formulation of ungeremine into the PLA/PEG polymer matrix** **38**
***Preparation and characterization of the spinning solutions*** **38**
***Electrospinning conditions*** **38**
***Attenuated Total Reflection Fourier Transform Infrared Spectroscopy (ATR-FTIR)*** **39**
***Differential Scanning Calorimetry (DSC)*** **39**
***Release experiments*** **39**
***Scanning electron microscope (SEM) and Porosities test of fibers*** **40**
***Wettability test*** **40**
**4.4. Extraction and purification of α-costic acid from *Dittrichia viscosa (Inula viscosa)*** **41**
**4.4.1. Preparation of polylactic acid (PLA) and Polylactic acid α-costic acid (PLA/α-CA) films** **42**

*Attenuated Total Reflection Fourier Transform Infrared Spectroscopy (FTIR-ATR) and Nuclear Magnetic Resonance Spectroscopy ($^1$HNMR)*....42
*Scanning Electron Microscopy (SEM)*.....43
*Gel Permeation chromatography (GPC)*.....43
*Differential Scanning Calorimetry (DSC)*.....43
*Thermogravimetric Analysis (TGA)*.....44
*Mechanical properties (Tensile test)*.....44
*Surface wettability: water contact angle measurements*.....44

**4.5. The NOVAMONT Stage**.....45

**4.5.1. Preparation of blends between Novamont polyester and chitosan-TPP microparticles (NPS/CH/TPP): tests HB1702- HB1705**.....45
**4.5.2. Preparation of blow moulding films based on Mater-Bi grades and including CH/TPP micro-particles (tests: FF3019, FF3020, FF3022 and FF3023)**.....45
**4.5.3. Formulation of neat chitosan and thermoplastic starch by extrusion (FF3024 and FF3025)**.....46
*Thermogravimetric analysis (TGA) of sub-micron particles, sheets and films*.....46
*Scanning Electron Microscopy (SEM) of sheets and films*.....47
*Tensile test of sheets and films*.....47

**5. RESULTS and DISCUSSIONS**.....48
**5.1. Antimould microbial and plant metabolites with potential application in intelligent food packaging (preliminary investigation)**.....48

**5.2. Development of HPLC method for the identification and quantification of cavoxin and cavoxone in *Phoma cava* culture filtrates**.....51
*Method development*.....51
*Method validation*.....52
*HPLC analysis of samples of cavoxin and cavoxone in the organic extracts of P. cava culture filtrates*.....52
**5.3. Physical-chemical characterization of CH/TPP/UNG beads**.....53
*Chitosan based beads stability, loading efficiency test and controlled releasing kinetics*.....53
**Biological activities**.....60
*Effect of ungeremine on cancer and normal cell line viability*.....60
*Antifungal activity of ungeremine contained in CH/TPP beads against P. roqueforti*.....60
*Scanning Electron Microscopy (SEM) analysis and porosity test*.....61
*Attenuated Total Reflection Fourier Transform Infrared (FTIR-ATR) Spectroscopy*.....63
*Thermogravimetric analysis (TGA)*.....65

**5.4. Physical and mechanical characterization of CH/TPP/UNG sub-micron particles formulated into Mater Bi films**……...**68**
***Antifungal activity and UV-Vis spectroscopy to evaluate ungeremine mass releasing***……...**68**
***Differential scanning calorimetry (DSC)***……...**71**
***Thermogravimetric analysis (TGA)***……..**73**
***Scanning electron microscopy (SEM)***……..**75**
***Water Vapor and Oxygen Permeability***……..**77**
***Tensile Test***……..**78**

**5.5. Physical-chemical characterization of PLA/PEG/UNG fibers**……..**80**
***Electrospinning of PLA, PLA/PEG solutions in the presence of ungeremine***……..**80**
***Attenuated Total Reflection Fourier Transform Infrared Spectroscopy (FTIR-ATR)***……**83**
***Differential Scanning calorimetry (DSC)***……..**83**
***Release rates*** ……...**86**
***Scanning electron microscope (SEM) analyses and porosity test of fibers***...**88**
***Wettability test***……..**93**
**5.6. Physical-chemical characterization of PLA/α-CA films**……...**94**
***Structural and morphological analyses: Attenuated Total Reflection Fourier Transform Infrared Spectroscopy (FTIR-ATR), Nuclear Magnetic Resonance Spectroscopy ($^1$HNMR, Scanning Electron Microscopy (SEM) and Gel Permeation Chromatography (GPC)***……**94**
***Differential Scanning Calorimetry (DSC)***……**100**
***Thermogravimetric Analysis (TGA)***……**103**
***Tensile test***……**104**
***Surface wettability: water contact angle (WCA) measurements***……..**105**
**5.7. The NOVAMONT Stage**……**106**
**5.7.1. Result and discussion**……...**106**
***Thermogravimetric analysis (TGA) of CH/TPP micro particles, sheets and films***……**109**
***Scanning Electron Microscopy (SEM) of sheets and films***……..**112**
***Tensile test of sheets and films***……..**114**
**6. CONCLUSION**……..**117**
**7. Acknowledgments**……..**118**
**8. REFERENCES**……..**119**

**ABSTRACT**

The food mold infestation is an extremely dangerous problem for the health of humans and animals. On the other hand, synthetic polymers massive impact on our life results in a serious problem in the term of both environmental issues and economical cost. Consequently, this project focused on the preparation of the smart packaging by incorporating the bioactive metabolites into eco-friendly biodegradable biofilm, a new frontier in the food packaging industry. As a preliminary investigation among 13 metabolites isolated from bacterial, fungal, and plants, three of them (cavoxin, ungeremine, and α-costic acid) showed the highest inhibition against *Penicillium roqueforti* and *Aspergillus niger*, the most common mold of bakery products. Besides, the incorporation potential of those three metabolites into a suitable biopolymer has been studied to generate 'intelligent food packaging' for the aim of increasing the quality of packaged food, extending the food shelf-life, improving microbiological safety, and preserving food nutritional values. The first metabolite was cavoxin, the HPLC method was developed to quantify the cavoxin. The qualitative and quantitative analysis of *Phoma cava* culture filtrates proved that cavoxin production in the stirred condition is significantly higher than the static one. The second metabolite was ungeremine (UNG), firstly encapsulated into the chitosan-tripolyphosphate (CH/TPP/UNG) microbeads and then formulated into the Mater-Bi (MBi) polymer matrix (MBi/CH/TPP/UNG) in both forms the microparticles and films showed 72 h of inhibitions against *P. roqueforti*. Additionally, ungeremine was directly formulated in polylactic acid and polyethylene glycol (PLA/PEG/UNG) nanofibers. The releasing pattern showed an initial burst release of ungeremine presented in the PEG followed by a sustained release, indicated the ungeremine is present in both the PLA and PEG domains of nanofibers. During the Novamot stage, the synthesis of ungeremine was developed in accordance with large scale production. Besides, the CH/TPP microparticles were successfully scaled up and formulated into the starch-based, transparent and polyester-based grades of MBi by film blowing and compression molding methods. The mechanical tests of the sheets and films

generally showed that microparticles increased the stiffness and decreased both stress and strain at break. Finally, α-costic acid (α-CA) was incorporated into polylactic acid (PLA). The Films did not have any antifungal activity due to the strong interaction between PLA and α-CA. Despite, α-costic acid could act as a plasticizer and improve both tensile strength and strain at break.

**Keywords**

Active packaging; *Penicillium roqueforti; Aspergillus niger*; biopolymers; Natural compounds; Antifungal activity.

## 1. INTRODUCTION

Molds in particular mycotoxigenic fungi can cause allergic reactions, respiratory problems, and mycotoxicosis. Hence, they can be considered as a risk for the health of humans and animals (Frisvad and Samson, 1991; Valerio et al., 2017). On the other hand, fungal contaminations due to the molds ability to grow at severe environmental conditions (low temperatures and water), could be potentially one of the main threats for fresh foods preservation which can be easily spoiled by molds such as bakery and dairy products, fruits and vegetables, preservation (Frisvad and Samson, 1991; Filtenborg, Frisvad and Thrane, 1996). The genera *Alternaria, Aspergillus, Penicillium, Eurotium, Botrytis, Rhizopus, Monilia, Cladosporium, Geotrichum, and Wallemia* are the common molds food contaminations (Valerio et al., 2017). Among them, *Aspergillus* and *Penicillium* exhibit the most food contamination to produce mycotoxins (Cakmakci et al., 2015). In this respect, Cakmakica et al investigated the several toxic metabolites produced by *Penicillium roqueforti* (Cakmakci et al., 2015). Furthermore, the studies showed *Aspergillus niger* could potentially produce two carcinogenic mycotoxins fumonisins and ochratoxins (Frisvad et al., 2011). In particular, in the bakery industry, *Aspergillus* and *Penicillium* genera are the foremost agents to deteriorate bread and bakery products (Frisvad and Samson, 1991; Nguyen Van Long et al., 2016). Previously, to protect food from spoilage antimicrobial metabolites such as bacteriocins, hydrogen peroxide, and organic acids were directly added as a food ingredient or incorporated into the package system (Axel et al., 2016). In the case of bakery products, benzoate, propionate, and sorbate have used as the ingredient (Suhr and Nielsen, 2005). However, this approach changed the flavor, odor, color, and textural properties of foods (Risch, 2009). To overcome this drawback, the new concept of food packaging known as “active packaging” has been developed by formulating active microbial compounds into the package system. In fact, active packaging designed to increase the food shelf-life, preserving their organoleptic properties and microbial infestation, and maintain or improve food quality by formulating different active and antimicrobial substances into the package

system (Atarés and Chiralt, 2016; Ghaani et al., 2016; Siracusa et al., 2008). In general, food packaging is used to protect foods from physical damage, chemical, and biological contamination along with preserving food quality, safety, and extending food shelf-life (Santagata et al., 2017). All materials that can extend the shelf-life or keep constant the packaged food condition could consider as an active package material (Ghaani et al., 2016). According to the European Commission, "active packaging materials are components that would release or absorb substances into or from the packaged food or the environment surrounding the food" (European Commission, 2004). Active natural compounds could be one of the most promising substances for incorporation into the polymer matrix to control mold growth and potentially act as an active packaging material. Plants and fungal microorganisms are the main sources of bioactive metabolites (Osbourn and Lanzotti, 2009; Tringali, 2001; Turner and Aldridge, 1983). In this regard, the studies could find out some antifungal bacterial (Puopolo et al., 2014) and fungal metabolites having the potential for practical application (Barilli et al., 2017; Evidente et al., 2006). Several plants and microorganisms belong to a different class of natural compounds, have already shown biological activities with potential application in different fields as agriculture (Cimmino et al., 2014, 2015a, 2015b; Evidente et al., 2011; Moeini et al., 2019) and medicine (Cimmino et al., 2013; Evidente et al., 2014; Mathieu et al., 2015) and as already mentioned as antimicrobial in the packaging system.

### 1.1. Preliminary investigation

In the term of packaging application of natural metabolites, as preliminary screening of this project, Valerio et al evaluated the potential of 12 bacterial, fungal and plant metabolites as natural fungicides **(Fig. 1)** and in particular their inhibitory effects against *P. roqueforti* and *A. niger* to investigate on their potential application as bakery product package systems (Valerio et al., 2017). They reported that among those metabolites α-costic acid and ungeremine are the most promising as potential bio-fungicide against both fungal strains. These metabolites inhibited fungal growth by more than 60% respect to the control at 72 h and this activity persisted also at 96 h. ungermine showed

MIC 90 lower than 0.003 mg/mL after 48 h of incubation and 0.025 mg/mL at 72 h against *P. roqueforti*. The MIC90 value for *A. niger* was 0.2 mg/mL at 48 h for both compounds. The α-costic acid showed generally MIC values at 48 and 72 h higher than ungeremine (Valerio et al., 2017). In another study, the authors showed that cavoxin can have an inhibitory effect against *P. roqueforti* IBT18687 and *A. niger* ITEM5132 and even they compared the cavoxin activity with calcium propionate, which is a chemical preservative for bakery products (European directive, 1995/2/CE). The result indicated that cavoxin not only influenced the growth of both fungal strains 100 fold lower concentration than calcium propionate but also could show activity even until 72 h up to its concentration (**Fig. 1**) (Santagata et al., 2017).

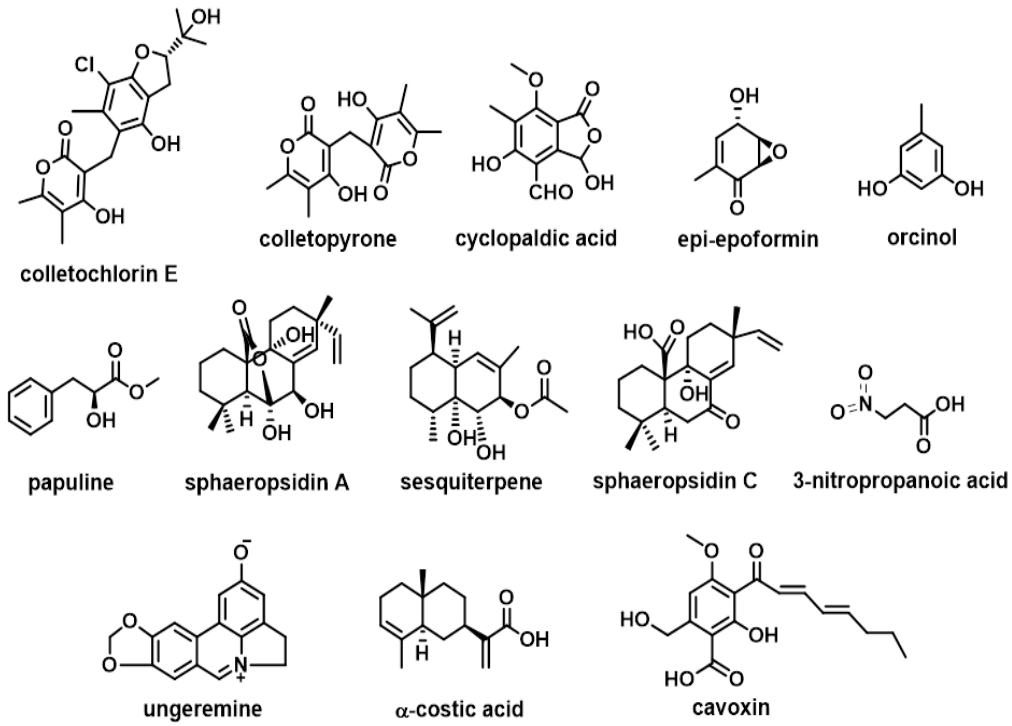


**Figure 1.** Structures of compounds (Santagata et al., 2017; Valerio et al., 2017).

### 1.1.1. Cavoxin

Cavoxin (CVX) is a tetrasubstituted benzoic acid **(Fig. 1)** and cavoxone **(Fig. 2)** is a chroman-4-one respectively isolated from *Phoma cava* from *Castanea* spp., a fungus isolated from chestnut (Evidente and Randazzo, 1985). However, cavoxone was biologically inactive. Therefore, researches mainly focus on cavoxin and its potential application in different fields.

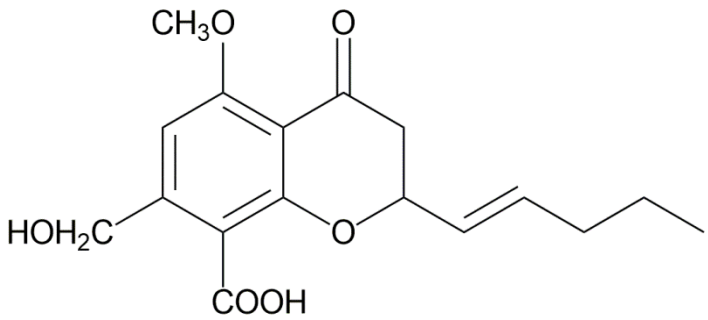


**Figure 2.** Cavoxone structure

There are lots of studies on cavoxin demonstrated its pesticide ability. In this regard, Barilli et al indicated that cavoxin strongly inhibited *Erysiphe pisi* (a major constraint for pea crops worldwide) germination and haustoria formation and reduced colony size (Barilli et al., 2019). Thus, Schrader et al proved cavoxin activity towards species of plant pathogenic fungi (Schrader et al., 2010). As it already mentioned cavoxin was an active antifungal metabolite against both *A. niger* and *P. roqueforti*. It was formulated into the polybutylene succinate (PBS). The PBS-CVX films maintained the antagonistic activity of cavoxin even after formulation into polymer matrix against two food mold contaminants (*A. niger* and *P. roqueforti*) (Santagata et al., 2017).

### 1.1.2. Ungeremine

Ungeremine (UNG) **(Fig. 1)** and zefbetaine **(Fig. 3b)** are two betaine type alkaloids isolated from *Pancratium maritimim* L., a known species of Amaryllidaceae collected on Egypt northern coasts (Abou-Donia et al., 1992). Ungeremine can be also synthesized by

$SeO_2$ oxidation of lycorine, the main Amaryllideacea alkaloids obtained in very high yield (11.2 g/kg of dried bulbs) by a green process which provide acid extraction, alkalinization and subsequently crystallization of the crude precipitated alkaloid **(Fig. 3a)** (Abou-Donia et al., 1992; Cimmino et al., 2017). The synthetic preparation of ungeremine was done according to (Fales et al., 1955) studies. Besides, Kornienko & Evidente collected all the studies about the effect of different oxidizing agents on lycorine (Kornienko and Evidente, 2008). Amaryllidaceae J. St.-Hil. **(photo. 1)** grows in several countries as wild species mainly in tropical and subtropical regions such as Andean South America, the Mediterranean basin, and southern Africa (Chase et al., 2009; Nair and van Staden, 2013). Thus, due to having beautiful flowers and volatile oils productions, they are cultivated as ornamental plants (Moeini et al., 2018). Amaryllidaceae species are classified in 60 genera and known as the herbal plant to make folk medicine especially in South Africa in which 1000 species wild growth (Chase et al., 2009). Also, they are a good source of biologically active alkaloids (Kornienko and Evidente, 2008). More recently, a study reported the stereostructure and biological activity of Amaryllidaceae alkaloids (Cimmino et al., 2017). *Stenbergia lutea Ker Gawl* which is a kind of Amaryllidaceae plant grows in the coasts of the Apulia region in South Italy and its rhizosphere is the best source of lycorine (Evidente et al., 1985).

Ungeremine could also obtain by the degradation of lycorine with *Pseudomonas sp*. ITEM 311 which grow on a minimal medium. The study could show ungeremine antibiotic activity against *Corynebacterium fascians* as well as other Gram-positive and Gram-negative bacteria (Evidente et al., 1985). The bioassay results showed that the antibiotic activity of ungeremine is due to the aromatization of the C ring and the oxidation state does not play role in antimicrobial activity (Evidente et al., 1985). It worth to mention that thanks to dipolar ion related to the azomethine cation and a negatively charged phenate group that is not adjacent to the cationic site ungeremine is a zwitterion (Carey and Sundberg, 2008). There are many other studies on the ungeremine biological activity to survey on other different potential applications of ungeremine. In this respect, Schrader et al could find out the ungeremine application in aquaculture by proving its antibacterial

activity against gram-negative bacterium *Flavobacterium columnare* which causes columnaris disease in channel catfish (*Ictalurus punctatus*) (Schrader et al., 2013). Besides, there is a lot of investigation on the medical application of ungeremine in different aspect such as anticancer activity and anti-alzheimer (Casu et al., 2011; Chen et al., 2017; Lamoral-Theys et al., 2010; Murray et al., 2013; Syad et al., 2013). As already mentioned, ungeremine is active against *P. roqueforti* and *A. niger* so, it could be considered as an antifungal additive in the active packaging system by potential application in food packaging mainly bakery products (Valerio et al., 2017). Interestingly, there is a direct relationship between the applicative potentialities of ungeremine with its easy availability thought one-step oxidation of lycorine without any further purification (Moeini et al., 2018).

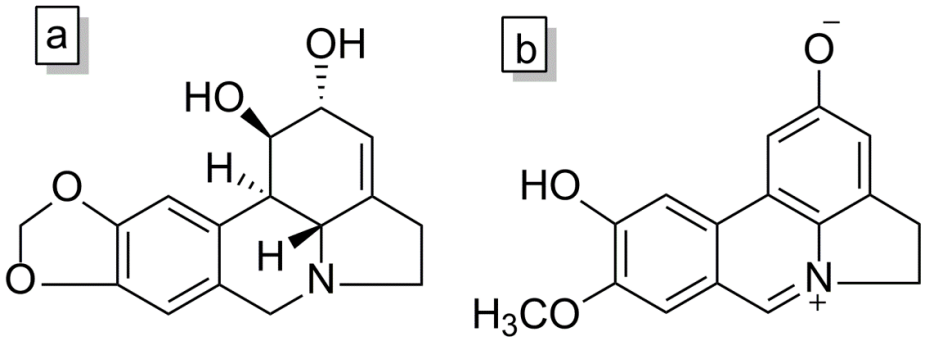


**Figure 3.** Lycorine (a) and zefbetaine (b)

### 1.1.3. α-costic acid

Another active metabolite against *P. roqueforti* and *A. niger* was α-costic acid, a sesquiterpenoid isolated from *Dittrichia viscosa (*Syn. *Inula viscosa)* **(photo. 1b)** (Andolfi et al., 2013; Valerio et al., 2017). It is also known as herbal plants in the Mediterranean area. The large number of studies on *D. viscosa* extractions proved their wide range of application in different fields like medicine as an antioxidant (Schinella et al., 2002), an anti-inflammatory (Hernández et al., 2005), antimycotic medication (Maoz and Neeman, 2000) and apoptosis in human melanoma cell line induced by the sesquiterpenes

tomentosin and inuviscolide (Rozenblat et al., 2008), and in agriculture known as a very strong natural herbicide (Moeini et al., 2019; Zermane et al., 2011), a fungicide of some important crops and plant disease (Mueller-Riebau et al., 1995; Omezzine et al., 2011; Stavrianakou, Sotiria, Liakopoulos, Georgios , Miltiadou, Despoina, Markoglou, Anastasios , Ziogas, Basil , Karabourniotis, 2010; Wang et al., 2004), phytopathogenic bacteria (Madanat et al., 2016; Stavrianakou, Sotiria, Liakopoulos, Georgios , Miltiadou, Despoina, Markoglou, Anastasios , Ziogas, Basil , Karabourniotis, 2010), insecticide (Madanat et al., 2016), plant parasitic nematodes (Oka et al., 2001) and parasitic and non-parasitic weeds (Vurro et al., 2009). Among the organic extract of plant aerial part, α-costic acid (α-CA) **(Fig. 1)** is a sesquiterpenoid acid which was isolated together with other four bi and tricyclic new phytotoxins belonging to different sesquiterpene subgroups and named inuloxins A-D (Andolfi et al., 2013; Johnson et al., 2018).

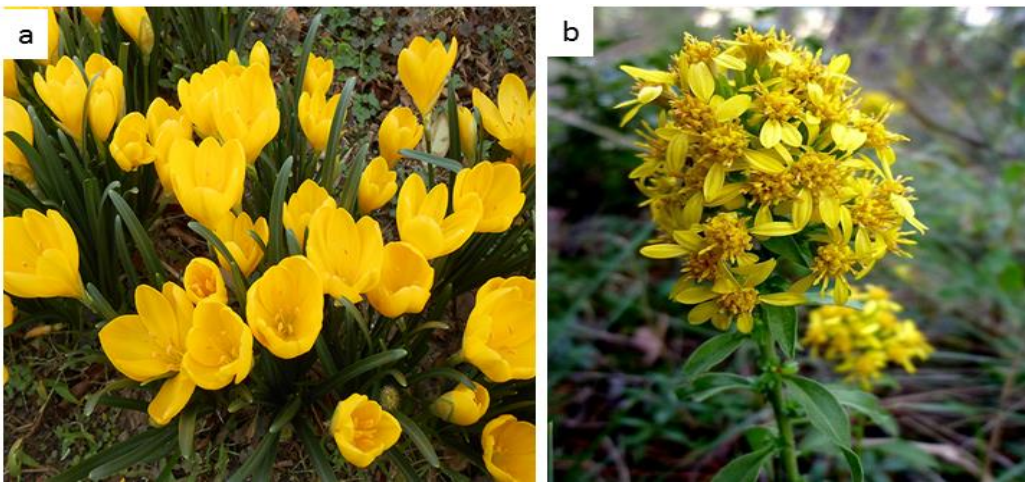


**Photo 1.** *Strenbergia lutea* (a) and *Dittrichia viscosa (Inula viscosa)* (b)

Shtacher and Kashman introduced α-costic acid as an antifungal (Shtacher and Kashman, 1970) and later its phytotoxic activity was assayed against crenate broomrape (*Orobanchecrenata*) and field dodder (*Cuscutacampestris*) (Andolfi et al., 2013). More recently, Valerio et al investigated α-CA potential application in food packaging. They

found out α-CA antifungal activity against two fungi responsible of bakery product contamination, *A. niger,* and *P. roqueforti* (Valerio et al., 2017).

### 1.2. Active packaging

An active package system is defined as a package system manufactured by formulated active compound or compounds into the package system to extend the food shelf-life. It should notice that the food shelf-life depends on the biological, chemical, and physical interaction between food surfaces with the package and the surrounded environment (Robertson, 2009). In general, there are two ways to control food contamination by including antimicrobial metabolites or chemical preservatives like bacteriocins, hydrogen peroxide, organic acids, benzoate, propionate, and sorbate either directly as a food ingredient or formulation into the package system as an active package system (Axel, 2015; Lavermicocca et al., 2000; Nguyen Van Long et al., 2016; Suhr and Nielsen, 2005). The main goal for packaged food could be certain delivery and the preservation of packaged foods before consumption. The traditional packaging system could change the flavor, odor, and color of foods (Risch, 2009). This is why lately industrial sectors and research centers have focused on developing active packaging systems. This new system protects food through both tangents interact with the food surface and having space between the package and the food system (Nguyen Van Long et al., 2016). A similar activity could be observed in antimicrobial food packaging to control the growth of microorganisms that may exist in packaged food (Santagata et al., 2017). Besides, the incorporation of natural bioactive substances into the active packaging has some advantages over the traditional preservatives such as protecting the food quality for prolonged times and reducing the possible change of food components (Muriel-Galet et al., 2013; Qin et al., 2015). Active packages have commonly manufactured by petroleum-based polymers because of their advantages over the biopolymers such as low cost, good mechanical properties, optical and barrier properties, heat sealability, resistance against water and oil, environmental microbial inertia, and easy processability (Riggi et al., 2011).

### 1.3. Synthetic polymers and their drawbacks

Fossil fuels based polymers such as polyethylene, polypropylene, and polystyrene because of their availability, low cost and good mechanical properties widely use as packaging materials (Montanheiro et al., 2014). Based on Plastics Europe, the consumption of plastics has been significantly increased from 65 mt (million tons) to more than 350 mt during the last decades from 1980 to 2017 so that 18.5% of this amount produced in Europe (PlasticsEurope, 2018) and more than one-third of this amount belongs to short-life products such as packaging (Schwarzböck et al., 2016). Since most synthetic plastics are not degradable and compostable, they have faced our world to numerous environmental concerns. Therefore, today recycling plastics become very important. To correctly realize the massive effect of the synthetic plastic on our environment, it would be helpful to consider precisely the European Commission's report. Actually, in spite of growing plastic production in the EU, just less than 25% of waste plastic is recycled and about 50% goes to landfills and others to oceans (European Commission, 2015). The 2030 Sustainable Development Goals implies to significantly diminish marine pollution of all kinds, including marine litter (European Commission, 2015). To achieve this goal, there is three mains point, first can be improving separate collection of plastics via using certification systems to avoid recyclable plastics away from landfills (European Commission, 2015). Second, using the chemical additive to enhance plastics biodegradability although, the presence of hazardous chemical additives not only could make technical difficulties but also can raise questions regards to plastics biodegradability (European Commission, 2015). The last one and the most important one is the investment of using biopolymers from natural and renewable resources can use as a replacement for oil-based plastics. Therefore, this project focused on the biopolymer-based active packaging system.

## 1.4. Biopolymers

The continuously growing public concern and environmental pressure resulted from petroleum-based polymers and plastic impact has aroused research interest in biodegradable polymers from natural resources as alternatives to conventional non-degradable polymers. According to the European Bioplastics, biopolymers defined as materials made from renewable resources which have to be biodegradable, biocompatible, and especially compostable, to be able to act as fertilizers and soil conditioners (Siracusa et al., 2008). These materials have several advantages like availability, biocompatibility, biodegradability, and non-toxicity (Kumar et al., 2011). These ecologically friendly properties, as well as the possibility of various modifications based on the desired application due to the presence of different functional groups, caused growing in popularity of biopolymers in the last decades. Besides, having different functional groups in natural biopolymers could lead to a wide range of applications in the packaging, paper coating, biomedical (reportable surgical sutures, implants, and drug delivery), chemical engineering and food science fields. Specifically, in the packaging sector material have to be renewable and compostable to reduce synthetic polymers consumption. Biopolymers can be derived either from different natural sources such as proteins, cellulosic, starch and other polysaccharides resources like microorganisms, plants, and animals, or chemically synthesized from biological materials such as sugars, starch, and natural fats or oils (Kumar et al., 2011). There are two methods for converting those materials into the biodegradable biopolymers: direct extraction of polymer from the plant or animal tissue, and chemical or biotechnological polymerization of the monomer. Thus, biopolymers can be classified according to the method of their production: (1) directly extracted from natural sources (mainly plants) like starch, cellulose, chitin and proteins (casein and wheat gluten), (2) produced by chemical synthesis from renewable bio-derived monomers like poly(lactic acid), poly(glycolic acid) and their bio polyesters, polybutylene succinate and etc. (3) produced by microorganisms or bacteria like the polyhydroxyalkanoates, mainly poly(hydroxybutyrates) and copolymers of hydroxybutyrate (HB) and hydroxy valerate (HV) (Mitrus et al., 2010). Especially, biopolymers directly obtained from natural sources

could examine as the most promising materials as an alternative for synthetic polymers due to their easy availability and cost-effectiveness regarded as the alternate materials (Fahnestock et al., 2011). This popularity in all applications is because of the renewable nature, biocompatibility, and biodegradability. The best definition of biodegradation again backs to European bioplastics which defined biodegradation as a chemical process, that depends on surrounding environmental condition (humidity and temperature) of materials, to convert materials into nature as water, carbon dioxide and compost (artificial additive are not needed) by environmental microorganisms **(Fig. 4)**. The degradation rate can be controlled by modifying the crystallinity. Indeed, the degradation rate is decreased by increasing the percentage of crystallinity. However, it could be also depended on other parameters such as the polymer molecular weight, its purity, ambient temperature, environmental pH, water permeability, its plasticity, and the additives.

On the other hand, due to being ecologically-friendly, nontoxic and edible materials plus all mentioned reasons, biopolymers are excellent materials for short-term and disposable applications in particular food packaging due to momentary self-life of the food package. Specifically, inactive packaging, the initial investigation on microbial packaging, which showed an increase in antimicrobial activity of bio-package against pathogenic and food spoilage bacteria, is an arisen field in the food packaging industry (Kalia and Avérous, 2011). However, working with biopolymers could be always a challenge for researchers which results from their lack of mechanical properties and lipid barrier as well as characteristic the antimicrobial inhibition of active package in the complex food system (Fahnestock et al., 2011). Among the biopolymers, the starch-based one is the most adaptable, abundant materials and low-cost material with potential application in polymer technology.

Among possible biopolymers chitosan, poly(lactic acid) (PLA), polybutylene succinate (PBS) and Mater Bi® selected as the main polymers for this project. Interestingly, all of those biopolymers could consider as in starch-based biopolymers either due to their structures, sources or additives. In the following part, each of the mentioned biopolymers is separately discussed in more detail.

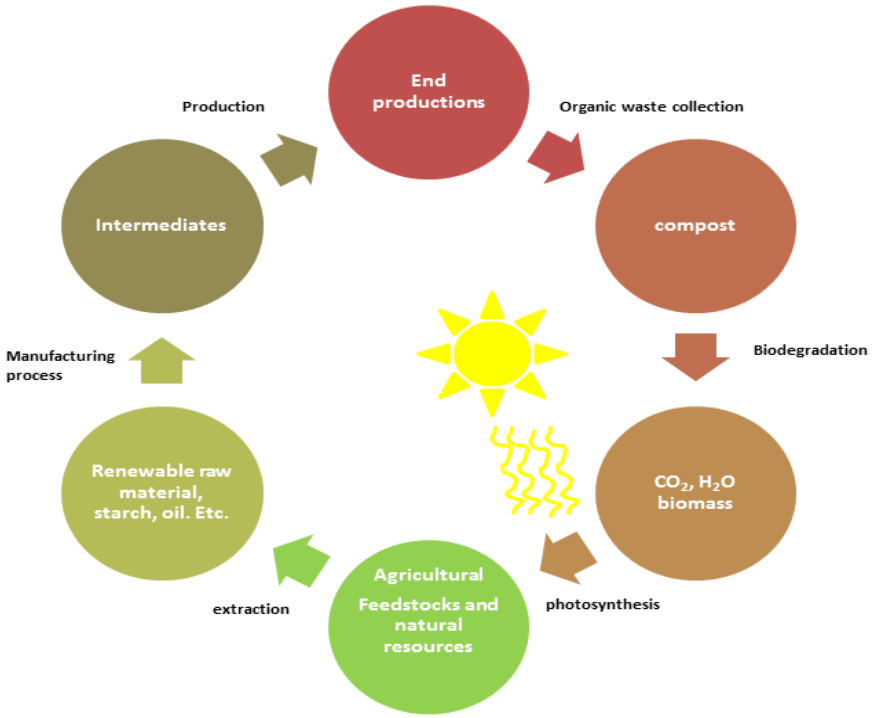


**Figure 4.** Packaging life cycle www.european-bioplastics.org

### 1.4.1. Chitosan

#### 1.4.1.1. Synthesis and characterization

Chitosan or β-(l-4)-2-amino-2-deoxy-D-glucopyranose is the main chitin derivative and linear polysaccharides with a pale yellow color which includes of N-acetyl-glucosamine and N-glucosamine units **(Fig. 5).** Chitin or poly-β-(1→4)-N-acetyl-D-glucosamine **(Fig. 5)** is one of the most abundant natural marine biopolymers with an estimated production of about one trillion tons per year (Morganti and Coltelli, 2019). Chitosan is produced by N-deacetylation of chitin by mean of the mixing of chitin with solid NaOH (weight ratio 1:5) at 180 °C. The number of N-glucosamine units of chitosan known as the degree of deacetylation (DDA), has a direct influence on the physicochemical properties, biodegradability, and immunological activity (Tolaimate et al., 2000). The degree of

deacetylation of chitosan can be measured by using different methods such as ninhydrin test, linear potentiometric titration, near-infrared spectroscopy, nuclear magnetic resonance spectroscopy, hydrogen bromide titrimetry, infrared spectroscopy, and first derivative UV-spectrophotometry (Khan et al., 2002). Due to the presence of the primary amino group, chitosan is soluble in a diluted organic acid (acetic, pyruvic and 10% citric and lactic acid) with pH lower than 6.5. Although chitosan is not soluble in water, it shows higher water absorbability than cellulose because of polyelectrolyte formation. Chitosan three average molecular weights are responsible of all chitosan physicochemical properties such as viscosity, solubility, elasticity, and tear strength. Chitosan with average Mw has the highest antimicrobial properties, and the lower one shows the highest inhibitory effect on human pathogen. However, regardless of molecular weight, chitosan is one of the most potent antibiotics toward gram-positive bacteria. Three functional groups of chitosan (amino, acetamido groups, primary and secondary hydroxyl groups) assumed for simple modification, appropriate to the proposed application (García-Valdez et al., 2018; Soundararajan, 2015). Chitin and chitosan are biocompatible, biodegradable, non-toxic, physiologically inertness, hemostatic, fungistatic, antitumor, and anticholesteremic (Badawy and Rabea, 2011). In spite of all the advantages, chitosan is not suitable for the controlled released formulation. That is why a crosslinking agent or crosslinker, is a reagent with specific functional groups used. In general, there are two kinds of crosslinking process, chemically or physically. The formation of intermolecular bridges between cross liking agent and chitosan segments resulted in an improvement in chitosan mechanical properties and its drug loading capacity. The three-dimensional network of chitosan can be formed by introducing cross-linking agents and through the formation of new inter chain linkage (Aggarwal S, Pahuja S, 2013). The interest of applying crosslinking agents could be due to many advantages such as easy preparation, relatively inexpensive prices, having various structures, and different functional groups. Besides, crosslinked chitosan are stable hydrophilic polymers resistance to high temperatures and low pH. Sodium tripolyphosphate (TPP) widely is used as a physical crosslinking agent

because of its nontoxic property and quick gelling ability through ionic interaction with chitosan amino groups in acidic conditions (Moeini et al., 2018, 2020b, 2020a).

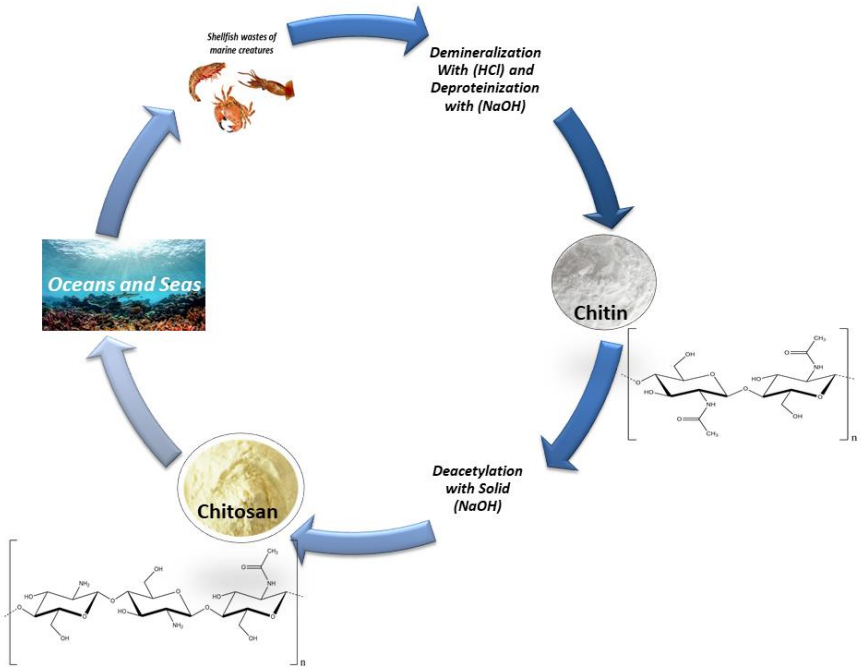


**Figure 5.** Chitosan preparation process (Moeini et al., 2020a)

### 1.4.1.2. Food packaging application

The global consumption of synthetic plastics is more than 200 million tons, with an annual growth of approximately 5% (Siracusa et al., 2008). Additionally, plastic packaging materials are usually contaminated by the foodstuff, and other substance, so their recycling is not practically economical. By considering, foodstuffs are exposed to the processing of microbial spoilage risks like mold growth and result in a serious hygienic problem, and an economic drawback for both consumers and manufacturers. On the other hand, chitosan is one of the most promising candidates for application in the food packaging industry, thanks to a wide range of properties such as being antimicrobial, eco-friendly, and

biodegradable, along with having encapsulation ability. Chitosan is widely used as outer layers films and can provide some supplementary and essential properties in the packaging system through controlling physiological, morphological and physicochemical changes in food products. The mechanism of extending shelf-life of food by the film coating includes controlling many effective criteria of packaging system such as water or moisture permeability, antimicrobial and antioxidants properties, package temperature, pressure of oxygen inside the package, respiration rate, impermeability to certain substances like fats and oils, structural reinforcement of food, coat flavor compounds, and leavening agents in the form of microcapsules. On the other hand, one of the main disadvantages of high-density polyethylene film, which is a common packaging material, is fermentation due to the depletion of oxygen and condensation of water result from the fluctuation of storage temperature, which promotes fungal growth. That is why it is necessary to use chitosan as a natural antimicrobial agent in food packaging. In this respect, Roller et al investigated the potential of using chitosan glutamate as a natural food preservative and evaluated the antimicrobial properties of chitosan glutamate in apple juice against 15 food spoilage yeasts and molds (Roller and Covill, 1999).

### 1.4.2. Poly (lactic acid) (PLA)

#### 1.4.2.1. Synthesis and characterizations

Poly (lactic acid) or polylactide (PLA) is a biopolymer from lactic acid (2- hydroxy propanoic acid) which thanks to bio resorbability and biocompatibility in the body, It has been widely used in the medical application (Tsuji et al., 2000). Due to higher production costs in comparison to conventional plastics, the initial attention on PLA as a package was on high-value films and rigid thermoforms packages for beverage containers and coated papers (Rafael et al., 2004). However, developing the technologies and decreasing the production cost of PLA resulted in a broader array of PLA packaging over time (Drumright et al., 2000; Tsui, 2002). It worth to point out some the PLA production advantages: (1) having renewable agricultural source (corn) (Barikani et al., 2014) (2) consumption large quantities of $CO_2$ during production process (Dorgan et al., 2001) (3)

significantly energy saving (Bogaert and Coszach, 2000) (4) recyclable and compostable (Pilla et al., 2009) (5) improving farm economies (Auras et al., 2004) and (6) adjustable mechanical and physical properties (Sarasua et al., 1998). In the term of packaging not only economic study confirmed the feasibility of PLA as a packaging polymer (Datta et al., 1995), but also medical studied proved that the amount of lactic acid (LA) migrates from package to food is lower than the amount uses as food ingredients. Therefore, PLA could be a good candidate for packaging applications (Hui et al., 2005). Currently, PLA is used for short-life products packaging materials like containers, drinking cups, sundae and salad cups, overwrap and lamination films, fresh fruit, and vegetable containers (Auras et al., 2004). As it shows in **(Fig. 6)**, lactide monomer has two different stereoisomers L-lactic acid and D-lactic acid which can result in the formation of three PLA stereoisomer: poly(L-lactide) (PLLA), poly(D-lactide) (PDLA), and poly(DL-lactide) (meso-lactide). Lactic acid or hydroxycarboxylic acid (2-hydroxypropionic acid) is a monomer of PLA which can be obtained either by chemical synthesis or by microbial fermentation of agricultural by-products (Madhavan Nampoothiri et al., 2010; Singhvi and Gokhale, 2013).

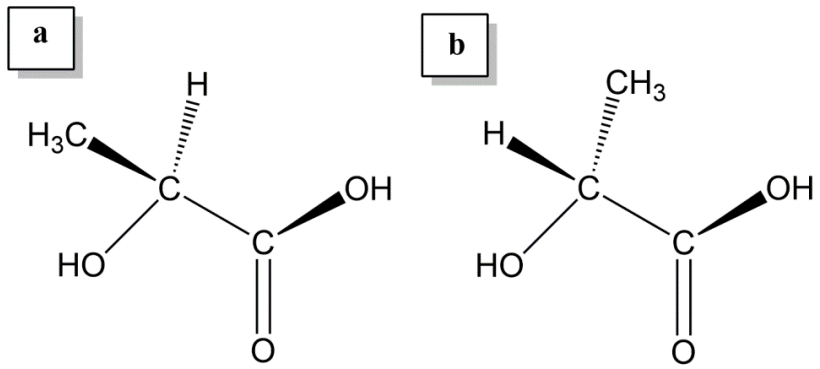


**Figure 6.** Lactic acid stereoisomers D- Lactic acid (a) and L- Lactic acid (b)

In principle, lactic acid can be manufactured in different ways (Siracusa, 2016): i) synthesized through the lactonitrile hydrolysis with strong acid ii) the catalyst degradation of sugars iii) microbial fermentation iv) the oxidation of propylene glycol v) the reaction of acetaldehyde, carbon monoxide, and water at high temperature and pressure vi) the

hydrolysis of chloropropionic acid and vii) the nitric acid oxidation of propylene **(Fig. 7)**. However, among those methods, the microbial fermentation production of lactic acid has gained more attention thanks to being environmentally friendly. Sugar in pure form (glucose, sucrose, lactose) or sugar-containing materials like whey, sugar cane and cassava bagasse, potato, tapioca, wheat, and barley could be a source of microbial fermentation (Ingrao et al., 2015).

As it showed in (**Fig. 7)**, there are three methods for the production of high molecular weight PLA: 1) direct polycondensation polymerization 2) azeotropic dehydrative condensation 3) polymerization through lactide formation.

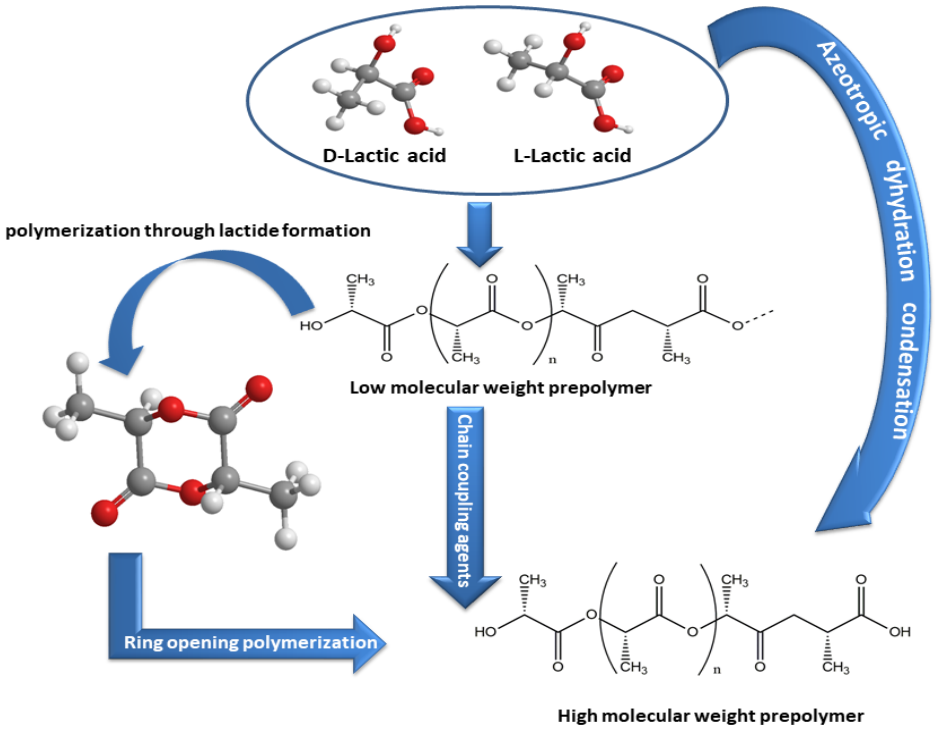


**Figure 7.** Synthesis methods for obtaining high molecular weight PLA

#### 1.4.2.2. Food packaging application

Since when the United States Food and Drug Administration (FDA) recognized PLA as a safe (GRAS) material for the food packaging, a large number of investigations have been done to find all potential food packaging applications of PLA (Conn et al., 1995). The similarity of PLA mechanical and physical-chemical properties to the commercial conventional thermoplastic polymer like polyethylene terephthalate (PET) (Auras et al., 2005) and in particular polystyrene (PS) (Drumright et al., 2000) has been resulted in a fast development of this application in food packaging industry as disposable cutlery, drinking cups, salad cups, plates, overwrap and lamination film, straws, stirrers, lids and cups, plates and containers for food dispensed at delicatessen to fast-food establishments (Conn et al., 1995; Groot et al., 2010). There are some food companies claimed that they use PLA for their products as lunch boxes, fresh food packaging, bottles of water, juices, and yogurts **(Photo. 2)** (Ahmed et al., 2009; Mutsuga et al., 2008). However, PLA's major drawback is weak mechanical and physical properties (low crystallinity, flexibility, and plasticity). To address this problem, there is two ways either manufacture the blend or composites of PLA with other polymers or addition of plasticizers. That's why many studies focused on a completely degradable packaging system by making blends or composites of PLA with other biopolymers (Homklin and Hongsriphan, 2013; Ke and Sun, 2003; Raghavan and Emekalam, 2001; Suyatma et al., 2004; Tawakkal et al., 2014). Regard to plasticizers, there are two kinds of plasticizers for improving polymer mechanical properties: low molecular weight substance (lactides, glyceryl triacetate, glucose, and citrate monoesters), and oligomer plasticizers such as polyethylene glycol (PEG), lactic acid oligomers (Liu and Zhang, 2011). Among them, poly(ethylene glycol) (PEG) and citrate derivatives, in particular, acetyl tributyl citrate (ATBC) are the most used plasticizers (Baiardo et al., 2003; Murariu et al., 2008).


**Photo 2.** PLA applications in food packaging (www.bio4pack.com)

Both PEG and ATBS could increase PLA elongation at a break along with a significant decrease in the glass transition temperature (Tg) and the crystallization temperature (Tc) (Courgneau et al., 2011). The effect of ATBC on mechanical properties confirmed by (Labrecque et al., 1997). PEG is polyether and knows with astonishing physico-chemical properties, water solubility, and low toxicity. There are different methods for the PLA and PEG incorporation such as physical blending and copolymerization (end-functionalized, branched or block copolymers), coatings, etc. However, due to simplicity, physical blending is more common (Toncheva et al., 2016).

### 1.4.3. MATER-Bi (MBi)

#### 1.4.3.1. Food packaging application

MATER-Bi (MBi) is a commercial polymer produced by Novamont Company. According to the company website, MBi is versatile and innovative bioplastic with wide range of application for daily products such as carrier bags, organic waste bags, nets for fresh fruit and vegetables, paper wrappings, cups and napkins, plates, cutlery, cups and spoons for ice

cream and a range of flexible packaging applications to reduce terrible environmental impact of conventional polymer **(photo. 3)** (http://materbi.com/). Mater-Bi is considered as a biodegradable and compatible starch-based polymer with different grades of starch. Therefore, there are various grades of MBi with diffident compositions and properties (Elfehri et al., 2015). Thus, biodegradability and compostability of MBi proven by Novamont company and the rate of degradation of MBi not only depends on its composite materials but also on the environmental conditions (humidity, oxygen availability, temperature, and presence of digestive bacteria) like other biodegradable polymers. However, according to them, the highest degradation rate could be achieved by providing industrial composting and anaerobic bacteria (http://materbi.com/).


**Photo 3.** MATER-Bi food industry applications (http://materbi.com/)

According to Bastioli, there are five classes of Mater-Bi for different applications (Bastioli, 1998). Class Z made of thermoplastic starch and poly-t-caprolactone with different methods such as film blowing, extrusion, casting, and injection molding can be processed. It applies as a bag, net, paper lamination, mulch films, twines, and wrapping film. Class Y made of thermoplastic starch and a cellulose derivative. This class is processed by

injection molding and used as cutlery, boxes, flower pots, seedling planter trays, golf tees, vending cups, and pens.

Class V can be processed through injection molding and used for loose fillers and packaging foams as a replacement of polystyrene, soluble cotton swabs, and soluble items. Class A made of starch and ethylene-vinyl alcohol copolymer and used in the applications that do not necessarily need to be compostable (Bastioli, 1998). Finally, class N made by poly(butylene adipate-co-terephthalate) (Elfehri et al., 2015). There are many studies on different classes of MBi to improve their mechanical properties and biodegradability. For instance, some studies on the effect of flax and sisal on class Y and Z mechanical properties and biodegradability proved the improvement of mechanical properties and biodegradation in the presence of flax and sisal (Alvarez and Vázquez, 2006; di Franco et al., 2004; Iannace et al., 2001; Puglia et al., 2003). Class N investigated by Morreale et al to evaluate wood flour effect on Mater Bi-N mechanical properties. The result showed that wood flour significantly increased young modulus and decreased elongation at break (Morreale et al., 2008). Besides, Elfehri et al analyzed the thermal and mechanical properties of raw and alkali state of Alfa fibers, dispersed in a bioplastic of the Mater-Bi (Elfehri et al., 2015). They showed that alkali Alfa fibers improved thermal stability by increasing in glass transition temperature (Tg) as well as by increasing Alfa fibers fraction modulus and tensile strength of biocomposites increased, but toughness and elongation at break decreased (Elfehri et al., 2015). However, as far as our knowledge, there are a few studies on the active packaging aspect of the Mater-Bi biopolymer matrix.

## 2. OBJECTIVES

The aim of the thesis was initially evaluating the antifungal activity of 13 fungal, plant and microorganism metabolites against *P. roqueforti* and *A. niger, and s*electing the most promising ones with the highest activity against both fungal strains.

In the next step, the selected metabolites had to formulate into suitable polymer matrices along with assessing the antifungal activity and chemical-physical properties of the biofilm. Finally, scale up the formulation method for the manufacturing of an active packaging system. The proposed steps summarized below:

- Finding new antifungal metabolites from the plant, fungal, and bacteria
- Discovering new protocols for the extraction and purification of bioactive metabolites in particular for the step-up production
- Developing the method for inclusion of active compounds in eco-friendly biofilms for food packaging, and agro-industrial
- Scaling-up the formulation methods to have active biofilms

# 3. MATERIALS AND METHODS

## 3.1. Natural metabolites

### 3.1.1. Fungi

Cavoxin isolated from culture filtrates of *Phoma cava* Schulzer from Castanea spp., a fungus belonging to a toxigenic genus (Evidente and Randazzo, 1985).

### 3.1.2. Plant materials

Whole aerial parts of *Dittrichia viscosa (*Syn. *Inula viscosa)* plants were collected fresh in Italy from naturally occurring populations. After harvesting, leaves were detached from the stems and dried in a ventilated oven at 50 °C for two days. The plant material was then grinded to obtain a powder by using a lab mill, and packaged in plastic bags under vacuum until its use (Andolfi et al., 2013).

Fresh ground bulbs of *Sternbergia lutea* Ker-Gawl was collected near Bari. The bulb gets dried in a ventilated oven at 50 °C and grinded as explained before (Evidente et al., 1984a).

## 3.2. Biopolymers

Chitosan (molecular weight 310,000–375,000 Da and deacetylation degree 75%) and sodium tripolyphosphate (TPP) were purchased from Sigma Aldrich (Milan, Italy). Commercial grade poly(lactic acid) 4042D resin was supplied by NatureWorks® LCC, Minnetonka Blvd, MN, USA. It consists of 92% L-lactide and 8% D-lactide units. The molecular weight is MW of ~390000 g/mol, with a polydispersity index of 2 and a density of 1.25 g/cm$^3$. Polyethylene glycol with Mw = 400 g/mol (PEG) was supplied by Sigma-Aldrich. All other reagents were purchased from Sigma Aldrich and used as received.

## 3.3. General procedures for natural metabolites characterization

$^1$H- and $^{13}$C-NMR spectrum was recorded at 400 MHz in $CDCl_3$ and $CD_3OD$ on Bruker spectrometers unless otherwise noted. The same solvent was used as an internal standard. UV spectra were taken in MeCN solution on a Perkin-Elmer Lambda 25 UV/Vis spectrophotometer.

Analytical and preparative TLC was performed on silica gel (Merck, Kieselgel 60 F254, 0.25 and 0.50 mm, respectively) or reversed-phase (Whatman, KC18 F254, 0.20 mm) plates; the spots were visualized by exposure to UV light or by spraying previously with 10% $H_2SO_4$ in methanol and then with 5% phosphomolybdic acid in ethanol, followed by heating at 110 °C for 10 min. Column chromatography was performed with silica gel (Merck, Kieselgel 60, 0.063-0.200 mm). The HPLC analysis was optimized using a system (HITACHI) consisting of a pump (5160) and a spectrophotometric detector (5410). Thus, the separations were performed using a Merk (Darmstadt, Germany) C-18 reversed-phase column Lichrocart (250 . 4.6 mm i.d.; 5 μm) and elution was done by acetonitrile-water 60–40% for 20 min.

### 3.4. General procedures for formulated films, composites and particles characterization

Attenuated Total Reflection Fourier Transform Infrared (FTIR-ATR) spectroscopy was carried out utilizing a Perkin-Elmer Spectrum 100 spectrometer (Waltham, USA), equipped with a Universal ATR diamond crystal-sampling accessory.

Thermogravimetric analyses (TGA) were carried out with a Mettler Thermogravimetric Analyzer Mod. TG50. Measurements were performed on samples of about 3–5 mg, placed in open ceramic crucibles and heated from room temperature to 600 °C at 20 °C/min in air atmosphere, with a nominal gas flow rate of 30 mL/min. Before the tests, a blank curve was measured and subtracted from the single thermograms, to correct from instrumental drift (Vyazovkin et al., 2014). The measurements were performed in triplicate (Moeini et al., 2018).

Morphological analysis of films was performed using a FEI Quanta 200 FEG Scanning Electron Microscope (SEM) on microbeads surface. SEM observations were performed in low vacuum mode (PH2O: 0.7 Torr), using a large field detector (LFD) and an acceleration voltage of 5–20 kV. Before the observation, the sample surfaces were coated with a homogeneous layer (18 ± 0.2 nm) of Au–Pd alloy using a sputtering device (MED 020, Bal-tec AG).

Gel permeation chromatography was performed using a GPC Max Viscotek system equipped with a TDA 305 triple detector (Refractive Index, Low Angle Light Scattering, Right Angle Light Scattering, and Viscometer). A Phenomenex pre-column and two columns Phenogel of 106 Å and 103 Å, respectively, were used. All the samples were dissolved and eluted in chloroform stabilized with ethanol. After complete dissolution, they were filtered on PTFE membranes of 0.22µm. The injection volume was 100µl, the flow rate 0.8 ml/min and the sample concentrations about 5mg/ml. The chosen method of analysis was a triple point, calibrated with a PS standard, provided by Viscotek, having narrow molecular weight distribution (Mw 104,959 Da, Mw/Mn 1.037). The measurements, performed at 35 °C, according to the temperatures of columns and detectors, ran for 50 min.

Differential Scanning Calorimetry (DSC Q2000, TA Instrument, equipped with an RCS cooling accessory). Samples of 5–8 mg were placed on sealed aluminum pans under a dry nitrogen flow of 50 mL/min. The samples were equilibrated at 25 °C and heated up to 180°C by a heating ramp of 20 °C/min to erase the previous thermal history. A brief isotherm step of one minute antedated a non-isothermal crystallization cooling step up to -80°C at a rate of 20°C/min. Finally, a second heating ramp up to 250 °C at 20 °C/min was recorded. All the samples were dried under vacuum at room temperature for 24 h before each DSC test.

Tensile tests were performed on dumbbell-shaped film specimens whose dimensions were respectively 4 mm in width and 28 mm in length, while the thickness of each film was measured at five random points and the result was not significantly different (0.073±0.002 mm). The tests were performed employing a dynamometer model LRX (LLOYD instruments, universal tensile tester equipped with a 1kN load, following ASTM D638-10 (2010). Five dumbbell-shaped samples were analyzed at room temperature 25±2 °C and 45 ± 5% RH, at a crosshead rate of 5 mm $min^{-1}$, without preload. The results of the evaluated parameters were expressed as the average values. Before testing, the samples were equilibrated in the climatic chamber settled at 25 °C and 50% RH for 24 hours.

# 4. EXPERIMENTAL

## 4.1. Antimold microbial and plant metabolites with potential application in intelligent food packaging (preliminary investigation)[1]

### 4.1.1. Biological assays

***Microbial strains and growth conditions***

To select the bioactive metabolites inhibiting mold growth, a spectrophotometric assay was performed with the Bioscreen C (Bioscreen C Oy‘growth curves AB Ltd; Helsinki, Finland). Microbial and plant metabolites (**Table 1**) were suspended in absolute methanol (MeOH, 99.9%) to obtain a stock solution (10 mg/mL). Each solution was diluted 1:100 with Potato dextrose broth (PDB-Biolife) to obtain an initial concentration of 0.1 mg/mL in PDB + MeOH 1% and solutions dispensed in 190 µl portions inoculated with 10 µl of a conidial suspension containing about 104 conidia, into sterile, disposable, and multi-well plates (“honeycomb” plates 10x10 wells; Labsystems, Helsinki, Finland). Each tested solution prepared in triplicate. Microplates were incubated at 26 ± 0.3 °C for 120 h in the Bioscreen C, and the growth of *A. niger* and *P. roqueforti* strains were automatically measured determining the optical density at 580 nm every 6 h using the turbidimetry method. The inhibitory efficacy of tested substances was expressed as growth inhibition percentage (calculated concerning the fungal growth in the inoculated PDB-MeOH 1% medium) and was obtained using OD580 values after 72 and 96 h growth.

***Antifungal microdilution test***

In order to determine the minimal concentration of the selected substances ungeremine and α-costic acid able to cause at least the 90% of growth inhibition respect to the control (PDB-MeOH 1%) (MIC90), each stock solution (20 mg/mL) diluted with Potato dextrose broth (PDB-Biolife) to obtain an initial concentration of 0.2 mg/mL in PDB + MeOH 1%. These solutions were serially diluted with PDB + MeOH 1% to obtain the following test

[1] The work was done in collaboration with CNR - ISPA - Institute of Sciences of Food Production and has been published in: Valerio, F., Masi, M., Cimmino, A., Moeini, S. A., Lavermicocca, P., & Evidente, A. (2017). Antimould microbial and plant metabolites with potential use in intelligent food packaging. Natural Product Research, 6419(October), 1–6. https://doi.org/10.1080/14786419.2017.1385018

concentrations: 0.1, 0.05, 0.025, 0.012, 0.006 and 0.003 mg/mL. In each experiment, an inoculated control not containing antifungal test solutions (PDB + MeOH 1%) was used as growth control. As a further control, an inoculated PDB + MeOH 1% solution containing calcium propionate (0.3% w/vol), generally used as a food preservative, was used. The efficacy of different concentrations of ungeremine and α-costic acid was expressed as inhibition percentage (inhibition %) calculated based on fungal growth reached after 72 h compared to the growth control (PDB + MeOH 1%) and as MIC90 and MIC50 values. These MIC values defined as the minimal inhibitory concentration able to cause at least 90% (MIC90) or 50% (MIC50) after 48 and 72 h. Additionally, optical density measurements recorded every 6 h from zero time to 162 h was used to generate growth curves for each fungal strain. The Gompertz model was used as a mathematical means of fitting growth curves to estimate microbial growth kinetics. Three points (optical densities at 72, 96, and 120 h) of the control growth curve were used to calculate with the Gompertz model the additional time (growth delay, GD, expressed in hours) required by ungeremine and α-costic acid solutions to reach the optical density of the control at that time. The growth delays concerning the control at these three times (GD72, GD96, and GD120, respectively) predicted by the Gompertz model in the cases where the optical density of the control not to reach within the experimental period, unpredictable data were obtained. The Sigma Plot program (SPSS Science Software Gmb, Erkrath, Germany) was used for graphics and data elaboration.

### 4.2. Extraction and purification of cavoxin and cavoxon from *Phoma cava* culture filtrates

Briefly, lyophilized solid residue corresponding to 9 liters of culture filtrate of *Phoma cava* was dissolved in distilled $H_2O$ (1 liter) and extracted with $CHCI_3$, (4 X 500 ml). The organic extracts were combined, dried ($Na_2SO_4$), filtered, and then evaporated under reduced pressure. The residue (1.762 g) was chromatographed on Sephadex LH-20 column according to a previously reported paper (Evidente and Randazzo, 1985). The first compound eluted with $CHC1_3$-iPrOH (9:1) was cavoxone **(Fig. 2)**, while the successive

toxic eluate contained cavoxin **(Fig. 1).** After removal of the solvent by rotary evaporator, both compounds obtained as homogeneous oil. Cavoxin crystallized as pale yellow needles (979 mg, 108 mg/liter) from EtOAc-petroleum ether (40-70°); cavoxone obtained as white needles (101.9 mg, 12.1 mg/liter) by crystallization from EtOAc (Evidente and Randazzo, 1985).

### 4.2.1. HPLC method for the identification and quantification of cavoxin in *Phoma cava* culture filtrates[2]

***Preparation of standard solution***

The stock solution (120 µg/ml) of cavoxin was prepared by dissolving 120 µg in 1.0 ml of chloroform: methanol (9:1).

***Preparation of calibration graph***

The mobile phase was MeCN–$H_2O$ at a flow rate of 1 mL $min^{-1}$. The analysis was performed using a MeCN–$H_2O$ gradient starting from 60–40%. Detection was performed at 280 and 325 nm which was the maximum adsorption wavelength of cavoxin a conjugated chromophore. The crystallized samples of both caxoxin and cavoxone were used as standards (Evidente and Randazzo, 1985). 20 µL of 120, 92 and 41µg/ml of the standard solution of cavoxin and 75, 32.5 and 16 µg/ml of the standard solution of were injected to obtain the calibration curve and monitored for 20min. Linearity was determined by analyzing different concentrations of cavoxin and covoxone obtaining a calibration curve. The calibration graph was prepared using values of peak area versus concentration of cavoxin and cavoxone applied (Masi et al., 2017a) .

[2] The work presented in this part has been published in: Masi, M., Moeini, S. A., Boari, A., Cimmino, A., Vurro, M., & Evidente, A. (2017). Development of a rapid and sensitive HPLC method for the identification and quantification of cavoxin and cavoxone in Phoma cava culture filtrates. Natural Product Research, 6419(October), 1–5. https://doi.org/10.1080/14786419.2017.1392950

***Method validation***

The method was established to compare the retention time (RT) values of the standard in the samples. The accuracy of the method determined through measurement of recovery. For the preparation of samples, the cavoxin standard (60 µg) was added to the organic extract of the stirred fungal filtrate culture (250 µg/ml) and the mixture

The bands of cavoxin and cavoxone were confirmed by comparing their RT ratio (about 2 minutes). To confirm the purity of the extraction of *P. cava*, UV absorbance spectra at 280 and 325 nm performed using cavoxin as reference. The sensitivity of the method was evaluated by the calculation of the linear regression equation with both the limits of detection (LOD) and the limit of quantification (LOQ).

The limit of detection defined the lowest amount of analyte able to be detected (LOD). Thus, the limit of quantification (LOQ) is the lowest amount of analyte, can be determined above the baseline noise. The LOD and LOQ for fungal stirred culture filtrate were determined by taking different concentrations (41-5 µg/ml).

### 4.3. Extraction and purification lycorine from *Sternbergia lutea*

Lycorine was obtained from acid extraction from minced bulbs of *Sternbergia lutea* Ker Gawl. Briefly, using the method developed by (Evidente et al., 1984b). Dried and minced bulbs of *S. lutea* (1 Kg) was extracted at room temperature for 24 h with 1% $H_2SO_4$. The liquid phase squeezed out through a cloth bag and then centrifuged. The residual bulbs were extracted again in the same condition. The combined aqueous phase was basified with NaOH (12 N) at pH 10. The solution was left in the dark overnight. The precipitate was first separated by decantation and then by centrifugation at 7000 rpm for 30 min. The brown cake was crystalized in boiling EtOH. Crystalline lycorine was collected as white prims (about 11g/kg dried bulbs).

#### 4.3.1. Synthesis of ungeremine

To synthesize ungeremine, lycorine (370 mg) dissolved in EtOH (20 ml) and $SeO_2$ (250 mg) was added. The oxidation reaction was carried out at reflux for 4 hours. The resulting suspension was filtered, to remove the selenium trace, and the solvent was

evaporated under reduced pressure to give a yellow solid. The solid residual was dissolved in water and the ungremine free base precipitated by the addition of ammonia (4 M). The compound was very soluble in hot water from which it was crystallized in bright yellow floccule (Evidente et al., 1984a; Fales et al., 1955).

### 4.3.2. Formulation of ungeremine into the polymer matrices

#### 4.3.2.1. Encapsulation of ungeremine in chitosan/tripolyphosphate (CH/TPP) microbeads[3]

Chitosan solution was prepared by dissolving chitosan (1 g) in 125 mL of dilute acetic acid (1% v/v), was kept under stirring for 24 h. Different concentrations of TPP solutions were prepared by dissolving 4%, 5% and 6% w/v of TPP in 25 mL deionized water. Hence, 2.5 mL of the prepared chitosan solutions were dropped into tripolyphosphate aqueous solutions, and kept under slight stirring for about 30 min, up to obtain spherical water-stable beads, following used as control. The microbeads were isolated by vacuum filtration on a paper filter and washed with 100 mL of deionized water to remove the excess of unreacted TPP from the surface of the beads. Finally, the microparticles were freeze-dried for 24 h. As far as concerning ungeremine inclusion inside CH/TPP microbeads, chitosan-ungeremine solution prepared by dissolving chitosan (1 g) and ungeremine (0.320 g) in 125 mL of dilute acetic acid (1% v/v), kept under stirring for 24 h. Hence, the same amount of ungeremine used for the preparation of the beads, i.e. 12.03 mmol. The same experimental procedure was done for obtaining of CH/TPP/UNG beads (Moeini et al., 2018).

[3] The work was done in collaboration with CNR - ISPA - Institute of Sciences of Food Production and CNR- IPCB- Institute for Polymers, Composites and Biomaterials and has been published in: Moeini, A., Cimmino, A., Dal Poggetto, G., Di Biase, M., Evidente, A., Masi, M., Lavermicocca, P., Valerio, F., Leone, A., Santagata, G., Malinconico, M., 2018. Effect of pH and TPP concentration on chemico-physical properties, release kinetics and antifungal activity of Chitosan-TPP-Ungeremine microbeads. Carbohydrate polymers 195, 631–641. https://doi.org/10.1016/j.carbpol.2018.05.005

- **Specific characterization methods for CH/TPP/UNG Microbeads**

***Loading efficiency test of ungeremine in CH/TPP/UNG beads***

In this work, an indirect method was used to calculate the drug loading efficiency (LE). It consisted of the evaluating of the amount of non-absorbed ungeremine in the beads. A known concentration of CH/UNG solution was dropped in the TPP solution. The maximum loading efficiency, by adjusting the pH to acidic conditions, could be evidenced by the visual observation from both the changing of the color of the beads and the TPP solution from white to yellow and vice versa respectively. The loading efficiency was evaluated by performing of UV-Vis from mother liquor. The same procedure was repeated in the other TPP solutions (TPP 5% and TPP 6%).

The loading efficiency (LE) tests were evaluated by means of UV-Vis spectroscopy, exploiting the Beer-Lambert law (A= εbc). The following equation **(Equation.1)** was used to calculate the percentage of the drug loading in the beads.

$$\%LE = 100 - \frac{concentration\ of\ mother\ liquor(mM)}{total\ concentration\ of\ ungeremine(mM)} \times 100 \qquad Equation\ 1$$

To evaluate the ungeremine concentration in mother liquor solution, and based on Lambert- Beer equation, the molar extinction coefficient ($\varepsilon$) was calculated by drawing the calibration curve; to this aim, six water solutions of ungeremine at 1% w/v of acetic acid was prepared, and UV-Vis absorbance was evaluated. By the curve slope, $\varepsilon$ was calculated **(Fig. 8).**

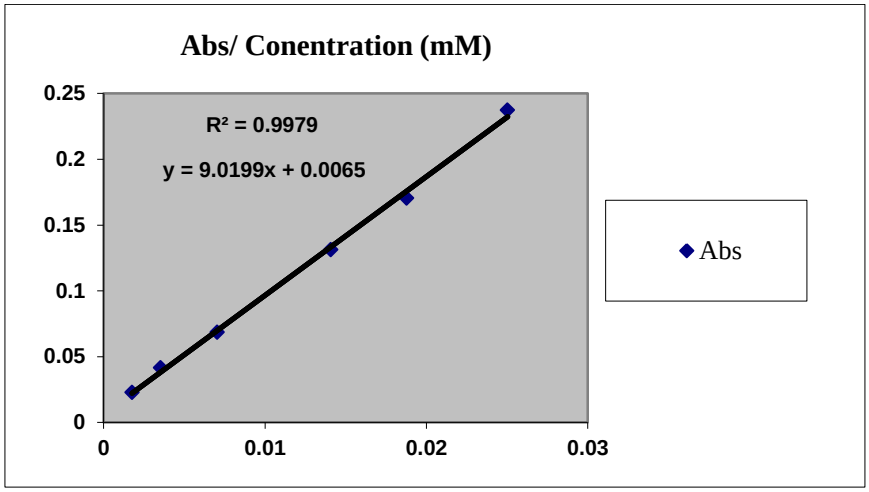


**Figure 8.** Calibration curve for molar extinction coefficient (ε) obtained

***Releasing kinetics***

Sodium hydroxide buffer solutions (pH= 5.7), and potassium phosphate (pH= 6.2) respectively prepared to assess the releasing profile of ungeremine from the beads. Equivalent volumes of the buffer solutions was added in six vials, three of them uploaded with CH/TPP/UNG microbeads with different concentrations of TPP, whereas CH/TPP microbeads was put in the other three vials, and used as the control. The concentration of ungeremine released from the microbeads regularly checked throughout the time, by performing UV-Vis spectroscopic analysis of buffer solution.

**Biological assay**

***Microbial strains and growth conditions***

*Penicillium roqueforti* IBT18687 (PR) was obtained from the Culture Collection of the Technical University of Denmark, Lyngby, Denmark. Fungal conidia collected from 7-day-old cultures on PDA was washed twice with sterile water, and a 50 µL aliquot of the conidial suspension was spread on PDA plates and incubated at 25 °C for 72 h. Conidia were collected using Triton X 100 0.05% (v/v), counted in the Thoma chamber and used in antifungal activity tests.

***Antifungal assays against Penicillium roqueforti***

Antifungal assays were performed as described before with slight modifications (Milovanovic et al., 2015; Seo et al., 2014). Briefly, chitosan beads (CH/TPP and CH/TPP/UNG) was sterilized by UV light for 30 min. Afterward, 20-25 chitosan beads were placed onto PDA plates which then inoculated with 20 μL of a spore suspension ($1 \times 10^5$ spores/ml) of the test microorganism *P. roqueforti* IBT18687. Mycelial growth observed after 1, 2, and 3 days of incubation at 25 °C.

***Porosity test***

To evaluate the porosity of the microbeads, porosity tests was evaluated by following the method reported by Schettini et al via a liquid displacement process (Bundela and Bajpai, 2008; Schettini et al., 2013). As non-solvent, n-hexan used, since its ability to easily penetrate the pores of beads without inducing shrinkage, swelling, or solubilization of the polymeric matrix (Zhang and Ma, 1999). The porosity of the beads was evaluated by following **(Equation 2)** reported: a known weight of beads (W0) immersed in a graduated cylinder containing a known volume (V0) of n-hexane. The beads kept in n-hexane for 24 h. Then the beads were extracted and weighed (W1). By knowing the density (ρ) of n-hexane, the porosity (P) of the beads was obtained (Bundela and Bajpai, 2008).

$$P = \frac{W1 - W0}{\rho V0} \times 100 \qquad Equation\ 2$$

**4.3.2.2. Preparation of sub-micron particles of CH/TPP/UNG**[4] (Moeini et al., 2020b)

Chitosan (1 g) was dissolved in 125 mL of dilute acetic acid (2 % v/v) water solution at 70 °C; after 45 min the polymer was completely solubilized, the solution was transparent

[4] The work was done in collaboration with CNR - ISPA - Institute of Sciences of Food Production, CNR- IPCB- Institute for Polymers, Composites and Biomaterials and Department of Chemistry and Polymer Science, University of Stellenbosch, Stellenbosch, and was published in: Moeini, A., Mallardo, S., Cimmino, A., Dal Poggetto, G., Masi, M., Di Biase, M., van Reenen, A., Lavermicocca, P., Valerio, F., Evidente, A., Malinconico, M., Santagata, G., (2020). Thermoplastic starch and bioactive chitosan sub-microparticle biocomposites: Antifungal and chemico-physical properties of the films. Carbohydrate Polymers 230, 115627.

and no solid and gelling particles were present; then, ungeremine (0.320 g) was added. CH/UNG blend was kept at the previous conditions for other 60 min up to reach a final clear solution. The preparation of sub-micron particles followed the method detailed by the authors in their previous article (Moeini et al., 2018). Briefly, a 4 %w/v of tripolyphosphate aqueous solution was prepared by dissolving TPP in water. This amount of crosslinking agent was selected after several experimental trials aimed to reach the highest beads water stability. Then, 4 mL and 8 mL of the CH/UNG solution were poured into 25 mL of TPP solution, under mild stirring, in order to produce CH/TPP/UNG cross-linked beads at CH-UNG/TPP weight ratio of 1/4; this mass ratio was previously assessed since at this proportion and at a pH 6.2, the crosslinking process was completed after 30 min, time at which the highest ungeremine loading efficiency could be reached, as proved and detailed by the authors in their previous article (Moeini et al., 2018). Finally, both solutions were ground for 20 min by means of a Homogenizer (Mod. IKA Ultra Turrax T25 Digital Homogenizer), at 13,500 rpm. DLS measurements were performed with a Malvern Zetasizer Nano ZS instrument equipped with a 4 mV HeNe laser operating at 633 nm, with a measurement angle of 173°. Mean size and polydispersity index were obtained by cumulated analysis of the correlation function. The distribution of molecular size evidenced that more than 91 % of particles were in the range of 800 nm, typical of sub-micron particle dimension. Finally, sub-micron particles were freeze-dried by lyophilizer for 48 h and then preserved in oven, under vacuum at 60 °C up to the next step.

**4.3.2.3. Formulation of sub-micron particles into the Mater Bi polymer matrix**

MBi pellets were previously ground and dried overnight, under vacuum at 60 °C, prior to extrusion. Two master batches of 10 g (total mass) of MBi and CH/TPP/UNG sub-microparticles were prepared by following two different matrix/dispersed phase weight ratio compositions: MBi/CH/TPP/UNG1 9.5 g/0.5 g and MBi/CH/TPP/UNG2 9 g/1 g. The powdered physical blends were melt mixed in a HAAKE MiniLAb extruder equipped with conical counter-rotating screws with a diameter of 5/14 mm and a length of 110 mm; the length to diameter ratios are ranged between 7.8-22 mm.

Extrusion was performed at 135 °C for 3 min at screws rotation speed of 20 rpm, in a flow-through mode. Samples were then collected in form of "spaghetti", pelletized and cooled at room temperature. They were dried overnight under vacuum at 60 °C, then compression-molded using a compression molding press (Model C, Carver Laboratory Press, USA), in order to prepare the films at different CH/TPP/UNG concentrations. About 2 g of pellets were placed between two steel plates, pre-heated at 137 °C for 2 min at 220 kPa and compression molded at 0 and 1 bar for 2 min, 7 and 14 bar for 1 min and subsequently cooled down to room temperature under pressure, by means of cold water circulating in the plates of the press. The processing temperatures did not influence the thermal stability of CH/TPP/UNG microbeads, i.e. chitosan and ungeremine, as evidenced by thermogravimetric analysis (TGA) detailed by the same authors in their previous article (Moeini et al., 2018). The thickness of films was measured at five random points, using a micrometer (Digital Micrometer Mitutoyo, IP-65 Japan) and the result was expressed as the average value. All the samples show an average thickness of 0.270 mm ± 10%. Finally, two different film compositions were obtained, MBi/ CH/TPP/UNG1 and MBi/CH/TPP/UNG2, in which the amount of CH/TPP/UNG were 0.5 g and 1 g, respectively.

- **Specific characterization methods for CH/TPP/UNG sub-micron particles formulated into Mater Bi**

### *Microbial strains and growth conditions*

#### *Antifungal activity of films by disc diffusion method*

MBi/CH/TPP/UNG1 and MBi/CH/TPP/UNG2 and neat Mater-Bi (used as a control) were tested for antifungal activity by the disc diffusion method (Santagata et al., 2017) on PDA plates (pH 5.6) and on bread-based medium agar plates (Bread Extract Broth, BEB) prepared as reported in (Di Biase et al., 2014). Briefly, the BEB medium was prepared by diluting 100 g of sliced bread, prepared in laboratory and not containing food preservatives, in 350 ml of distilled water. The suspension was homogenized for 2 min in a stomacher (Seward, London, UK), filtered through filter paper (Whatman no. 1). HCl 1 M

was used to adjust the pH from 6.2 to values of 5.7 and 4.9, typical of different food bakery formulations, and agar was added (16 g/L) for the antimicrobial tests. The pH was measured by using the pH meter CRISON GLP 31 EC. The medium was sterilized at 121 °C for 15 min. For the antifungal test, 100 μL of spore suspension in sterile water containing about $1\times10^4$ spores/mL was spread on the agar media (PDA and BEB). The discs (1.3 cm) of MBi/CH/TPP/UNG1 and MBi/CH/TPP/UNG2 and plain MBi were placed on the agar plates previously inoculated with the test microorganism; plates were incubated at 25 °C for 3 days. The antifungal activity of the films was assessed by comparing the halo of inhibition of fungal growth occurring in presence of MBi/CH/TPP/UNG1 and MBi/CH/TPP/UNG2 with respect to control plate hosting neat MBi disc.

***Determination of residual ungeremine mass in biocomposites after antifungal tests by means of UV–Vis Spectroscopy***

After testing the antifungal activity, disc samples were preserved in 1 mL of $CHCl_3$ up to the determination of residual ungeremine mass. A 2 mL volume of distilled water (pH 5) was added to the suspensions to extract ungeremine and all other water-soluble molecules. The aqueous layers were analyzed throughout UV-Vis spectroscopy by means of UV-Vis spectrophotometer (V−570, Jasco Easton, USA) double beam system, with a single monochromator. The solutions were poured in 1 cm quartz cells, the scan speed was 400 nm/min and the wavelengths ranged in between 190 and 600 nm. The amount of ungeremine was evaluated considering UV–Vis absorbance at 360 nm. The mass percentage values were averaged on three different measurements.

***Differential scanning calorimetry (DSC)***[5]

Differential scanning calorimetry (DSC) analysis was performed by means of a TA Instruments Q100 calorimeter (TA Instruments, Waltham, MA, USA). The sample weights were in the range of 6 mg. The DSC cell was purged by nitrogen gas at the flow rate of 10 °C/min. All the samples were kept in isotherm at 5 °C for 5 min. and then heated up to

[5] This part has been done at Stellenbosch University at Department of Chemistry and Polymer Science.

200 °C; after a second isotherm at that temperature for 5 min, the samples were cooled up to 5 °C and then re-heated up to 200 °C; all the thermal ramps were performed at a rate of 10 °C/min.

***Thermogravimetric analysis (TGA)***

Thermogravimetric analyses (TGA) were carried out by using a Mettler Thermogravimetric Analyzer Mod. TG 50. Measurements were performed on samples of about 8–10 mg, placed in open ceramic crucibles and heated from room temperature to 600 °C at 20 °C/min in nitrogen atmosphere, with a nominal gas flow rate of 30 mL/min. Before the tests, a blank curve was measured and subtracted from the single thermograms, to be free from instrumental drift (Vyazovkin et al., 2014).

***Permeability test***

Water and oxygen permeability were tested on neat MBi and biocomposite films by means of an Extra Solution $O_2$ and Multi Perm Equipment, operating at 25°C and 50% relative humidity (RH). The instrumental apparatus consists of a double chamber diffusion cell. The films were inserted between the two chambers: water and oxygen enters the lower one, and a dry nitrogen flux flows in the upper one. A zirconium oxide sensor detects the gases diffusion across the film. The exposed area of the film was 50 $cm^2$. Collected data were converted in water and oxygen transmission rate (WVTR and OTR) that is the time rate of water and oxygen flow between two parallel surfaces under steady conditions at specific temperature and RH. Water and oxygen permeability were calculated from WVTR and OTR data.

***Scanning Electron Microscopy (SEM)***

Cryogenically fractured cross-section of all samples were morphologically analysed by using a FEI Quanta 200 FEG Scanning Electron Microscope. SEM observations were performed in low vacuum mode (pressure 0.7 torr), using a large field detector (LFD) and an acceleration voltage of 5–20 kV. Prior to the observation, the sample surfaces were coated with a homogeneous layer (18 ± 0.2 nm) of Au–Pd alloy by means of a sputtering device (MED 020, Bal-Tec AG).

***Tensile test***[6]

The tensile properties were tested using a LRX (LLOYD instruments) universal tensile tester equipped with a 1 kN load, in accordance with ASTM D638-10 (2010). Six dumbbell shaped samples were analyzed at room temperature 25±2 °C and 45 ± 5% RH, at a crosshead rate of 5 $mm.min^{-1}$, without preload. Before testing, the samples were equilibrated in climatic chamber settled at 25 °C and 50% RH for 24 hours.

**4.3.2.4. Formulation of ungeremine into the PLA/PEG polymer matrix**[7] (Moeini et al., 2020c)

***Preparation and characterization of the spinning solutions***

PLA and PLA/PEG, in three different ratios, with obtained both with a total polymer concentration of 9 % (w/v). The PLA solution was prepared by dissolving of PLA in the required amount of dichloromethane (DCM) at 50 °C under stirring while the PLA/PEG blends were prepared by addition of PEG to the PLA solution in three different (w/w) ratios (95/5, 87/13 and 74/26) (Toncheva et al., 2016). Similarly, solutions containing UNG were prepared by adding UNG, dissolved in methanol (DCM/MeOH = 9:1 v/v), at ratios 1, 2 and 3 % (w/v) to the polymer solution while stirring. The final solutions were obtained after stirring for a further for 30 minutes.

***Electrospinning conditions***

The electrospinning was set up by mean of a standard single needle electrospinning apparatus with a high voltage power supply of up to 30 kV and 1 ml syringe equipped with a positively charged metal and an aluminum plate as a collector of the mat. The electrospinning conditions for all samples were a voltage difference of 17 kV, a tip-to-collector distance of 17 cm and a feed rate of 0.075 ml/min. The exception was PLA/PEG/UNG 2% in which electrospinning condition were a voltage difference of 27 kV, a feed rate was 0.65 ml/min and a tip-to-collector distance of the 22 cm. All the

[6] This part has been done at Stellenbosch University at Department of Chemistry and Polymer Science.

[7] This part has been done at Stellenbosch University at Department of Chemistry and Polymer Science, and published in: Moeini, A., Cimmino, A., Masi, M., Evidente, A., & Van Reenen, A. (2020). The incorporation and release of ungeremine, an antifungal Amaryllidaceae alkaloid, in poly(lactic acid)/poly(ethylene glycol) nanofibers. Applied Polymer Science.

experiments were conducted at 25 °C. Note that the electrospinning conditions were selected after experimentation and in order to reproducible produce fibres with similar diameter and morphology.

***Attenuated Total Reflection Fourier Transform Infrared Spectroscopy (ATR-FTIR)***

ATR Fourier transform infrared (ATR-FTIR) spectroscopic analysis of mats was performed on the all the samples (PLA, PLA/PEG, PLA/UNG and PLA/PEG/UNG) from 500 to 4000 $cm^{-1}$ with a resolution of 4 $cm^{-1}$ and 64 scans by using a Nicolet™ iS™ 10 Fourier transform infrared spectrophotometer fitted with a smart diamond ATR accessory (Thermo Fischer Scientific, Waltham, USA).

***Differential Scanning Calorimetry (DSC)***

The thermal characteristics of fibers were investigated by differential scanning calorimetry (DSC), the analysis was performed by means of a NETZSCH-Gerätebau GmbH (Wittelsbacherstraße-Germany) in the range of -30 °C to 200° with the heating rate 10 °C/min**.** the crystallization degree of PLA ($\chi_C^{PLA}$) was calculated by following equation **(Equation 3).**

$$\chi_C^{PLA}\% = \left[ \left( \Delta H_m^{PLA} - \Delta H_{cc}^{PLA} \right) / \, W \times \Delta H_m^{\circ} \right] \qquad (\textit{Equation 3})$$

where $\Delta H_m^{PLA}$ is the PLA enthalpy of fusion in the fibers, $\Delta H_{cc}^{PLA}$ is the enthalpy corresponding to the temperature of cold crystallization, $\Delta H_m^{\circ}$ is the theoretical heat of fusion of 100% crystalline PLA (93.7 J/g) and WPLA is the mass fraction of PLA in the mats (Wu et al., 2014).

***Release experiments***

The release of UNG from the fiber mats were evaluated by incubating the electrospun fibers and at 34 °C in vials with 25 ml of buffer solution based on sodium acetate/ acetic acid (pH=5.4) for 72 hr. After that, the hydrophilic medium was replaced with a hydrophobic medium of Sörensen/ethanol (30:70 v/v) for another 72 hr. The concentration of ungeremine released from the micro and nano fibers was followed by means of UV-vis

spectroscopy of the buffer solution. The calibration curve of ungeremine was obtained by plotting the absorbance measurement at 260 nm. The values reported are an average of three experiments

***Scanning electron microscope (SEM) and porosities test of fibers***

The morphology of the fibrous materials was observed by a scanning electron microscope (SEM). In order to observe the effect of the buffer solution on the fibers, selected fibers were immersed in the sodium acetate/acetic acid buffer solution (pH=5.4) for 24 h, 48 h and 72 h. Samples were removed, rinsed with distilled water and dried under vacuum at 30 °C. All the samples were vacuum-coated with gold and observed by Sigma VP FE-SEM with Oxford EDS Sputtering System (Carl Zeiss, Germany). The fiber morphology was analyzed in terms of the criteria for complex evaluation of electrospun materials by using the ImageJ software by measuring the diameters of at least 20 fibers from each SEM micrograph.

The porosities of fibers were measured by means of liquid intrusion method. As non-solvent, heptane was used due to its ability to easy penetrate into porosities without shrinkage, swelling or solubilization of the PLA/PEG blend. The fibers were weighed before immersion in heptane as intrusion liquid and the mats left for 1 hour on shaker. The fibers then are taken out and weighed immediately and porosity (P) was calculated based on the following equation:

$$P = [(m_w - m_d)]/d_s / \left\{ [(m_w - m_d)]/ d_s \right] + [m_d^{PLA}/d_{PLA}] + [m_d^{PEG}/d_{PEG}] \right\} \qquad (Equation\ 4)$$

Where ds is a solvent density, $m_w$, md, $m_d^{PLA}$ and $m_d^{PEG}$ are weights of the wet mats, dry mats and PLA fraction and PEG fraction in the dry fibers, respectively.

***Wettability test***

The wettability was measured on neat PLA, PLA/PEG and PLA/PEG/UNG fibers in a different ratio of PEG. For this purpose, an optical contact angle DSA 125 (KRÜSS GmbH, Hamburg, Germany) equipped with the aid high-resolution camera was used and the data were analyzed by KRUSS software. The static contact angle of water at room

temperature (θ, deg) was measured by a sessile drop method by dropping 10 drops of distilled water (2 μl) onto the surface film with a syringe. The entire droplet is released from 0.5 cm above the polymer surface to ensure the consistency of the measurements. The contact angle is calculated 1 minute after droplet deposition by means of the angle between the baseline of the drop and the tangent and the boundary average angle values at all the drops was calculated (Introzzi et al., 2012).

### 4.4. Extraction and purification of α-costic acid from *Dittrichia viscosa (Inula viscosa)*

Plant material (400 g) was extracted by water–methanol (1:1,1L) under stirred conditions at room temperature for 24 h. The suspension was then centrifuged at 7000 rpm for 30 min and the supernatant extracted by $CH_2Cl_2$ (3 X 400 ml). The organic extracts were combined, dehydrated ($Na_2SO_4$) and evaporated under reduced pressure, giving a brown–red oily residue (6.12 g) with high phytotoxic activity. This latter residue was chromatographed by silica gel column eluted with solvent system $CHCl_3$-i-PrOH (95:5), and nine groups of homogeneous fractions were obtained. The second and third fractions, highly toxic in the bioassay activity, contained the main metabolite. The residues of these two fractions were combined (800 mg) and purified by a RP-18 column at medium pressure, using system solvent $H_2O$-MeCN (1:1), giving three fractions. The two lesser polar fractions, both obtained as homogeneous yellow oil, contained the main metabolite identified as α-costic acid (9, 455 mg, 1.14 g/kg, Rf 0.35) (Andolfi et al., 2013).

### 4.4.1. Preparation of polylactic acid (PLA) and Polylactic acid α-costic acid (PLA/α-CA) films[8] (Moeini et al., 2020d)

PLA films were obtained by dissolving 210 mg of the polymer in 20 ml of $CHCl_3$, at 50 °C, under stirring for 3 hours. The obtained solution was poured on 6 cm diameter of glass Petri dish, kept in the plane to ensure the homogeneous thickness of the films. All films were allowed to dry during exposure to the atmosphere for 3 days. The glass plates were covered with aluminum and capped by glassware in order to avoid a fast solvent evaporation. Preliminary investigation (not reported) was performed by preparing films with different PLA/α-CA weight ratios to consider the effect of α-CA on PLA mechanical properties. Among them, PLA/α-CA weight ratio of 7:1 (w/w) evidenced the best results; for this reason, this weight concentration was used for film preparation and characterization. Specifically, PLA/α-CA films were prepared by dissolving PLA, as previously described. After dissolution, 30 mg of α-CA was added and left for other 3 h in continuous stirring at the same temperature. The solutions were casted on glass Petri dish and left to dry in the same condition as previously reported. Petri dish and left to dry as previously reported.

***Attenuated Total Reflection Fourier Transform Infrared Spectroscopy (FTIR-ATR) and Nuclear Magnetic Resonance Spectroscopy ($^1$HNMR)***

FTIR-ATR analysis was recorded on neat α-CA and on PLA and PLA/α-CA films from 500 to 4000 $cm^{-1}$ with a resolution of 4 $cm^{-1}$ and 32 scans by using a Nicolet™ iS™ 10 Fourier transform infrared spectrophotometer fitted with a smart diamond ATR accessory (Thermo Fischer Scientific, Waltham, USA).

For $^1$HNMR analysis, PLA/α-CA film samples were dissolved in $CDCl_3$ and sealed in NMR tubes. The analysis was performed with an NMR spectrometer (Bruker AVANCE

[8] This part has been done at Stellenbosch University at Department of Chemistry and Polymer Science in collaboration with CNR- IPCB- Institute for Polymers, Composites and Biomaterials and has been published in: Moeini, A.,Van Reenen,A., Van Otterlo,W., Cimmino, A., Masi, M., Lavermicocca, P., Valerio, F., Immirzi, B., Santagata, G., Malinconico, M., & Evidente, A. (2020). α-costic acid, a plant sesquiterpenoid from Dittrichia viscosa, as modifier of Poly (lactic acid) properties: a novel exploitation of the autochthone biomass metabolite for a wholly biodegradable system. Industrial Crops and Products (In press).

III 600, Billerica, MA, USA) with a 5 mm BB probe at 600 MHz operating frequency and a spectral window of 0–10 ppm.

***Scanning Electron Microscopy (SEM)***

Morphological analysis of films was performed by means of a Scanning Electron Microscope (SEM) (Quanta 200 FEG, 338 FEI, Eindhoven, The Netherlands), on cryogenically fractured film cross sections. Film surfaces were coated with a homogeneous layer (18 ± 0.2 nm) of Au and Pd alloy by means of a sputtering device (MED 020, Bal-Tec AG, Tucson, AZ, USA). The micrographs were performed at room temperature, in high vacuum mode and internal water vapor pressure of 66.66 Pa, by using a large field detector (LFD) and an acceleration voltage of 20 kV.

***Gel Permeation chromatography (GPC)***[9]

The molecular weight distributions of PLA and PLA/α-CA films were measured by Gel permeation chromatography. The analysis was performed using a GPC Max Viscotek system equipped with a TDA 305 triple detector (Refractive Index, Low Angle Light Scattering, Right Angle Light Scattering and Viscometer). A Phenomenex pre-column and two columns Phenogel of $10^6$ Å and $10^3$ Å, respectively, were used. All the samples were dissolved and eluted in chloroform stabilized with ethanol. After complete dissolution, they were filtered on PTFE membranes of 0.22μm. The injection volume was 100μl, the flow rate 0.8 ml/min and the sample concentrations about 5mg/ml. The chosen method of analysis was triple point, calibrated with a PS standard, provided by Viscotek, having narrow molecular weight distribution (Mw 104,959 Da, Mw/Mn 1.037). The measurements, performed at 35 °C, according to the temperatures of columns and detectors, ran for 50 min.

***Differential Scanning Calorimetry (DSC)***

Thermal properties of PLA based films were studied by Differential Scanning Calorimetry (DSC Q2000, TA Instrument, equipped with a RCS cooling accessory). Samples of 5–8 mg were placed on sealed aluminium pans under a dry nitrogen flow of 50 mL/min. The

[9] This part has done in Institute for Polymers, Composites and Biomaterials, National Research Council, Italy.

samples were equilibrated at 25 °C and heated up to 180 °C by a heating ramp of 20 °C/min to erase the previous thermal history. A brief isotherm step of one minute antedated a non-isothermal crystallization cooling step up to -80 °C at a rate of 20 °C/min. Finally, a second heating ramp up to 250 °C at 20 °C/min was recorded. All the samples were dried under vacuum at room temperature for 24 h before each DSC test. All the experiments were repeated three times to ensure reproducibility and for each analysis, a fresh specimen was used.

***Thermogravimetric Analysis (TGA)***

Thermogravimetric analyses (TGA) were carried out with a TA Q500 thermogravimetric analyzer (TA Instruments, New Castle, USA). Measurements were performed on samples of about 3-5 mg, placed in open ceramic crucibles and heated from room temperature to 600 °C at 20 °C/min in nitrogen atmosphere, with a nominal gas flow rate of 30 ml/min. The measurements were performed in duplicate.

***Mechanical properties (Tensile test)***

Tensile tests were performed on dumbbell shaped film specimens whose dimensions were respectively 4 mm in width and 28 mm in length, while the thickness of each film was measured at five random points and the result was not significantly different (0.073±0.002 mm). The tests were performed by means of a dynamometer model LRX (LLOYD instruments, universal tensile tester equipped with a 1kN load, in accordance with ASTM D638-10 (2010). Five dumbbell shaped samples were analyzed at room temperature 25±2°C and 45 ± 5% RH, at a crosshead rate of 5 mm $min^{-1}$, without preload. The results of the evaluated parameters were expressed as the average values. Before testing, the samples were equilibrated in climatic chamber settled at 25 °C and 50% RH for 24 hours.

***Surface wettability: water contact angle measurements***

Water contact angle measurements were performed on neat PLA and PLA/α-CA films. An optical contact angle DSA 125 (KRÜSS GmbH, Hamburg, Germany) equipped with the aid high-resolution camera was used and the data were analyzed by KRUSS software. The static contact angle of water at room temperature (θ, deg) was measured by a sessile drop method by dropping 11 drops of distilled water (2 μl) onto the surface film by using a

syringe. The entire droplet was released from 0.5 cm above the polymer surface to ensure about the consistency of the measurements. The contact angle was calculated immediately after droplet deposition by means of the angle between the baseline of the drop and the tangent. Finally, the boundary average angle values at all the drops were calculated.

## 4.5. The NOVAMONT Stage[10]

### 4.5.1. Preparation of blends between Novamont polyester and chitosan-TPP microparticles (NPS/CH/TPP): tests HB1702- HB1705

Novamont polyester (NPS) and CH-TPP microparticles in ratio 95:5 have been extruded by Rheomix twin HAAKE extruder with total weight of 50g for each batch. The raw materials were fed manually up in a extruder. The extrusion was performed at 145 °C, 2 min at 50 RPM and then the rotation rate increased to 100 RPM for other 10 min. The resulting blends were then collected and weighed for next step. As benchmark, NPS extruded with the same conditions was used.

The collected samples including NPS (HB1704 and HB1702) and NPS/CH/TPP (HB1705 and HB1703) were further processed by compression molding. In order to prepare the compression sheets, 10 g of each samples were weighed and placed between two steel plates, pre-heated at 150 °C for 2 min at 5 bar and subsequently at 15 bar for 3 min then cooled down to room temperature under pressure, by means of cold water. The film thickness was measured at ten random points using a micrometer (Digital Micrometer) and the result expressed as the average value for NPS and NPS/CH/TPP sheets were 540±40 μm and 570±30 μm respectively.

### 4.5.2. Preparation of blow molding films based on Mater-Bi grades and including CH/TPP micro-particles (tests: FF3019, FF3020, FF3022 and FF3023)

The strategy to incorporate CH/TPP in films based on Mater-Bi grades included: (a) the preparation of a master-batch with CH/TPP with Novamont polyester as a matrix; and (b) the preparation of films starting from dry blends obtained from the CH/TPP master-batch and a suitable Mater-Bi grade.

[10] This part has been done at Novamont Company.

In particular, the first step of the process involved the preparation of the master batch NPS/CH/TPP (MB) with ratio 90:10 by means of anti-rotating twin-screw extruder (test HB1706). The obtained pellets were collected and weighed for the next step.

The first film (**FF3020**) was based on a starch based grade and was prepared starting from a dry blend with a ratio 90:10 between SBG-MBi (Starch Based Grade – Mater-Bi) and MB.

The second film (**FF3023**) was based on a transparent grade (TG) and was prepared starting from a dry blend with a ratio 90:10 between TG-MBi (Transparent Grade – Mater-Bi) and MB. In both cases the total amount of microbeads was 1%. Benchmark TG-MBi and SBG-MBi films were produced by means of film blowing as well. 50 m of each film with average thickness of 20 μm and width of 12 cm were collected and kept at room temperature for further characterization. During film blowing of SBG-MBi/MB films, the processing temperature increased in order to study the effect of temperature in microparticles compatibility and mechanical properties of the films.

### 4.5.3. Formulation of neat chitosan and thermoplastic starch by extrusion (FF3024 and FF3025)

Based on Novamont proprietary processes, polyesters, starch and additive have been processed by reactive extrusion to obtain the reference compound and film (**FF3024**). The same process was repeated with the addition of 1% of chitosan in formulation (**FF3025**). In this way, chitosan was directly added to the film blowing formulation through a reactive extrusion process.

- **Specific characterization methods for the films**

***Thermogravimetric analysis (TGA)***

Thermogravimetric analyses (TGA) was carried out by using a Thermogravimetric Analyzer. The measurements performed on samples of about 2-5 mg, placed in open platinum crucibles and heated profile started from room temperature to 600 °C at 20 °C/min in nitrogen atmosphere with one hour isotherm at 105 °C to remove the trace water, and a nominal gas flow rate of 30 mL/min.

***Scanning Electron Microscopy (SEM)***

Morphological analysis of films was performed on cryogenically fractured cross-section of all samples by using a Scanning Electron Microscope instrument. SEM observations was performed in low vacuum mode (Pressure 0.7 torr), using a secondary electron detector and an acceleration voltage of 5–20 kV. Prior to the observation, the sample surfaces coated with a homogeneous layer (18 ± 0.2 nm) of Au by means of a sputtering device.

***Tensile test***

The tensile properties were measured in accordance with ASTM D1822. Ten dumbbell shaped samples were analyzed at room temperature 25±2 °C and 50% RH, without preload. Before testing, the samples equilibrated in climatic chamber settled at 25 °C and 50% RH for 48 hours.

## 5. RESULTS and DISCUSSIONS

### 5.1. Antimould microbial and plant metabolites with potential application in intelligent food packaging (preliminary investigation) [11]

The natural metabolites used for the study (**Fig. 1, Table 1**) belong to different classes of natural compounds as colletochlorin E and colletopyrone (Masi et al., 2017b), α-costic acid (Andolfi et al., 2013), cyclopaldic acid (Graniti et al., 1992), *epi*-epoformin (Andolfi et al., 2014), 3-nitopropanoic acid (Andolfi et al., 2015), orcinol (Monde et al., 1998), papuline (Evidente et al., 1990), sphaeropsidins A and C (Evidente et al., 1997; Masi et al., 2016), sesquiterpente (1,8a-dihydroxy-3,8-dimethyl-5-(prop-1-en-2-yl)-1,2,4a,5,6,7,8,8a octahydronaphthalen-2-yl acetate (Masi et al., 2013), and ungeremine (Abou-Donia et al., 1992). All fungal metabolites are a pyran-2-one, sesquiterpene, isobenzofuranone, cyclohexene oxide, aliphatic acid, benzendiol, pimaranediterpenes and sesquiterpene (Table1). Papuline, the methyl ester of the antifungal compound phenyllactic acid (Lavermicocca et al., 2000), is a bacterial metabolite, while α-costic acid, a sequiterpene, and ungeremine, a betaine belonging to the lycorine type of Amaryllidaceae alkaloids, are plant metabolites **(Table 1)**. Data resulting from the antifungal test performed with all natural metabolites highlighted the inhibitory efficacy, at percentages higher than 60%, mainly of the plant metabolites ungeremine and α-costic acid , at the concentration tested (0.1 mg/mL) against both fungal strains (Table 2). The inhibition persisted also at 96 h. In particular, ungeremine was mainly active against *P. roqueforti*, while *A. niger* was more sensitive to α-costic acid. In order to better investigate on the antifungal properties of these two compounds, a broth microdilution test was performed to identify a MIC value. The test allowed highlighting the higher efficacy of ungeremine against the two fungal strains over the time **(Table 1 and 2)**. In **Table 1** are reported the $MIC_{90}$ and $MIC_{50}$ values after 48 and 72 hours growth. Ungeremine confirmed to be most efficacious against *P. roqueforti*

[11] The work was done in collaboration with CNR - ISPA - Institute of Sciences of Food Production and has been published in: Valerio, F., Masi, M., Cimmino, A., Moeini, S. A., Lavermicocca, P., & Evidente, A. (2017). Antimould microbial and plant metabolites with potential use in intelligent food packaging. Natural Product Research, 6419(October), 1–6. https://doi.org/10.1080/14786419.2017.1385018

showing $MIC_{90}$ lower than 0.003 mg/mL after 48 h of growth and of 0.025 mg/mL at 72 h, even allowing the reduction of more than 50% (MIC50) with concentration lower than 0.003 mg/mL. The growth of *A. niger* was inhibited by more than 90% only at 48 h using a 0.2 mg/mL concentration but a 0.003 mg/mL level, or lower at 48 h, was enough to obtain a 50% growth reduction. The α-costic acid generally showed MIC values at 48 and 72 h higher than ungeremine against the fungal strains. The fungal growth in the presence of the two selected compounds was compared to a growth control and to calcium proprionate 0.3% (w/vol), a food preservative generally used to control the fungal spoilage. Data deriving from the spectrophotometric measurements allowed obtaining the fungal growth curves. By fitting the growth curves with Gompertz parameters referring to the control growth at 72 h, 96 h and 120 h, the growth delays reported in **Table 2** were obtained. *P. roqueforti* was more sensitive to both substances since unpredictable growth delays were obtained until 0.025 mg/mL for ungeremine and 0.05 mg/mL for α-costic acid after 96 and 120 h. After 72 h ungeremine caused growth inhinition percentages even higher than 80% respect to the control at all concentration tested with concomitant growth delays by more than 40 h (0.003 mg/mL). The α-costic acid was less efficacious than ungeremine even if a level of 0.05 mg/mL determined more than 50% of *P. roqueforti* growth inhibition respect to the control. The common food preservative 0.3% calcium proprionate had higher growth delay at 72 h (42.84 h vs. 23.45 h). In the case of *A. niger*, ungeremine and α-costic acid behaved similarly, mainly at the higher concentration tested, causing growth inhibition at 72 h comparable to calcium proprionate until concentrations of 0.006 mg/mL for ungeremine and 0.025 mg/mL for α-costic acid. However, for *A. niger*, the growth was delayed by more than 2 days using 0.025 mg/mL of ungeremine and 0.05 mg/mL of α-costic acid.

**Table 1.** Antifungal activity of microbial and plant metabolites by spectrophotometric assay (Valerio et al., 2017)

| Time | ***PR*** | ***AN*** | ***PR*** | ***AN*** | ***PR*** | ***AN*** | ***PR*** | ***AN*** | ***PR*** | ***AN*** |
|---|---|---|---|---|---|---|---|---|---|---|
| | **ungeremine 0.1** | | sesquiterpene 0.1 | | sphaeropsidin C 0.1 | | papuline 0.1 | | Cyclopaldicacid | |
| **72h** | **98.36±0.35** | **77.52±2.09** | 36.45±1.25 | 49.83±24.93 | 54.38±3.16 | 64.63±11.90 | 37.81±4.98 | 40.11±9.02 | 29.34±1.41 | - |
| **96h** | **94.18±1.32** | **56.53±3.69** | 14.65±9.82 | 18.10±5.66 | 58.97±10.53 | 11.29±0.49 | 18.18±12.31 | 12.62±6.80 | 59.48±1.78 | - |

| Time | ***PR*** | ***AN*** | ***PR*** | ***AN*** | ***PR*** | ***AN*** | ***PR*** | ***AN*** | ***PR*** | ***AN*** | ***PR*** | ***AN*** |
|---|---|---|---|---|---|---|---|---|---|---|---|---|
| | 3-nitropropionic acid 0.1 | | **α-costic acid 0.1** | | orcinol 0.1 | | colletopyrone 0.1 | | colletochlorin E 0.1 | | *epi*-epoformin | |
| **72h** | 34.72±5.77 | 42.92±20.26 | **62.34±5.20** | **81.93±1.46** | 34.27±3.76 | 49.67±3.57 | 20.23±5.99 | 54.08±10.63 | - | 3.43±2.65 | 48.15±2.62 | - |
| **96h** | 8.76±1.13 | 28.22±3.04 | **77.66±3.25** | **77.54±3.07** | 7.02±1.41 | 18.05±7.71 | 3.29±2.74 | 18.62±4.03 | - | 5.84±6.33 | 59.48±1.78 | - |

**Table 2.** $MIC_{90}$ and $MIC_{50}$ values of ungremine and α-costic acid after 48 and 72 h. (Valerio et al., 2017)

| Sample | $MIC_{90}$ 48h | $MIC_{50}$ 48h | $MIC_{90}$ 72h | $MIC_{50}$ 72h |
|---|---|---|---|---|
| | **ungeremine (mg/mL)** | | | |
| ***P. roqueforti*** | <0.003 | <0.003 | 0.025 | <0.003 |
| ***A. niger*** | 0.2 | <0.003 | >0.2 | 0.003 |
| | **α-costic acid (mg/mL)** | | | |
| ***P. roqueforti*** | 0.1 | 0.05 | 0.1 | 0.012 |
| ***A. niger*** | 0.2 | 0.012 | >0.2 | 0.025 |

## 5.2. Development of HPLC method for the identification and quantification of cavoxin and cavoxone in *Phoma cava* culture filtrates[12] (Masi et al., 2017a)

***Method development***

Among different types of chromatography, high performance liquid chromatography (HPLC) has been most widely used as an essential analysis tool for research, manufacturing, clinical tests, and diagnostics (Hayes et al., 2014). The HPLC method was developed for quantification of cavoxin and cavoxone in culture filtrates of *P. cava* grown in different conditions. The HPLC analysis was optimized using a system (HITACHI) consisting in a pump (5160) and a spectrophotometric detector (5410). Thus, the separations were performed using a Merk (Darmstadt, Germany) C-18 reversed phase column Lichrocart (250 . 4.6 mm i.d.; 5 μm) and elution was done by acetonitrile - water 60-40% in 20 min. Detection was performed at 280 and 325 nm which correspond the UV maximum absorption of cavoxin and cavoxone, respectively (Evidente and Randazzo,

[12] The work was presented in this part has been published in: Masi, M., Moeini, S. A., Boari, A., Cimmino, A., Vurro, M., & Evidente, A. (2017). Development of a rapid and sensitive HPLC method for the identification and quantification of cavoxin and cavoxone in *Phoma cava* culture filtrates. Natural Product Research, 6419(October), 1–5. https://doi.org/10.1080/14786419.2017.1392950

1985) crystallized standard samples of both caxoxin and cavoxone were used (Evidente and Randazzo, 1985) and samples were injected 20 µL loop and monitored for 20 min.

***Method validation***

The method was established by comparing the peak purity of the cavoxin and covoxone standards obtained as previously described with fungal filtrate extracts (Evidente and Randazzo, 1985). The identification of cavoxin and cavoxone in the crude organic extracts has been based on the retention time of the standards and confirmed by their co-injection. The accuracy of the method is well assured by the clear separation of the peaks by the peak symmetry and without any shoulder. The calibration curves for cavoxin and cavoxone were obtained in the range of 120-41 µg/mL and 75–16 µg/mL, respectively, and appeared to be linear. Regression equation for both cavoxin and cavoxone were obtained as y = 2E+08x – 100829 and y = 2E+08x + 276440; $R^2$ (correlation coefficient) values were 0.9907 and 0.9989 respectively which showed a good linear regression for the developed method. LOD (limit of detection) and LOQ (limit of quantification) values for cavoxin were found to be 2.5 µg/mL and 5 µg/mL, respectively, indicating a good sensitivity for quantification. Thus, the accuracy of the method was expressed as percent recovery of cavoxin in the organic extracts of stirred and static fungal culture filtrates and ranged 98.79-110.34%, showing a good recovery rate. The percentage recovery values higher than 100% indicated that there was no interference in the fungal filtrates organic extracts. Other needed data are reported in **Table 3.**

***HPLC analysis of samples of cavoxin and cavoxone in the organic extracts of P. cava culture filtrates***

The organic extracts of *P. cava* culture filtrate were analyzed by HPLC as detailed previously in experimental part. The results summarized in **Table 3** showed that the absolute amount of cavoxin is 60.84±3.30 mg/L when the fungus was grown in stirred condition. This yield is three times higher compared to the static condition. For cavoxone, produced in very low amounts, the fungus performed better in stirred condition than in static one (**Table 3**).

**Table 3.** Quantification of cavoxine and cavoxone in the organic extract of *P. cava* culture filtrates grown in stirred and static condition (Masi et al., 2017a)

| Condition | Filtrate (L) | Extract (mg) | Cavoxin (mg/L) | Cavoxone (mg/L) |
|---|---|---|---|---|
| **Stirred** | 0.8 | 249.8 | 60.8390 | 0.0590 |
| **Static** | 0.9 | 117.1 | 16.0576 | 1.1340 |

Thus, the developed method provides a simple and rapid and sensitive assay for detection and estimation of cavoxin and covaxone in complex matrixes.

### 5.3. Physical-chemical characterization of CH/TPP/UNG microbeads[13] (Moeini et al., 2018)

***Chitosan based beads stability, loading efficiency test and controlled releasing kinetics***

CH/TPP micro-beads have been widely investigated for improving the drug delivery of both small and large molecular weight drugs (Dash et al., 2011) and may therefore be considered a promising encapsulating system of ungeremine, since the bioactive molecule, like chitosan is soluble in acetic acid water solution and can be easily dissolved inside the polymeric solution before the gelation process. Moreover, as previously detailed, UNG is a zwitterion (Carey and Sundberg, 2008). Hence, it could be hypothesized that during the crosslinking process between chitosan and TPP, ungeremine could take part in the ionic interaction, thus inducing the formation of a strong three-dimensional network by means of ionic physical entanglements. The nature and extent of ionic interactions between chitosan and TPP are reliant to parameters as the charge density of both electrolytes, strongly dependent on the solution pH. Indeed, the study reported that the chitosan beads prepared with TPP could both increase the loading efficiency of active compounds and prolong their release period, by opportunely modulating the pH (Shu and Zhu, 2000, 2001). As

[13] The work was done in collaboration with CNR - ISPA - Institute of Sciences of Food Production, CNR- IPCB- Institute for Polymers, Composites and Biomaterials and Department of Chemistry and Polymer Science, University of Stellenbosch, Stellenbosch, and was published in: Moeini, A., Mallardo, S., Cimmino, A., Dal Poggetto, G., Masi, M., Di Biase, M., van Reenen, A., Lavermicocca, P., Valerio, F., Evidente, A., Malinconico, M., Santagata, G., (2020). Thermoplastic starch and bioactive chitosan sub-microparticle biocomposites: Antifungal and chemico-physical properties of the films. Carbohydrate Polymers 230, 115627.

concerning the investigated system, the TPP water solution (pH 8.6) contained both $OH^-$ groups and $P_3O_{10}^{5-}$. Therefore, the ionic interaction with the available $–NH_3^+$ binding sites could occur by deprotonation (interaction between $OH^-$ and $-NH_3^+$ groups) of charged amines or by ionic crosslinking (interaction between $P_3O_{10}^{5-}$ and $-NH_3^+$ groups) processes. When chitosan solutions were dropped in TPP basic solution, gelled microbeads, by ionotropic gelation, were obtained. They showed irregular shape and their easy smashing in TPP solutions, supported their instability (see **Fig. 9**). It is worthy to highlight that, in the TPP solution, the coexistence of both counterions triggered a sort of their competition in reacting with the protonated amine groups; it was likely that, when the chitosan droplets were in contact with TPP solution, the gelling mechanism of the chitosan beads was mainly ruled by the phase inversion process (coacervation of $–NH_3^+$ and $OH^-$ groups), at the expense of only few crosslinking junction points between $–NH_3^+$ and $P_3O_{10}^{5-}$. Thus, at high pH, the coacervation process was characterized by a weak ionic crosslinking and the randomly coiled chitosan repeating units provided a slackened loop conformation. This effect, sharpened by the increasing of TPP concentration and hydroxyl groups, induced further deprotonation of chitosan amine groups with following weakening of ionic complex formation **(Fig. 10a)**. By progressively adding acetic acid to TPP solution, the pH was reduced, passing by pH=7 up to pH=6.1. The concentration of hydroxyl ions was drastically reduced, and an in-liquid curing mechanism occurred, involving the chitosan amine groups protonation, the strong positive charge repulsion, and the ionic crosslinking process between $P_3O_{10}^{5-}$ and $-NH_3^+$ groups. Therefore, the beads formed were more spherical, homogeneous and stable over the time. In addition, they were smaller with respect to the ones obtained at basic pH **(**see **Fig. 10b)**. These outcomes were consistent with a tight crosslinked CH/TPP structure, responsible of both higher stability and lesser swelling ability of the beads. Hence, at low pH, crosslinked chitosan resulted in a more extended loop and ladder shaped three-dimensional network (Fwu-Long et al., 1999), as evidenced in **(Fig. 10b,c).**

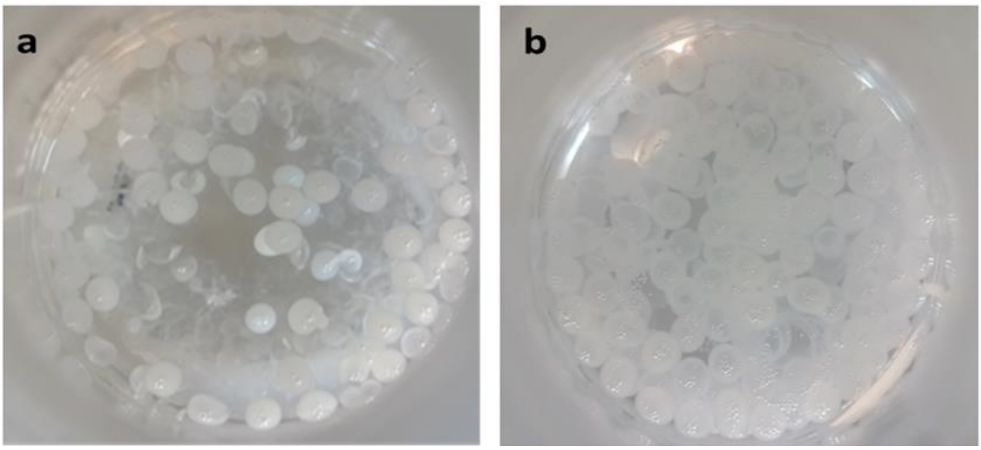


**Figure 9.** CH/TPP bead formation at basic (a), and acidic (b) pH. (Moeini et al., 2018)

As far as CH/TPP/UNG beads preparation, chitosan and ungeremine were previously dissolved providing a yellow-orange colored solution, since the chromophores groups present in the alkaloid. Anyway, the presence of the color played a key role in the enlightenment of the crosslinking process occurring during the external gelation method (see **Fig. 11**). Actually, when CH/TPP solution was dropped into TPP basic solutions, two macroscopic opposite phenomena could be observed: at the beginning, the beads formed and were yellow, thus indicating that the crosslinking process physically involved ungeremine. Anyway, after few seconds, ungeremine was rapidly squeezed out from the beads, as evidenced by the drastically changing of beads color from yellow to white. Actually, the fast gelation process between chitosan and TPP basic solutions allowed ungeremine charged molecules to be physically entrapped in the weak ionic crosslinked layer formed on the bead surface, that for this reason, became yellow; anyway, as previously described, at high pH, the beads coacervation is controlled by phase-inversion gelation process, since both the higher concentration of hydroxyl groups and their smaller size with respect to TPP anions.

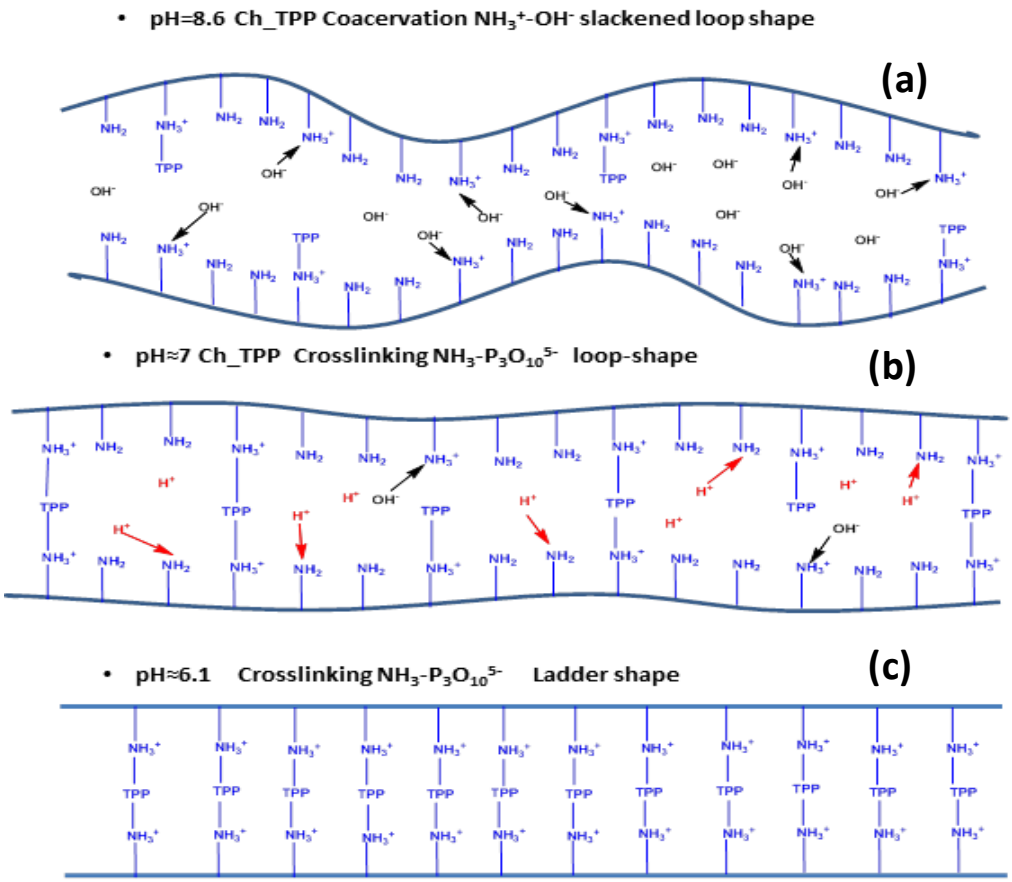


**Figure 10.** In liquid curing mechanism of chitosan in TPP solutions at basic (a), neutral (b) and acidic pH (c) (Moeini et al., 2018)

Moreover, it should be stressed that the UNG steric hindrances due to the presence of aromatic and heterocycles residues, induced its squeezing out from the surface gelation layer at basic condition, thus allowing beads becoming newly white **(Fig. 11a).** By increasing CH/TPP concentration inside TPP solution, pH decreased, and the active molecule started to diffuse into the beads, even if some yellowness could be still observed in TPP solution, indicating that UNG was not completely absorbed in CH/TPP microbeads (**Fig. 11b**). With the following lowering of pH at about 6.1, the gelation process, as previously detailed, was controlled by the ionic crosslinking between $P_3O_{10}^{5-}$ and $-NH_3^+$. This experimental condition matched with the higher

loading efficiency of the antifungal molecules inside the crosslinked network, resulting in the development of yellow and stable CH/TPP/UNG beads **(Fig. 11c**). It could be assumed that, being a zwitterion, ungeremine could take actively part to the ionic crosslinking process with both TPP and -$NH_3^+$ groups, by means of ionic physical entanglements (Carey and Sundberg, 2008; Ko et al., 2002).

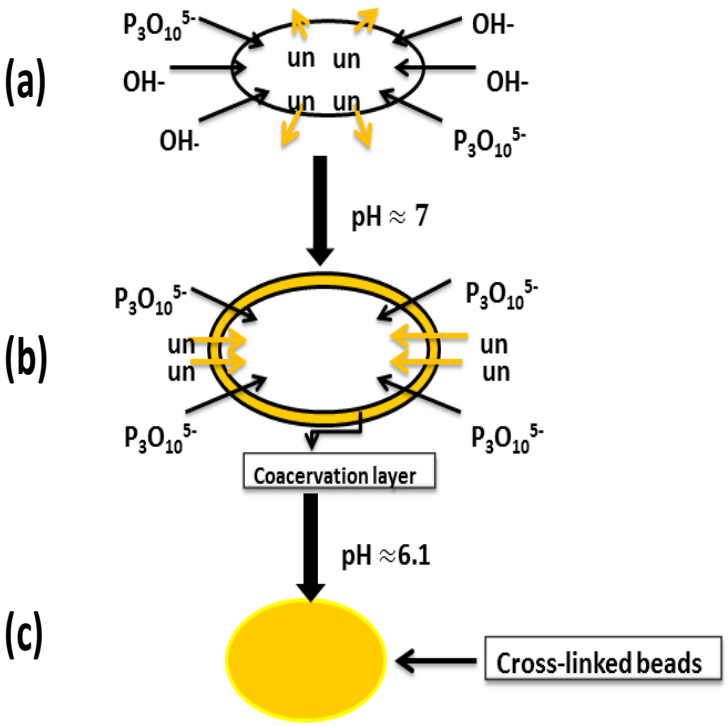


**Figure 11.** In-liquid curing mechanism of CH/TPP/UNG beads in TPP solution: (a) basic, (b) neutral and (c) acidic pH (Moeini et al., 2018)

In **Table 4,** the loading efficiency of ungeremine in CH/TPP/UNG beads at different concentration of TPP has been detailed. The analysis of data highlighted that for all the samples, the loading efficiency was very high; in particular, it is possible to underscore that by increasing TPP concentration, the loading efficiency of the antifungal metabolite was slightly enhanced. This outcome could be explained by considering the increase of the crosslinking junction points occurring between ungeremine positive

charged nitrogen and TPP polyanion. At the same time, this significant result evidenced that, besides being physically entrapped in the CH/TPP network, ungeremine played an active role during the crosslinking process, as confirmed by FTIR data.

In order to follow the kinetics of ungeremine releasing from chitosan-based beads, UV-Vis spectroscopic analysis was performed by using two different pH buffer solutions 5.7 and 6.2 as releasing media. These two pH were selected as they are typical of bakery products. An intense UV absorption at 370 nm was observed (spectrum not reported) according to the presence of ungeremine conjugated chromophore and the percentage of ungeremine released from the chitosan microbeads formulations vs time, at pH=5.7 and pH=6.2, was plotted in **(Fig. 12a,b)** respectively. The diffusion properties and the release kinetics were functions of ungeremine concentration, changing of beads stability at different pH, water absorbed, dissolution of ungeremine and desorption of the same via swelling controlled mechanism (Dini et al., 2003). Each curve was built by evaluating the ungeremine content inside the buffer solutions at different times. Specifically, three beads of each composition were subsequently dipped inside buffer solutions and periodically collected at the same time intervals. The average value of the ungeremine amount detected from the beads was reported as a function of the time. From the analysis of the curves, worthy difference in releasing behavior could be marked at the two pH. Specifically, at pH=5.7, CH/TPP/UNG beads highlighted a similar trend independently from TPP concentration, with a high UNG releasing in the first three hours and a slower one up to 48 hours, where about 20% of UNG was squeezed out **(Fig. 12a)**. At pH=6.1, the kinetics pattern followed a substantial different profile, depending on TPP concentration. During the first 24 hours, a burst and faster ungeremine releasing was observed **(Fig. 12b)**, particularly accentuated in CH/TPP/UNG4 composition. In the following 24 hours, a sort of a plateau was detected for all formulations, even if CH/TPP/UNG4 sample experienced the highest rate of release, reaching up to 35% of ungeremine weight delivery. It could be hypothesized that the starting fast release was

mainly caused by desorption of the ungeremine from the outer layer of crosslinked systems. Anyway, at both pH, from 24 up to 48 hours of treatment, the releasing process followed a tailoring-off behavior, likely due to a more convoluted pathway for ungeremine dissolution from the inside core of CH/TPP crosslinked network (Forni et al., 1992) towards the solution. Moreover, it deserves of note that, generally, by increasing TPP concentration, the ungeremine releasing from the beads decreased since the stronger interaction occurring between ungeremine and rising concentration of TPP counterions, as previously shown by the loading efficiency percentage and following detailed by FT-IR spectra evaluations. Probably, since the degree of swelling and following desorption of ungeremine is mostly ruled by the crosslinking density of the polymeric network and by the strength of the network formed, as previously described and reported in literature (Harris et al., 2011; Higuera-Ciapara et al., 2004), a decrease in the amount of crosslinking agent and increasing of pH as in the case of CH/TPP/UNG4 system, induced as expected effect, the enhancement of ungeremine releasing. Thus, at higher pH **(Fig. 12b)**, as expected, the curves followed a faster releasing kinetics, since the increasing of $OH^-$ residues and following decreasing of ionic complex. Hence, depending on the specific bakery substrate, it could be possible to modulate ungeremine release.

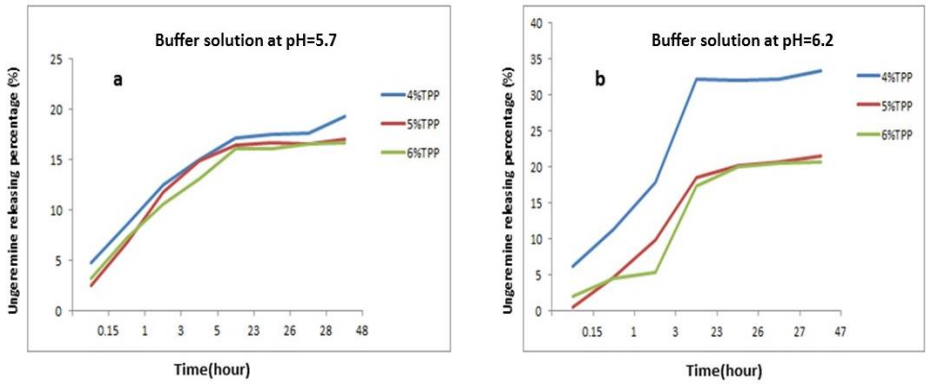


**Figure 12.** Kinetics release profile of ungeremine (%w) in buffer solution at pH= 5.7 (a) and pH= 6.2 (b) vs time (hours) (Moeini et al., 2018)

**Biological activities**

***Effect of ungeremine on cancer and normal cell line viability***

Since ungeremine is released from the CH/TPP/UNG microbeads, the absence of toxicity of the neat substance was demonstrated both on breast cancer cell line (MCF-7), and on normal human epidermal keratinocytes-adult (HEKa) in a range of concentrations from 0.2 to 100 μg/mL (equivalent to about 0.8 - 376 μM, respectively). In particular ungeremine, at all the tested concentrations was not cytotoxic for both the considered cell types, treated for 24 h. At longer incubation time, 48 h and 72 h, only the two higher concentrations of ungeremine slightly decreased cell viability in MCF-7 cells, but none relevant cytotoxicity was detectable, as demonstrated by the $IC_{50}$ values (106.6 μg/mL, 124.4 μg/mL and 30.8 μg/mL, respectively, equivalent to 396, 459 and 115 μM), confirming previous data on a panel of cancer cells (Van Goietsenoven et al, 2010). Significantly, none cytotoxicity was detectable for normal epidermal keratinocytes at the tested concentrations and at all treatment times as the $IC_{50}$ values for HEKa were very high ($IC_{50}$>111 μg/mL). At our best knowledge, there is no literature data about exposure by the skin or epithelial mucosae (short or long-term exposure) to ungeremine.

***Antifungal activity of ungeremine contained in CH/TPP beads against P. roqueforti***

The antifungal properties of ungeremine against *P. roqueforti* was previously shown and detailed by (Valerio et al., 2017). The antifungal test was performed using the CH/TPP/UNG based beads and CH/TPP, used as control, to assess the release of ungeremine from the CH/TPP beads into the agar plates previously inoculated with the fungal strain. The assay confirmed the antifungal activity of ungeremine released from the beads at different concentrations of TPP, as evidenced in **(Fig. 13)**.

Antifungal activity was determined by evaluating the inhibition zones formed around the beads. All the tested samples were strongly active in inhibiting the fungal growth; indeed, after 72 h, fungal mycelia were observed only in all control beads (CH/TPP), with a contamination mostly starting from the beads core, maybe because the UV sterilization was not completely effective.

This outcome suggested that already at the lowest concentration of TPP, ungeremine could exploit its antifungal activity. For this reason, aimed to use the above formulated microparticles as additives in bioactive food packaging material, a first challenge could be represented by testing CH/TPP4/UNG composition.

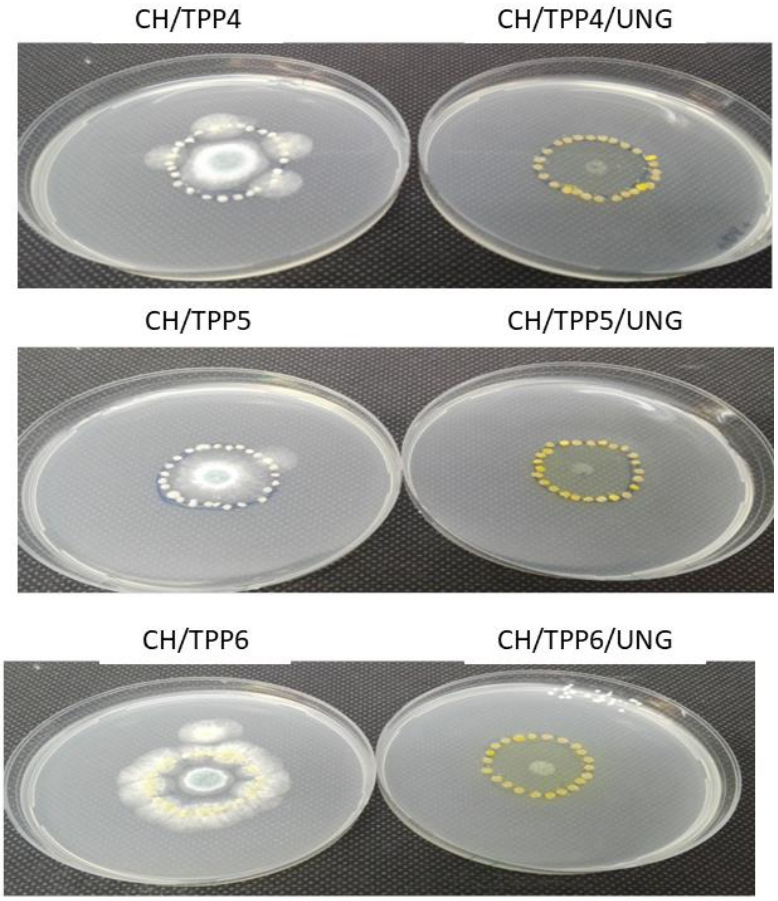


**Figure 13.** Antifungal assay of ungeremine released from the CH/TPP beads after 72 h, at different TTP concentration (Moeini et al., 2018)

***Scanning Electron Microscopy (SEM) analysis and porosity test***

SEM analyses were performed on three samples for each composition in order to obtain more detailed information on morphology of chitosan microbead surfaces. In **(Fig. 14a,b)**, as an example, the micrographs of CH/TPP4 and CH/TPP4/UNG are respectively reported.

The neat beads evidenced a microporous and wrinkled surface with regular distribution of holes, whose diameter was in the range of 200 μm.

The ungeremine loading induced a strong effect on the architectural morphology of the microbeads; indeed, it provided a deeper regularity of the surface associated with more closely packed holes, showing thicker walls and smaller size diameters of about 100μm. This peculiar morphology suggested a substantial increment of the structural crosslinking density, since the presence of a tighter network, as previously detailed. Similar results were found by (Chung and Park, 2007; Srinatha et al., 2008).

The evaluation of void spaces of chitosan based beads, by means of porosity tests, played a key role in providing information related to the polymeric network structure, following to the crosslinking process occurring with different concentration of TPP and UNG. The porosity data, reported in **Table 4**, evidenced a peculiar behavior of CH/TPP and CH/TPP/UNG samples. By the increasing of crosslinking junction points, following to the high concentration of TPP, the porosity of samples increased and the effect was particularly marked in samples containing ungeremine. This peculiar result could be explained considering that the crosslinking process of chitosan beads, responsible of the junction points development, occurred during the samples soaking in water solutions of TPP; so chitosan crosslinked while swelling, i.e., adsorbed some water during the formation of three-dimensional stable network, as also shown by thermal analysis. Hence, the conformation of crosslinked polymeric backbone attained in wet condition did not change after freeze-drying process (Russo et al., 2007, 2010). This outcome induced the increasing of free volume and porosity of the samples, particularly heightened in the beads containing ungeremine where more crosslinking junction sites were formed and preserved after drying process.

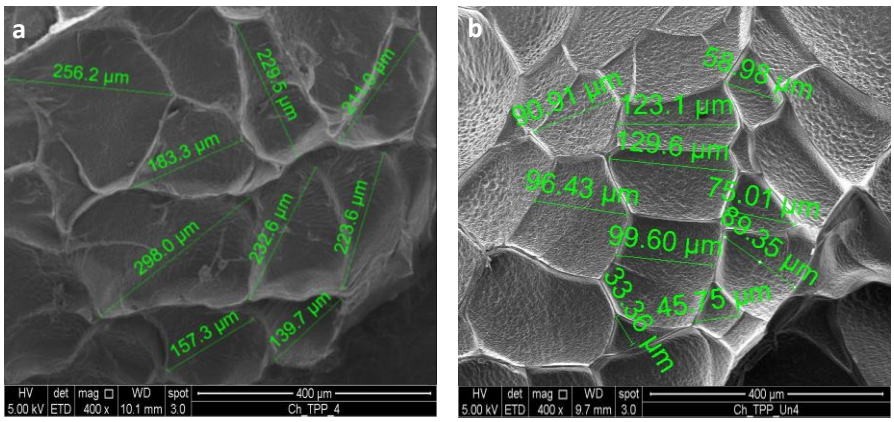


**Figure 14.** SEM micrographs of CH/TPP4 (a) and CH/TPP4/UNG (b) surface (Moeini et al., 2018)

***Attenuated Total Reflection Fourier Transform Infrared (FTIR-ATR) Spectroscopy***

All chitosan based beads cured in TPP solution at pH≈6.1, were analyzed by FT-IR spectroscopy, in order to follow the structural changes of chitosan after crosslinking process with trypolyphosphate and ungeremine. In order to compare the spectroscopic behavior of the crosslinked based beads with the ones of the neat polymer, a film of plain chitosan was prepared by casting from a water acidic solution (pH≈6.1). In **(Fig. 15.a,b)**, as an example, FT-IR spectra of CH, CH/TPP6 and CH/TPP6/UNG are reported. In particular, in the region of high frequency absorption peaks **(Fig. 15a)**, FT-IR spectrum of neat chitosan evidenced a band with two sub-maxima at 3362 $cm^{-1}$ and 3292 $cm^{-1}$ attributed to -OH and -NH groups stretching vibrations. In CH/TPP6 and CH/TPP6/UNG systems, this bands became wider, flattened and underwent a shift towards lower frequency (at about 3166 $cm^{-1}$), thus suggesting the physical interactions between the functional polar groups of chitosan, sodium polyphosphate and ungeremine, mainly occurring via hydrogen bonding (Jia-hui et al., 1999). Carbonyl and finger print regions of the spectra are reported in **(Fig. 15b)**. Neat chitosan displayed two strong vibration peaks at 1653 $cm^{-1}$ and 1564 $cm^{-1}$. These peaks were respectively assigned to C=O stretching vibration (amide I) and to N-H bending vibration (amide II) of N-acetylglucosamine residues (Smitha et al., 2005). However, since the chitosan used showed a DA of 75%,

only 25% of the nitrogen atoms occurred as amides, whereas the remaining atoms as expected were neutral and protonated amines, since both films and beads were prepared in acid conditions. Considering that protonated amines display asymmetric deformation in 1650-1570 $cm^{-1}$ range and symmetric vibrational mode in 1550-1505 $cm^{-1}$ range, it is plausible that besides the amide I, the band at 1653 $cm^{-1}$ also contains the asymmetric -$NH_3^+$ deformation, whereas the peak at 1564 $cm^{-1}$ resulted from the overlapping of both amide II, primary deacetylated amines N-H stretching vibrations and the symmetric -$NH_3^+$ vibrational mode. Actually, the band at 1564 $cm^{-1}$ showed a larger intensity than the one at 1653 $cm^{-1}$, thus indicating the prevalence of amine groups (Lawrie et al., 2007). FT-IR technique is a valid tool aimed to assess the physical or chemical interactions between components in polymeric based systems. By comparing FT-IR spectra of plain chitosan and CH/TPP, it is worthy to highlight several differences correlated to the evidence of the ionic crosslinking process occurring. Indeed, following to the development of chitosan three-dimensional networks, the peak of 1653 $cm^{-1}$, assigned to the amide ν(C=O) mode shifted towards 1635 $cm^{-1}$ and the peak at 1564 $cm^{-1}$ moved to 1543 $cm^{-1}$. These results could be ascribed to the formation of physical entanglements occurring among the functional groups of CH/TPP beads during the crosslinking process by means of both ionic interactions and hydrogen bonding. The development of tighter linkages was responsible of the local energy stretching vibrations inhibition with following decreasing of corresponding absorption frequency (Bhumkar &Pokharkar, 2006; Xu & Du, 2003). Moreover, at 1545 $cm^{-1}$, a new shoulder weak peak could be evidenced, likely assigned to the δ vibrational mode of protonated amine groups in chitosan, as confirmed by (Souza et al., 2015). In ungeremine loaded beads, the previous bands were furthermore shifted towards lower frequencies; in particular, the amide I peak moved to 1622 $cm^{-1}$ whereas the peak at 1564 $cm^{-1}$ shifted to 1526 $cm^{-1}$. These results evidenced that ungeremine were not only physically entrapped inside the crosslinked network, but keenly took part to the new linkages occurring in the three-dimensional network, thanks to their positive nitrogen and negative oxygen reactive functional groups. Finally, at 1218 $cm^{-1}$, in CH/TPP and CH/TPP/UNG spectra, it was possible to detect the P=O stretching peak, related to the

presence of tripolyphosphate groups (spectrum not reported) (Fwu-Long et al., 1999; Gan and Wang, 2007).

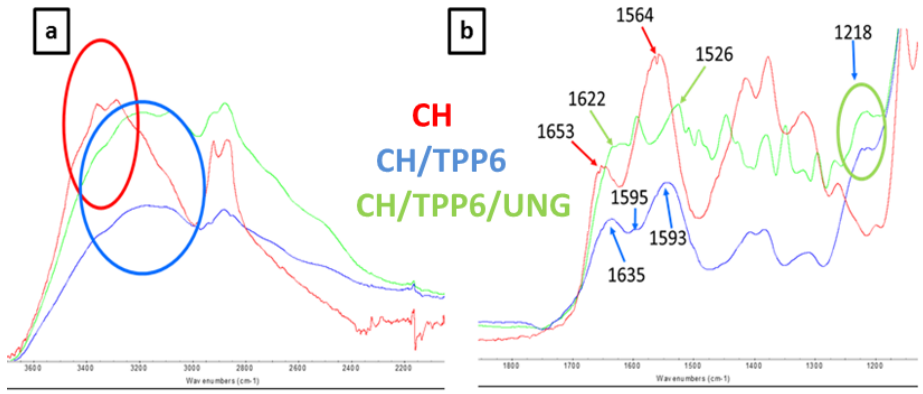


**Figure 15.** FT-IR spectra of CH, CH/TPP6 and CH/TPP6/UNG in the range of 3600-2200 $cm^{-1}$ (a) and in the range of 1800-1100 $cm^{-1}$ (b) (Moeini et al., 2018)

***Thermogravimetric analysis (TGA)***

In **(Fig. 16)**, the mass loss (TGA) of all chitosan based beads **(Fig. 16a)** and their derivative curves (DTG) **(Fig. 16b)** are reported. In **Table 4**, the weight loss percentage at 100 °C and 150 °C ($W_{Loss}$%100 °C and $W_L$%150 °C), the temperature of main degradation step ($T_{onset}$°C), and the temperature of maximum degradation rate ($T_{peak}$°C) are reported. All data were opportunely normalized with respect to the sample sizes.

Thermogravimetric analysis is a valid tool to determine the different water adsorption of films and to investigate the different pattern of polymeric degradation; moreover, information related to the physical interaction between the components of a polymeric system, are detectable too (El-hefian et al., 2012). From the analysis of the curves, three different stages of mass loss may be recognized: the first from room temperature to about 100 °C, the second between 100 °C and about 200 °C, and the third at temperatures above 200 °C. Higuchi and Iijima proposed that water exists in three states in hydrophilic polymer matrices: (i) free water, (ii) freezable bound water, (iii) non-freezable bound water (Higuchi and Iijima, 1985). On the base of the above claims, analyzing the thermograms in

(**Fig. 16a)**, it is possible to claim that the first two steps of weight loss up to about 200 °C concerned the elimination of water (Russo et al., 2010). Lastly, around 200 °C, the decomposition process of polysaccharides starts, involving a random split of the glycosidic bonds, vaporization and elimination of volatile products (Nieto et al., 1991). Nevertheless, it is worthy to highlight a severe different thermal behavior passing by neat chitosan to CH/TPP and CH/TPP/UNG samples. In fact, the water loss of CH was of about 9% at 150 °C, whereas, at the same temperature, the crosslinked samples without and with ungeremine released about 18% (CH/TPP6) and 14% (CH/TPP6/UNG) of their water contents. This outcome suggests that the three-dimensional networks induced the absorption of high water amount. Moreover, this trend is enhanced by increasing TPP concentration. This outcome is cleared up by taking in account that crosslinking occurred while swelling as previously detailed. Since in the swollen samples some macromolecular chain segments, before interacting with each other, could interact with water molecules via hydrogen bonds, the free volume of the polymeric based system increased (Russo et al., 2007).

**Table 4**. Sample identification codes, UNG concentration (mmol), ungeremine loading efficiency (%), Beads porosity (%), Weight Loss percentage at 100 °C ($W_L$%100 °C) and at 150 °C ($W_L$%150 °C), Temperature of degradation onset ($T_{onset}$°C), Temperature of maximum degradation rate ($T_{peak}$°C) (Moeini et al., 2018)

| Data Sample | UNG (mmol) | LE(%) | Por(%). ±10% | $W_{.Loss}$ (%) 100 °C±5% | $W_{.Loss}$% 150 °C±5% | $T_{onset}$ (°C) | $T_{peak}$ (°C) |
|---|---|---|---|---|---|---|---|
| **CH** | --- | --- | --- | 8.2 | 8.9 | - | 295 |
| **CH/TPP4** | --- | --- | 0.17% | 12.4 | 14.8 | 165 | 252 |
| **CH/TPP5** | --- | --- | 0.25% | 13.4 | 14.9 | 155 | 269 |
| **CH/TPP6** | --- | --- | 0.29% | 15 | 18 | 156 | 268 |
| **CH/TPP4/UNG** | 11.39 | 94.67% | 0.85% | 10 | 12.7 | --- | 256 |
| **CH/TPP5/UNG** | 11.52 | 95.75% | 1.1% | 11.5 | 12.4 | --- | 250 |
| **CH/TPP6/UNG** | 11.62 | 96.55% | 1.3% | 12.2 | 13.6 | --- | 250 |

The degradation profile of the films (DTG curves) and the relative temperature pattern are reported in (**Fig. 16b)** and **Table 4**, respectively. The first worthy observation is related to the hastening of thermal decomposition process of all cross-linked samples, particularly

accentuated in CH/TPP/UNG samples, where the lowest $T_{onset\ .degr}$ and $T_{peak}$ could be found. Similar results were also found by Kim and Lee, Neto et al, and Russo et al when working with crosslinked samples of chitosan (Kim and Lee, 1993; Neto et al., 2005; Russo et al., 2007). As a matter of fact, usually cross-linked samples experience a delay in the onset of degradation. The lowering of chitosan thermal stability after the crosslinking process could be associated to changes in the macromolecular backbone structure of the polymer. In particular, the heterogeneous cross-linking reactions between polysaccharides chains and crosslinking agent induced the weakening of attractive intra-inter-molecular hydrogen bonds. Thus, according to literature data, the less packed chitosan macromolecular chains, resulting more exposed to the random splitting of the glycosidic bonds, fastly underwent to the thermo-degradation process. This phenomenon is particularly stressed in ungeremine-loaded samples (see **Table 4**), where the main degradation process was severely anticipated with respect to both pristine polymer and unloaded beads. It was likely that, even at higher concentration of TPP, the excess of protonated amine groups on chitosan backbone could not be stabilized by negative counterions. Hence, some domains in which the electrostatic repulsion prevailed could trigger a less packed structure more prone to the thermal degradation (Pieróg et al., 2012).

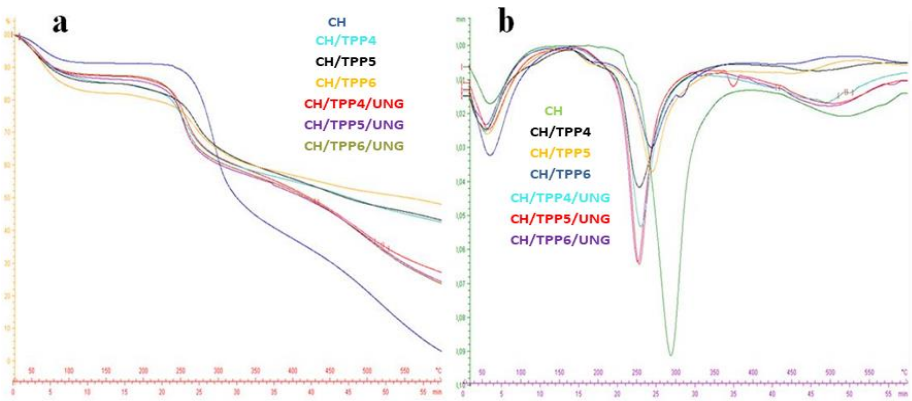


**Figure 16.** Chitosan based beads thermograms: Weight loss (%) (TGA) (a) and thermal degradation rate (DTG) (b) (Moeini et al., 2018)

## 5.4. Physical and mechanical characterization of CH/TPP/UNG sub-micron particles formulated into Mater Bi films[14] (Moeini et al., 2020b)

***Antifungal activity and UV-Vis spectroscopy to evaluate ungeremine mass releasing***

Previously, Valerio et al demonstrated the antifungal properties of ungeremine against *P. roqueforti* (Valerio et al., 2017). Moeini et al detailed the strong ungeremine antifungal effect when it was included in CH/TPP cross-linked microbeads, paving the way for the development of novel biodegradable packaging materials for food preservation, particularly for bakery products (Moeini et al., 2018). For this reason, CH/TPP/UNG sub-micron particles were included in Mater-Bi polymer in two different concentrations and tested against *P. roqueforti* on a routinely used growth medium (PDA) and on a medium mimicking bread composition (BEB).

After 48 hours only the MBi/CH/TPP/UNG2 film on PDA medium (pH=5.7) inhibited the fungal growth, as evidenced in **(Fig. 17a)**, whereas in the presence of MBi/CH/TPP/UNG1 a slight inhibition was observed indicating that an effective CH/TPP/UNG sub-micron particles formulation can be represented by CH/TPP/UNG2. Indeed, as was evidenced by the UV-Vis analysis, a higher concentration of ungeremine was released from CH/TPP/UNG sub-micron particles for the MBi/ CH/TPP/UNG2 film, proving both its enhanced solubility in the agar medium at pH 5.7, and justifying the observed antifungal activity. Actually, as deeply explained by the same authors in the previous paper Moeini et al, and briefly recalled in the section 2.2 of this manuscript, the three-dimensional network obtained by crosslinking chitosan and TPP by optimizing the mass ratio CH:TPP (1:4), evidenced a strong and long-lasting physical stability even at acidic pH; this outcome deserves being emphasized considering that the ungeremine releasing from the sub-micron particles occurred at low pH and did not encompassed the chitosan solubilization since its

[14] The work was done in collaboration with CNR - ISPA - Institute of Sciences of Food Production and CNR- IPCB- Institute for Polymers, Composites and Biomaterials and was published in: Moeini, A., Mallardo, S., Cimmino, A., Dal Poggetto, G., Masi, M., Di Biase, M., van Reenen, A., Lavermicocca, P., Valerio, F., Evidente, A., Malinconico, M., Santagata, G., (2020). Thermoplastic starch and bioactive chitosan sub-microparticle biocomposites: Antifungal and chemico-physical properties of the films. Carbohydrate Polymers 230, 115627.

strong involvement in the ionic crosslinked structure. Hence, the UNG releasing followed a diffusion pathway from the polymeric matrix and, during the antifungal assays, no chitosan bulk erosion could be observed (Moeini et al., 2018).

The results after 3 days of incubation on BEB plates evidenced no bioactivity for neat MBi and slight one for MBi/CH/TPP/UNG1 films, whereas notable antifungal activity was obtained from MBi/CH/TPP/UNG2 sample. In order to investigate the MBi/CH/TPP/UNG2 bioactivity and its application at different pH conditions, the pH of BEB medium (pH 6.2) was modified at values of 5.7 and 4.9 to mimic different bread types such as yeast-leavened and sourdough bread, respectively (Valerio et al., 2015). The results, shown in **(Fig. 17b)**, indicated that by decreasing the pH, the inhibition halo was slightly larger, thus suggesting that bioactivity was influenced by the acidic conditions. This result is once more in accordance with both the higher ungeremine content inside MBi/CH/TPP/UNG2 and its higher solubility in acidic condition.

In **Table 5**, the absorbance values of the samples and the corresponding residual ungeremine mass, evaluated by considering Lambert Beer (LB) law, and were detailed. Based on LB equation, only the absorbance interval in the linearity range (0.1 and 1.1) is appropriate. Hence, all the values below 0.1 are negligible and, as a consequence, the amount of ungeremine in the polymeric matrix is not estimable. From the analysis of the table, it is worthy to highlight that the absorbance peak areas of film MBi/CH/TPP/UNG2 were always the larger, thus confirming the ungeremine higher concentration found in that film. The amount of ungeremine released from the polymeric matrix and sub-micron beads, generally increased in MBi/CH/TPP/UNG2 films, confirming its improved antifungal activity both on PDA and BEB plates, at different pH.

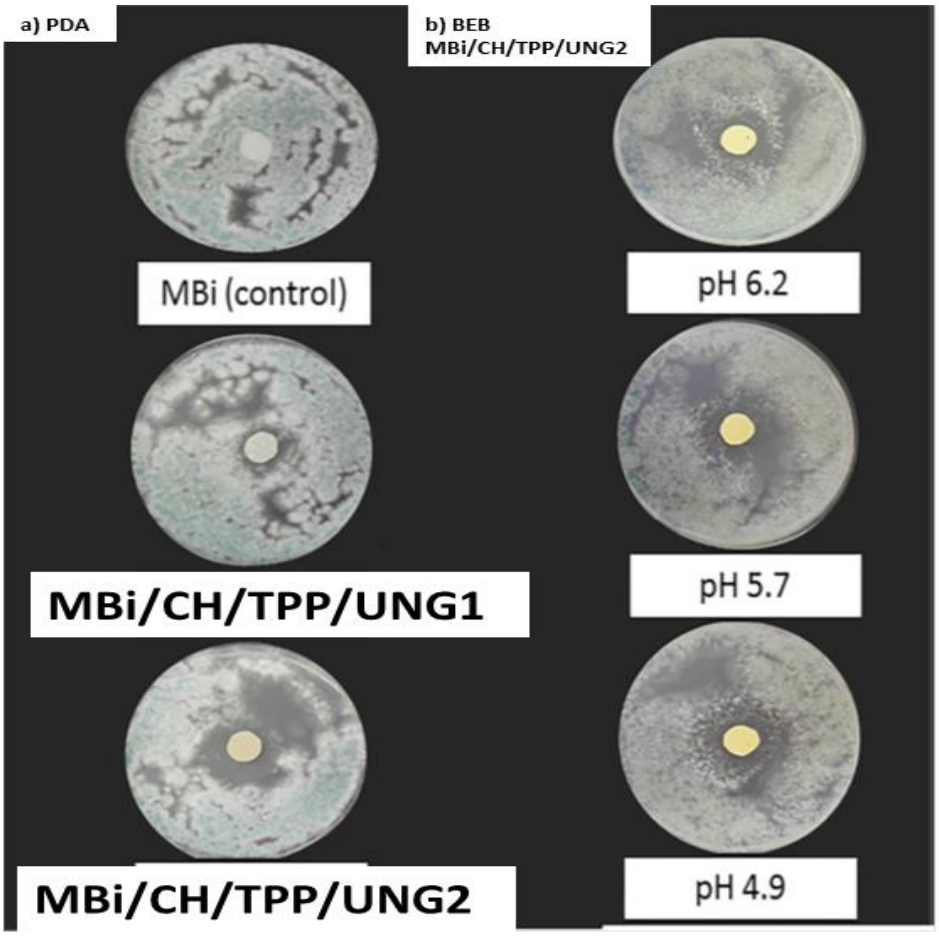


**Figure 17.** Antifungal activity against *P. roqueforti* of films on PDA plates at pH=5.7 (a), and MBi/CH/TPP/UNG2 film on BEB plates at different pH, after 3 days of incubation at 25 °C (b). (Moeini et al., 2020b)

**Table 5.** Residual ungeremine mass (%w) in MBi/ CH/TPP/UNG1 and MBi/CH/TPP/UNG2 on PDA and BEB media at different pH. (Moeini et al., 2020b)

| SAMPLES | | Absorbance (λ360nm) | Ungeremine Mass (mg) |
|---|---|---|---|
| **1** | **PDA pH (5.7) MBi/CH/TPP/UNG1** | 0.113 | 3.5 |
| **2** | **PDA pH (5.7) MBi/CH/TPP/UNG2** | 0.166 | 2.6 |
| **3** | **BEB pH (6.2) MBi/CH/TPP/UNG1** | 0.161 | 5.0 |
| **4** | **BEB pH (6.2) MBi/CH/TPP/UNG2** | 0.342 | 4.5 |
| **5** | **BEB pH (5.7) MBi/CH/TPP/UNG1** | 0.095* | ---- |
| **6** | **BEB pH (5.7) MBi/ CH/TPP/UNG2** | 0.255 | 4.0 |
| **7** | **BEB pH (4.9) MBi/CH/TPP/UNG1** | 0.047* | ---- |
| **8** | **BEB pH (4.9) MBi/CH/TPP/UNG2** | 0.181 | 2.8 |

***Sample 5 and 7 are outside the linearity range of LB equation.**

### *Differential scanning calorimetry (DSC)*

The first heating run of the compression molded films erased their previous thermal history. DSC thermograms recorded during the cooling ramp and second heating of MBi based films are reported in **(Fig. 18 a,b)**, respectively, while DSC parameters are detailed in **Table 6**. All data were normalized with respect to MBi content inside the biocomposites. The analysis of the cooling thermograms evidenced the crystallization of MBi in the plain and doped polymer. . As expected, the sub-micron particles included in the polymer matrix affected the crystallization process. Indeed they acted as nucleating agents able to both anticipate the onset of melt crystallization, and to move $T_{peak}$ towards higher values. The effect was particularly emphasized in MBi/CH/TPP/UNG2 biocomposite, since the higher concentration of nucleating agents (**see Table 6**). This outcome suggested that the dispersed phase was able to promote the development of crystalline nuclei in the biodegradable polymer during the cooling step. Nevertheless, in both composites, crystallization enthalpy (ΔHc) decreased by increasing of CH/TPP/UNG

content. This result, apparently in antithesis with the hastening of nuclei development, could be explained by considering that, in presence of the sub-micron particles, the macromolecular motion could be restricted, in this way avoiding the growing of polymeric crystals around the small nuclei. At the same way, the decreasing of melting enthalpy ($\Delta H_m$) in both composites could be attributed to the strong interfacial adhesion occurring between the polymer matrix and CH/TPP/UNG, able to restrict the polymer chain orientation during the packing process. Similar results were observed by Lee & Wang that investigated the thermal properties of biocomposites based on PLA and PBS including bamboo fibers (Lee et al., 2006) and by Dae-Hyun et al, when short pulp fibers were incorporated into corn starch plasticized with glycerol (Dae-Hyun et al., 2003).

In (**Fig. 18b)**, the thermograms of the second heating run of the samples are reported too. It is worthy to highlight the severe increasing of MBi glass transition temperature (see also **Table 6**), as a consequence of the introduction of the rigid sub-micron particles inside the macromolecular network. The decreasing of macromolecular mobility is likely due to the strong physical interaction occurring between the polar residues of starch component of the polymeric matrix and the hydroxyl and amine groups of both chitosan and ungeremine zwitterion of the dispersed phase (Jandas et al., 2011). The increasing of MBi Tg from 60 to 103-104 °C positively affect its application potentialities, approaching this polymer to other conventional food packaging materials, such as poly(ethylene terephthalate) (Tg = 67−81 °C) and polystyrene (Tg = 70−115 °C). Indeed, just to give you an idea, a packaging vessel or cup exposed to hot foodstuffs or drinks should have a Tg sufficiently higher than the application temperature, in order to both preserve the high mechanical strength and avoid the lessening of dimensional stability, also responsible of the contaminant releasing from polymeric matrix (Luzi et al., 2019). Moreover, the inclusion of dispersed phase inside MBi resulted in both a decreasing of thermal capacity associated to glass transition phenomena and in a consequent broadening of Tg range. A broadened Tg is often observed in polymer-filler systems, and is generally linked to good interfacial adhesion between the matrix and the dispersed particles, together with a restriction of molecular mobility of polymeric segments near the filler surface (Mallardo et al., 2016).

**Table 6.** Thermal properties of neat MBi, MBi/CH/TPP/UNG1 and MBi/CH/TPP/UNG2 films. (Moeini et al., 2020b)

| Sample | $Tc_{Onset}$ (°C) | $T_{peak}$ (°C) | $\Delta Hc_{melt}$ (J/g) | Tg (°C) | $T_m$ (°C) | $\Delta H_m$ (J/g) |
|---|---|---|---|---|---|---|
| **MBi Film** | 113 | 101 | 12.8 | 60 | 142.4 | 8.43 |
| **MBi/CH/TPP/UNG1** | 115 | 102 | 11.2 | 103 | 142.3 | 7.82 |
| **MBi/CH/TPP/UNG2** | 121 | 105 | 8.9 | 104 | 143.5 | 5.07 |

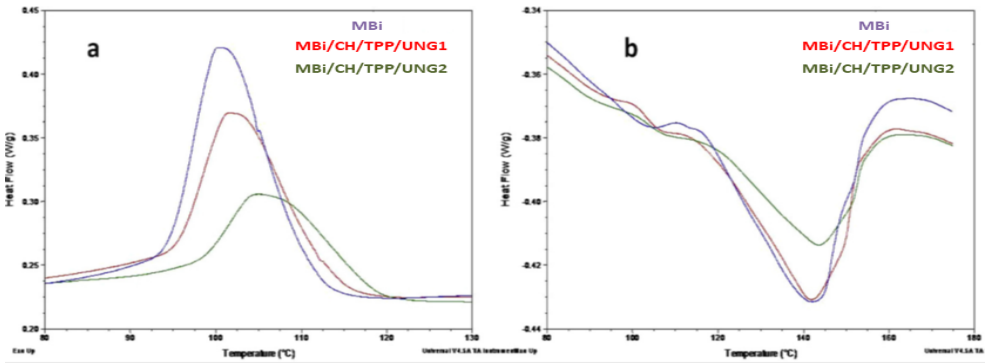


**Figure 18.** DSC thermograms of cooling ramp (a), and second heating ramp of MBi (blue), MBi/CH/TPP/UNG1 (red), MBi/CH/TPP/UNG2 films (green) based samples (b). (Moeini et al., 2020b)

### 3.3. Thermogravimetric analysis (TGA)

TGA thermograms of neat MBi film, MBi/CH/TPP/UNG1 and MBi/CH/TPP/UNG2 films and their first derivatives curves (DTG) are reported in **(Fig. 19 a,** and **b)**, respectively. All the curves were normalized with respect to starting sample weights. In **Table 7**, the temperatures of 10% weight loss ($T_{10\%}$) and the maximum decomposition rate temperature of both degradations step ($T_{max1}$ and $T_{max2}$), are shown. From the analysis of thermograms, it is possible to observe that, at about 100 °C, all the samples showed an initial mass loss consistent with the desorption of water molecules, corresponding to roughly 6% of the original sample weights. Nevertheless, the main decomposition processes occurred at higher temperature; specifically, as widely reported in literature, in the range of 280-340 °C, the degradation of the starch fraction occurs, accounting for approximately 20% weight loss (Cerruti et al., 2011), whereas at temperature higher than 300 °C and

involving about 70% mass loss, the polyester segments degradation occurred (Angelini et al., 2014). It is worthy to note that the presence of CH/TPP/UNG1 and CH/TPP/UNG2 sub-micron particles, respectively, decreased both the onset of degradation by about 10 °C and 35 °C respectively, and the starch fraction maximum decomposition rate was about 10 °C and 20 °C respectively, with respect to the neat polymer.

**Table 7.** Temperature of 10% weight loss ($T_{10\%}$), maximum decomposition temperatures rate ($T_{peak1}$ and $T_{peak2}$), for MBi, MBi/CH/TPP/UNG1 and MBi/CH/TPP/UNG2 Films. (Moeini et al., 2020b)

| Samples | $T_{10\%}$ (°C) | $T_{peak1.}$ (°C) | $T_{peak2.}$ (°C) |
|---|---|---|---|
| **Mbi** | 310 | 320 | 400 |
| **MBi/CH/TPP/UNG1** | 300 | 310 | 405 |
| **MBi/CH/TPP/UNG2** | 275 | 290 | 402 |

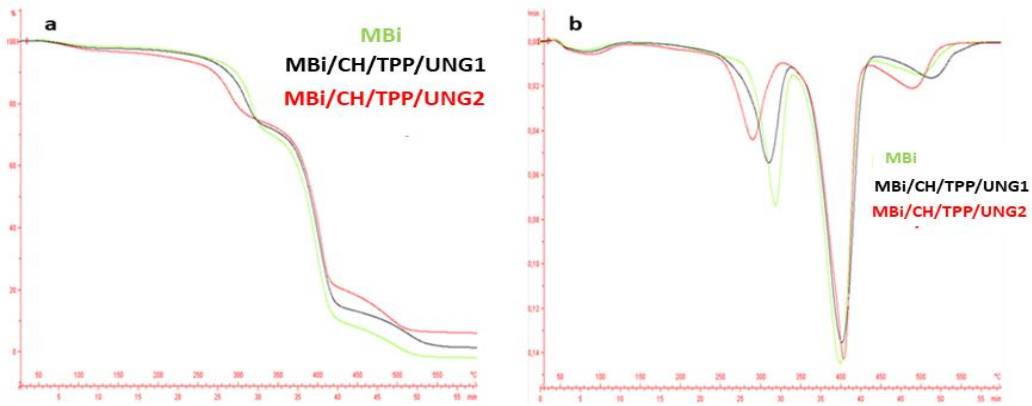


**Figure 19.** Weight loss (%), thermograms (TGA) of MaterBi based samples (a) and their derivative curves (DTG) (b) (Moeini et al., 2020b)

On the other side, it deserves to mention that the polyester fraction did not show any substantial modification in thermal behavior, as evidenced by the degradation kinetics of the neat and doped MBi samples and by the value of their $T_{peak2}$, occurring at about 400°C. These outcomes suggested that in MBi films, the starch fraction and the chitosan based sub-micron particles physically interacted, by means of hydrogen bonding, as was

expected since the common polysaccharide nature. In a previous paper, Moeini et al reported that neat chitosan and CH/TPP/UNG $T_{peak}$ occurred at 295 °C and 256 °C, respectively (Moeini et al., 2018). Hence, their thermal degradation could induce and trigger the starch decomposition process. In addition, it is likely that their fine dispersion between starch macromolecular chains induced the weakening of intra-inter-molecular hydrogen bonds of the polysaccharide, reducing the packing of its backbone structure and providing a higher liability to both the random splitting of the glycosidic bonds and to a fast thermo-degradation process, as found by (Pieróg, Ostrowska-Czubenko, & Gierszewska-Druzyńska, 2012).

***Scanning electron microscopy (SEM)***

SEM analyses were performed in order to obtain information on CH/TPP/UNG filler distribution inside MBi film. In **(Fig. 20a)**, the cross-sectional fracture of neat MBi film is reported. The rough, irregular and wrinkled surface of neat MBi film revealed a rather homogeneous dispersion of gelatinized starch particles embedded in a continuous matrix (the synthetic polymeric component of the formulation); moreover, several regularly sized microvoids can be detected, whose diameters closely resemble those of the original starch particles. This finding could be explained by the starch particles debonding and pulling out, following to the mechanical stress applied during cryogenic fracture of the films for the surface delamination. As concerning the doped samples, in (**Fig. 20b,c)** and **(Fig. 20d,e)**, MBi/CH/TPP/UNG1 and MBi/CH/TPP/UNG2 film micrographs at different magnifications, are respectively reported. From the analysis of micrographs c and e, it is worthy to highlight the presence of CH/TPP/UNG dispersed phase, whose dimension was ranged between 100 and 800 nm. In addition, it is possible to observe a fairly rough cross-sectional surface with a pronounced coarsening due to the homogeneous dispersion of the submicro beads well embedded inside the polymeric matrix. The general absence of voids and the presence of several discrete micro-domains, homogenously sourranded by a polymeric halo, suggested the development of physical interactions occurring between the polar groups of both polysaccharide fractions. It’s not by chance that this outcome was

particularly enhanced in MBi/CH/TPP/UNG2 sample (**Fig. 20d**), where a substantial higher concentration of CH/TPP/UNG particles could be spotted.

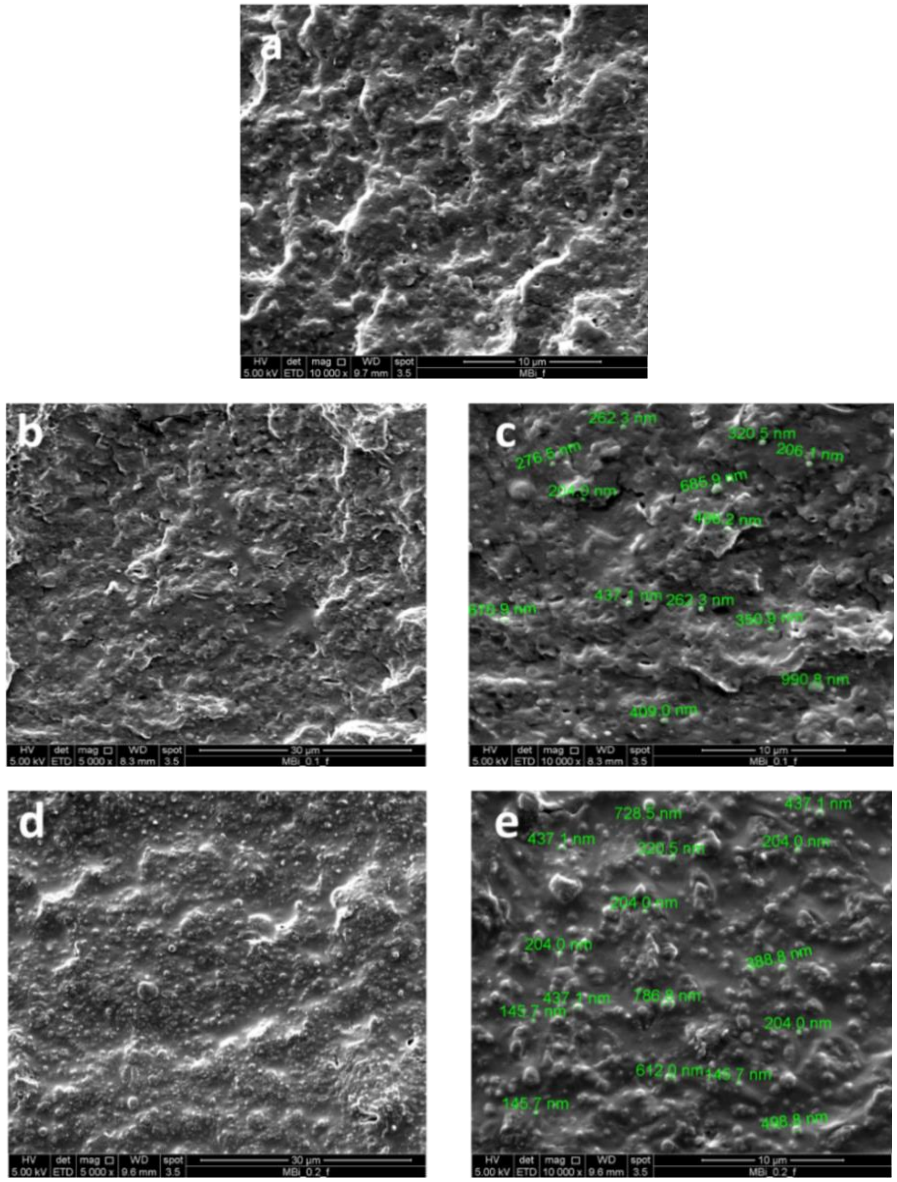


**Figure 20.** SEM micrographs of cryogenically cross-sectional surface of neat MBi (a), MBi/CH/TPP/UNG1 (b,c), and MBi/CH/TPP/UNG2 (d,e) at 5000x (b,d) and 10000x magnifications (c,e) (Moeini et al., 2020b)

***Water Vapor and Oxygen Permeability***

In semi-crystalline polymers, small molecules diffusion occurs only through the amorphous phase, whereas the crystalline fraction does not contribute to permeability. This entails that the permeability values are functions of the amorphous volumetric fraction. The addition of fillers into a polymer affects the gas diffusion mechanism through the material. Thus, the permeability of a multiphase system, such as biocomposites, accounts for the amorphous volumetric fraction, the filler volume fraction, the tortuosity pattern and the thickness of the films (Crispin et al., 2003). Generally, biocomposites evidence high barrier properties with respect to the neat polymeric matrix, due to the nucleating effect induced by the dispersed phase (Mahmoodi et al., 2019). In the specific case, CH/TPP/UNG sub-micron particles acted as nucleating agents able to promote the formation of several crystalline nuclei to the detriment of the amorphous phase, as previously discussed in DSC section; as a consequence, a tightened and tortuous structural pattern developed, hindering the both solubility and diffusion of oxygen molecules in MBi doped samples, as shown in **Table 8**. Similar results have been widely described in literature (Ortega-Toro et al., 2016; Persico et al., 2009; Russo et al., 2010). Nevertheless, from the analysis of Table 8, it is possible to highlight a slight increasing of water permeability in the biocomposites. Since CH/TPP/UNG sub-micron particles are not water-soluble, it is plausible that the increase of WVP was mainly due to the diffusion of water vapor molecules. Actually, differently from oxygen, it is likely that in presence of the water molecules flow, the high concentration of polar groups from both starch and chitosan polysaccharides induced a sort of macromolecular swelling, able to widen the interstitial spaces between macromolecular chains and sub-micro particles junction points, thus hastening the diffusion of water molecules throughout the membrane; This effect was particularly enhanced in MBi/CH/TPP/UNG2 sample where the concentration of hydrophilic groups was higher. Turco et al., found similar results for Poly (Lactic Acid)/Thermoplastic Starch based blends (Turco et al., 2019).

In literature, transmission rates and permeabilities values can be interchangeably used for discussion of barrier properties. Actually, the obtained results could extend the potential

applications of MBi based composites as packaging of a wide range of oxygen sensitive food products, such as processed meat packaging (with OTR and WVTR requirement of 3.1 to 15.5 cc/$m^2$×24 h and 3.1 to 7.75 g/$m^2$ ×24 h) and cheese (with OTR and WVTR requirement of 9.3 to 15.5 cc/m 2×24 h and 1-15.5 g/m 2 ×24 h), as evidenced by (Yee Bond et al., 2016). The water vapor and oxygen barrier properties found are comparable to those of some traditional polymers commonly used as food packages, such as PET, EVOH, PP, while they result being higher than those of PS and biodegradable plastics, such as polylactic acid (PLA), as reported by Ortega-Toro et al 2016. These outcomes highlight that the MBi based biocomposites could be a promising resource for the packaging industry, even more targeted towards the employment of eco-sustainable plastic materials (Ortega-Toro et al., 2016).

**Table 8.** Water Vapor and Oxygen Permeability at 25°C and 50% RH. (Moeini et al., 2020b)

| **Samples** | **Water Vapor Permeability (±10%) (g/Pa*m*24 h)** | **Oxygen Permeability (± 5%) ($cm^3$/Pa*m*24 h)** |
|---|---|---|
| **Mbi** | $2.07*10^{-7}$ | $1.68*10^{-7}$ |
| **MBi/CH/TPP/UNG1** | $3.17*10^{-7}$ | $1.07*10^{-7}$ |
| **MBi/CH/TPP/UNG2** | $3.28*10^{-7}$ | $9.78*10^{-8}$ |

***Tensile Test***

Tensile tests were performed in order to investigate the influence of CH/TPP/UNG sub-micron particles on the modulus and ultimate behavior of MBi based samples. The results are listed in **Table 9**. The analysis of data of all samples evidenced a common elastic behavior followed by a plastic deformation up to sudden rupture of the samples. In particular, neat MBi polymer was characterized by a high ductility and tenacity, since the high both tensile strength and strain at break. Moreover, it is possible to highlight that, for a long duration upon tensile loading, the strain increased with constant stress due to the inherent ductile behavior of the polymer. Anyway, the mechanical properties of the

biocomposites were affected by the presence of the dispersed phase, as widely occurring for similar systems (Raj et al., 2011).

Indeed, it should pointed out that strength and elongation at break for filled systems depend on the state of the polymer-particle interface, since when there's a good adhesion between filler and matrix, an enhanced stress transfer occurs at the interface (Ratanakamnuan and Aht-Ong, 2006). The introduction of CH/TPP/UNG sub-micron particles inside MBi polymeric matrix induced a progressive increasing of elastic modulus, suggesting the effectiveness of the filler reinforcement. The higher weight fraction of CH/TPP/UNG resulted in the greater stiffness of the composites. The improvement of MBi rigidity is due to the strong physical interaction occurring with the polar groups of CH/TPP/UNG particles, by means of hydrogen bonding, accounting for an improvement of the filler–matrix interaction (Belhassen et al., 2008). In addition, upon tensile loading, the presence of CH/TPP/UNG sub-micron particles and their good interface with Mater Bi, led to improved mechanical stress-transfer from the matrix to them, leading to high tensile strength properties. Hence, CH/TPP/UNG particles exerted good reinforcing effect in the polymeric matrix and increased the tensile strength of the composite. This result supported both the previous finding of Tg increasing, and the morphological analysis related to the fine distribution of the dispersed phase.

As a consequence of the reduced macromolecular mobility, the strain at break of the biocomposites dropped down (Elfehri et al., 2015). Anyway, the low values of standard deviation associated with strain at break values of the two samples containing the filler, supported the good interfacial adhesion between MBi and CH/TPP/UNG dispersed phase.

**Table 9.** Young's modulus (*E*), stress at break ($\sigma_b$) and strain at break ($\varepsilon_b$) of neat MBi, MBi/CH/TPP/UNG1 and MBi/CH/TPP/UNG2 films. (Moeini et al., 2020b)

| Sample | E(MPa) | σ(MPa) | ε(%) |
|---|---|---|---|
| **MBi** | 157.7±3.8 | 11.1±0.3 | 281.3±3.8 |
| **MBi/CH/TPP/UNG1** | 163.6±6.8 | 14.5±0.2 | 46.8±3.4 |
| **MBi/CH/TPP/UNG2** | 174.1±5.2 | 20.9±0.2 | 26.5±1.1 |

## 5.5. Physical-chemical characterization of PLA/PEG/UNG fibers[15] (Moeini et al., 2020c)

***Electrospinning of PLA, PLA/PEG solutions in the presence of ungeremine***

The aim of this work was to investigate the effect of hydrophilicity of fibers on the release of the metabolite. In order to optimize the electrospinning condition, several solvents and blend mixtures were initially tested under a variety of electrospinning conditions (voltage, flow rate, polymer concentration, and needle-collector distance). In order to have a suitable solvent, the polymer solubility and spin ability were investigated. According to Luo et al, a better solvent requires a higher polymer concentration to avoid forming a droplet during electrospinning, while a solvent with partial solubility is appropriate for a more dilute solution (Luo et al., 2010). Due to the very similar solubility parameters that was reported for PLA (i.e., 20.18 $MPa^{0.5}$) and PEG (20.08–20.90 $MPa^{0.5}$), it seems feasible to use the same solvent system for PLA/PEG blend electrospun solution (Llorens et al., 2014). Dichloromethane is a suitable solvent for rendering fibers, even at a relatively low concentration of polymer (Llorens et al., 2014; Toncheva et al., 2011, 2012, 2016). However, ungeremine is not soluble in DCM, so MeOH was used as a co-solvent in all blend solutions.

In the second step, different polymer concentrations and blend ratios were investigated in order to optimize the continuous fibers. From our experiments, no continuous fibers were observed below concentrations of 9%. Therefore, PLA and PLA/PEG blends of microfibrous mats were fabricated in three different ratios (PLA/PEG5, PLA/PEG13, and PLA/PEG26) with a total polymer concentration of 9% w/v. Before incorporation of the metabolite, the influence of PEG on the hydrophilicity of the PLA polymer matrix was investigated by a contact angle test. The preliminary observation of electrospun fibers showed that fibers appeared continuous even when the lowest amount of PEG (5%) was added to the PLA solution.

[15] This part has been done at Stellenbosch University at Department of Chemistry and Polymer Science, and published in: Moeini, A., Cimmino, A., Masi, M., Evidente, A., & Van Reenen, A. (2020). The incorporation and release of ungeremine, an antifungal Amaryllidaceae alkaloid, in poly(lactic acid)/poly(ethylene glycol) nanofibers. Applied Polymer Science.

In this study, ungeremine (UNG) was used as an antifungal metabolite. In the absence of UNG, PLA/PEG26 formed cylindrical and continuous fibers that were considered high quality. However, when UNG was incorporated, altering the configuration of the blend, the PLA/PEG/UNG1%-13 formed similar quality fibers to the PLA/PEG26 configuration. The effect of UNG on the fibers could be attributed to two different aspects. First, in terms of the ionic nature of ungeremine (**Fig. 21a and b**), UNG is a zwitterion, (Moeini et al., 2018) and the presence of positive and negative charges in the structure of ungeremine coupled with an increasing charge density probably resulted in ionic interactions between UNG (**Fig. 21c)**, which could lead to the formation of UNG agglomeration in the fibers. This was simulated by "Chem3D Pro" software (**Fig. 21d)**, and was also practically observed in the PLA/UNG1% fibers **(Fig. 25e)**. Indeed, even 1% of UNG resulted in some agglomerates in the PLA/UNG1% fibers which probably resulted from immiscibility of the PLA and ungeremine in the PLA/UNG solution mixture and through ionic interactions between UNG molecules. For other fiber blends, the same was observed in at UNG concentrations above 1%, and no fibers could be fabricated in the presence of 3% of ungeremine in any of the electrospun solutions **(Table 10)**. The second aspect that might have an effect on fiber morphology was the hydrogen bonds between $N^+$ and $O^-$ of UNG with hydroxyl groups of PEG. It seems that the formation of the good and continuous fibers in the presence of UNG was directly influenced by PEG content. In particular, it was observed that continuous fibers could form only at PLA/PEG/UNG2%-13 when 2% of ungeremine was used. It could be hypothesized that in the presence of a certain ratio of PEG and UNG, hydrogen bonds can have priority over ionic interactions. Finally, an effect of increased charge density was observed in the presence of a high percentage of UNG (2%) during the electrospinning process. In order to observe the formation of fibers from PLA/PEG/UNG2%-13, and to prevent the fibers from being retained in the tip of the needle, the voltage for this sample was changed by increasing the differences between positive (+) and negative (-) charges as well as increasing flow rate and the distance between the needle and collector.

**Table 10.** The summary of the fibers formation from the different blend solutions and ungeremine concentration (positive and negative known as a successfully formed fiber and not formed fiber respectively) (Moeini et al., 2020c)

| Blend solutions | Ungeremine concentration | | |
|---|---|---|---|
| | 1% | 2% | 3% |
| PLA | + | - | - |
| PLA/PEG5 | + | - | - |
| PLA/PEG13 | + | + | - |
| PLA/PEG26 | + | - | - |

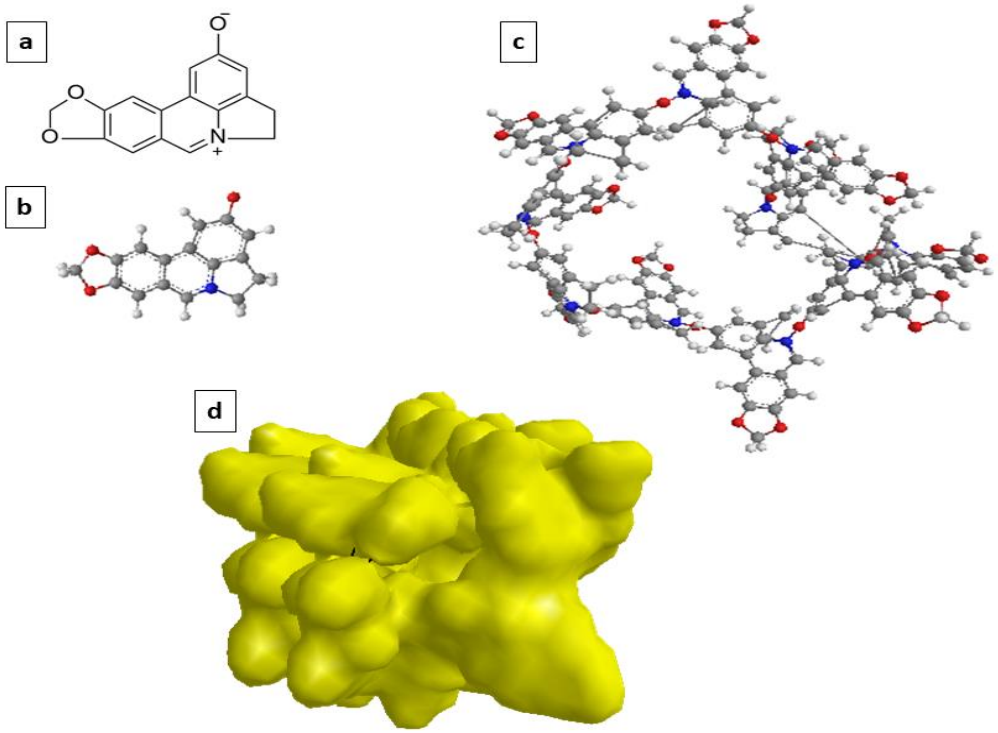


**Figure 21.** Ungeremine structure 2D (a), 3D (b), the ionic interaction of UNG molecules (c) and 3D simulated UNG agglomeration in solvent (d) (All the pics were drawn by ChemDraw software) (Moeini et al., 2020c)

***Attenuated Total Reflection Fourier Transform Infrared Spectroscopy (FTIR-ATR)***

The presence of antifungal metabolite in the electrospun fibers was evaluated by FTIR spectroscopy; the FTIR spectra of the PLA, PLA/PEG and PLA/PEG/UNG are shown in (**Fig. 22)**. A qualitative analysis of the fiber composition was performed by IR spectroscopy. In the spectrum of PLA, the peaks at 1753 $cm^{-1}$ correspond to C=O. The –$CH(CH_3)$- bonds are observed at 1353 $cm^{-1}$ and 1452 $cm^{-1}$. The strong bands at 1083 $cm^{-1}$, 1128 $cm^{-1}$ and 1181 $cm^{-1}$ were assigned to C-O-C stretching vibration **(Fig. 22a)**. The peaks at the range of 2800-3000 $cm^{-1}$ are related to $CH_3$ asymmetric, $CH_3$ symmetric and –CH groups. The peak at 2999 $cm^{-1}$ is attributed to CH stretching is used for the characterization of PLA (Yuniarto et al., 2016). In the PLA/PEG fibers, the board peak at 3300-3500 $cm^{-1}$ corresponds to PEG hydroxyl group. In addition, the appearance of the peak at 2875 is characteristic of the presence of PEG **(Fig. 22 a** and **c)**. The addition of the PEG into the PLA/PEG blends fibers lead to a decrease in the intensity of –CH peaks at 2999 $cm^{-1}$, and an increase in the intensity of the peak at 2945 $cm^{-1}$ and the appearance of a peak at 2878 $cm^{-1}$ **(Fig. 22c)** (Boua-In et al., 2010). The hydroxyl group broad peak at the range of 3300-3500 $cm^{-1}$ appeared after addition of PEG into PLA/PEG blends and it was broadened by increasing the percentage of PEG. This occurrence could also be observed in PLA/PEG/UNG fibers in which the peak widened in comparison with PLA/PEG fibers. In addition, a shift to higher frequencies was observed, in ungeremine loaded fibers from 3427 $cm^{-1}$ in PLA/PEG fibers to 3497 $cm^{-1}$ in PLA/PEG/UNG. This result might be attributed to physical interaction by hydrogen bonding formation between UNG with hydroxyl group PEG (**Fig. 22c)**.

***Differential Scanning calorimetry (DSC)***

As it is shown in **Table 11**, the thermal properties of the fibers were studied by mean of DSC. For the PLA mats $T_g$ and $T_m$ were observed at 59 °C and 148.6 °C respectively. The melting temperature ($T_m$) of PLA in all fibers regardless of the PEG percentage does not change significantly. However, the plasticizing effect of PEG in PLA/PEG blend was observed by the effect of polyether on PLA polymer matrix. This effect was increased by increasing the percentage of PEG content into PLA/PEG blends and it was proved by a

shifting in $T_g$ and $T_{cc}$ of PLA to lower temperature as well as narrowing and sharping $T_{cc}$ peak (Toncheva et al., 2016) **Table 11** and (**Fig. 23)**. The addition of PEG into PLA has similar effect of semi-crystalline sample and resulted in an increase in PLA melting enthalpy ($\Delta H_m$) by increasing PEG content into PLA/PEG blend (Llorens et al., 2014). It has also observed that due to low molecular weight, PEG facilitated the orientation of PLA matrix in the electrospinning process which resulted in an increasing in degree of crystallization ($\chi_C$). On the other hand, the addition of ungeremine into PLA and PLA/PEG blends fibers was resulted in a shift in Tg, Tcc and Tm to lower temperatures as well (**Table 11** and **Fig. 23)**. Furthermore, incorporation of ungeremine caused an increase in $\Delta H_{cc}$ and $\Delta H_m$ which lead to an increase in degree of crystallization ($\chi_C$) of PLA/PEG blends.

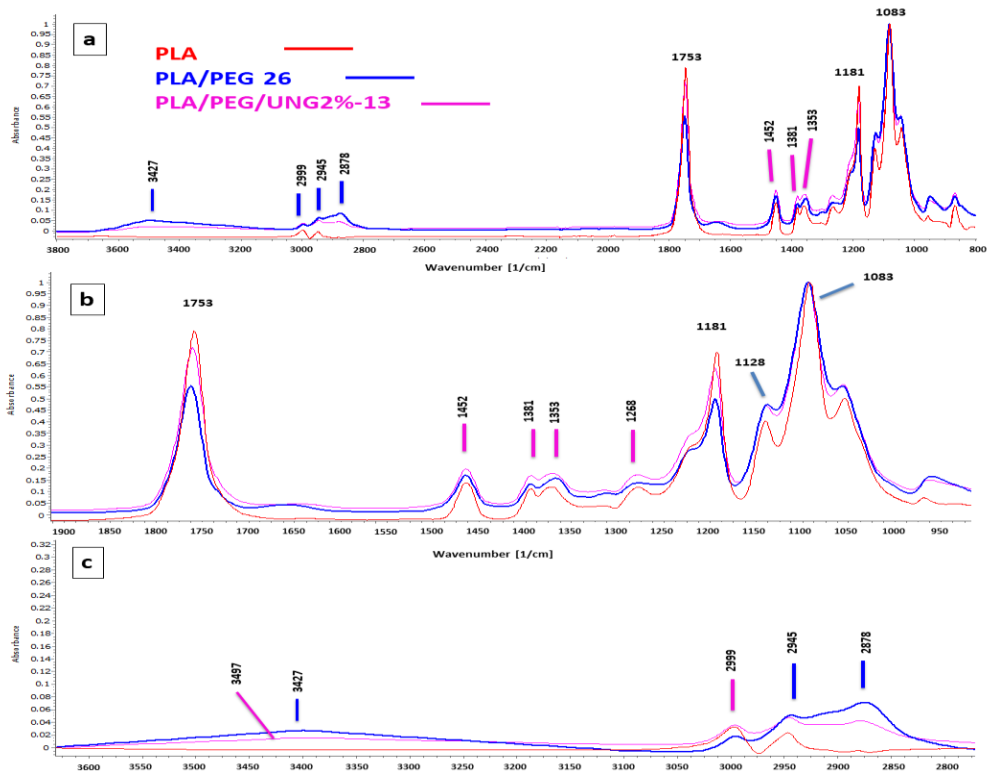


**Figure 22.** FT-IR spectra of PLA, PLA/PEG26 and PLA/PEG/UNG2%-13 (a) PLA, PLA/PEG26 and PLA/PEG/UNG2%-13 at the range of 1800–800 $cm^{-1}$ (b) and in the range of 3600–2200 $cm^{-1}$ (c) (Moeini et al., 2020c)

**Table 11.** Thermal characteristics of the PLA and PLA/PEG blends fibers (Moeini et al., 2020c)

| Mats | $T_g$ (°C) | $T_{cc}^{PLA}$ (°C) | $\Delta H_{cc}^{PLA}$ ($Jg^{-1}$) | $T_m^{PLA}$ (°C) | | $\Delta H_m^{PLA}$ ($Jg^{-1}$) | $\chi_c^{PLA}$ |
|---|---|---|---|---|---|---|---|
| | | | | $T_{m1}$ | $T_{m2}$ | | |
| **PLA** | 59.3 | 127 | 3.1 | 148.6 | ---- | 4.9 | 4.09 |
| **PLA/PEG 5** | 30.6 | 95.5 | 20.55 | 136.6 | 145.3 | 25.94 | 10.93 |
| **PLA/PEG 13** | 17.0 | 75.1 | 20.17 | 122.8 | 141.9 | 27.74 | 15.68 |
| **PLA/PEG26** | 15.4 | 71.8 | 15.73 | 127.5 | 138.7 | 24.2 | 23.64 |
| **PLA/UNG1%** | 54.2 | 124.7 | 3.92 | 147.8 | ---- | 6.84 | 8.53 |
| **PLA/PEG/UNG1%-5** | 29 | 85.2 | 26.46 | 130.9 | 146.2 | 35.21 | 13.06 |
| **PLA/PEG/UNG1%-13** | 12.0 | 68.8 | 21.04 | 122.5 | 141.7 | 33.13 | 20.92 |
| **PLA/PEG/UNG2%-13** | 19.8 | 75.7 | 16.98 | 126.1 | 143.9 | 27.76 | 22.32 |
| **PLA/PEG/UNG1%-26** | 15.4 | 71.9 | 18.8 | 126.8 | 140.5 | 29.25 | 24.13 |

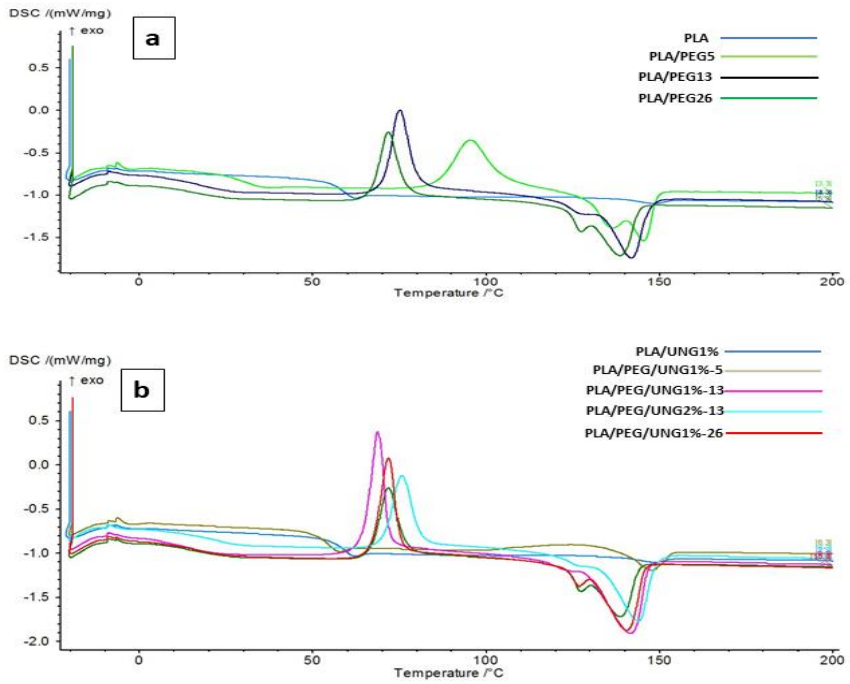


**Figure 23.** DSC thermograms of fibrous materials from blank fibers (a), and ungeremine included fibers (b) (Moeini et al., 2020c)

It could be assumed that the ionic nature of UNG causes nucleation sites into the fibers and result in a decrease in the mobility and increase in the degree of crystallization ($\chi_C$) of the fibers in the presence of UNG. The two $T_m$ peaks in observed for the PLA/PEG blends is probably a result of the uneven distribution of PEG in the PLA matrix. This leads to two different crystalline domains, one being affected by the PEG and the other not. This is supported by the FTIR results regarding the association between PEG and PLA. A similar double melting event was reported by (Toncheva et al., 2016).

***Release rates***

The release behavior of UNG from PLA and PLA/PEG blends fibers is shown in **(Fig. 24)**. In order to observe the effect of PEG content in the fibers releasing behavior, the fibers were successively exposed to a hydrophilic medium (sodium acetate/acetic acid) and then to a more hydrophobic Sörensen/ethanol (30:70v/v) solution. The release profile of all samples regardless of the percentage of PEG showed similar pattern which could be explained in four steps.

In the first step (first 7 hours of exposure), we have a fairly rapid release of UNG from all the fibers except for the PLA. The release rate is directly related to the PEG content in the fibers (from 1.5% for PLA to 14% for PLA/PEG/UNG1%-26). Thus, as the hydrophilicity of the fibers increase, so the release of UNG is increased **(Fig. 24b)**. It could be postulated that the water medium would selectively dissolve the PEG from the fibers thus increasing the available surface area for ungeremine to be released from, or that some of the ungeremine is preferentially included in the PEG domains in the fiber. The latter is supported by some of the results obtained by SEM and ATR-FTIR. It is clear that the more hydrophobic PLA matrix is hardly affected by the aqueous medium in the first 72 hours, resulting in little or no release of the ungeremine. Similar patterns were reported with regards to the release of triclosan from PLA/PEG blends (Llorens et al., 2014; Zurita et al., 2005).

Interestingly, when the PLA/PEG13 fibers were compared to the concentration of the UNG seems to have little effect in the first few hours of exposure. It is only after the first 6 or 7 hours that the 2% UNG fibers release at a higher rate than the 1%. After the first step

(7 hours) there is a steady release rate of UNG in all the fibers, while the more hydrophilic fiber mats maintain a higher release of UNG. This is in line of what was observed and postulated with regards to the SEM and ATR-FTIR results. It appears as if some of the ungeremine is more likely to associate with the PEG domains in the fibers than the PLA. What is really interesting here is the sustained slow release of the ungerimine in the hydrophilic medium. In many other cases, a typical release profile is that of an initial burst release followed a slow release over the remainder of the test period.

The PLA/PEG/UNG1%-5 fibers increased their release rates between 7 and 72 hours, but still released significantly less UNG than the other, more hydrophilic fibers (the PLA/PEG/UNG1%-26 fibers reached 32% release after 72 hours and the PLA/PEG/UNG1%-5 only about 5%).

The third step in the release profiles was started by replacing the aqueous solution with a more hydrophobic solution (Sörensen/ethanol). The result was a reversal of the release rate for most of the fibers, with the more hydrophobic fibers (PLA) more rapidly releasing the ungeremine (PLA increased from 1.7% to 25.6% within this period and PLA/PEG/UNG1%-5 from 5.4% to 19.9%). This could be due to the solubility of the ungeremine into the medium or the affinity for the more hydrophobic segments of the fibers with the medium, or both. After this initial new burst release a steady increase was observed for all the fibers. The apparently final or equilibrium release point was reached at a time that was inversely proportional to the PEG content of the fibers (PLA/PEG/UNG1%-26) reached an equilibrium first and so on). What is notable is that the amounts released for the PLA/PEG1% fibers were all similar (48 – 55% after 150 hours) but the amount released from the PLA/PEG/UNG2%-13 was much higher than that of the similar fibers containing 1% ungeremine. This shows that a considerable amount of the ungeremine was still contained in the PLA segments of the fibers, and that the metabolite was evenly dispersed in the fibers during the production process.

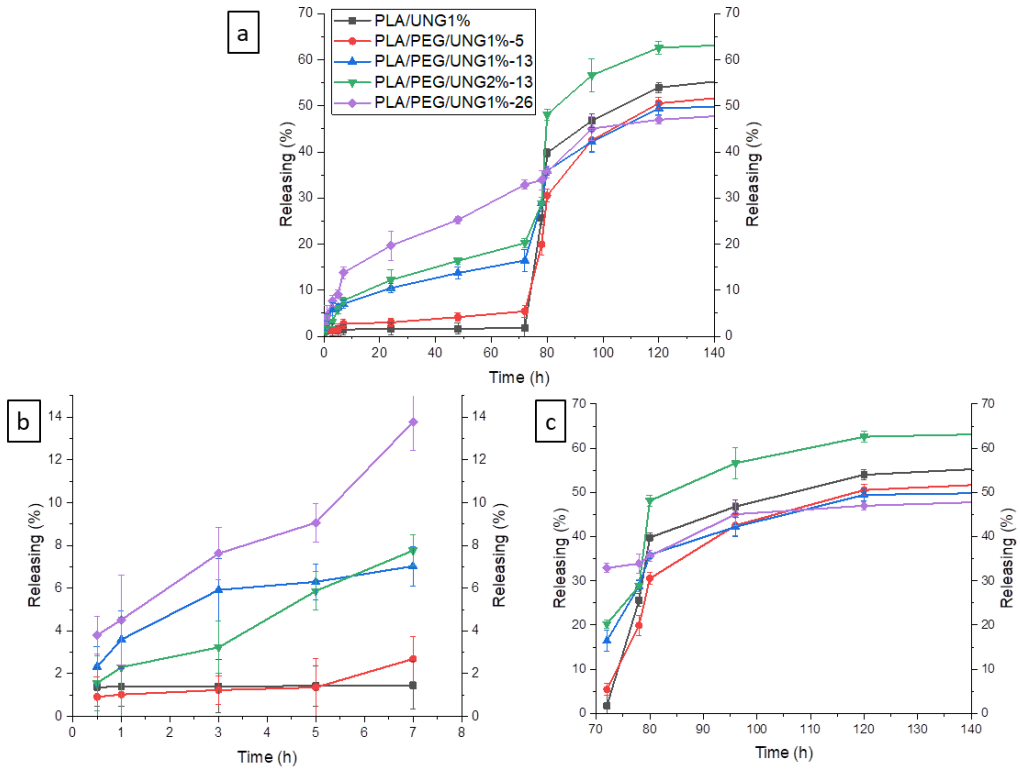


**Figure 24.** Ungeremine release curves for PLA/UNG1% (black), PLA/PEG/UNG1%-5 (Red), PLA/PEG/UNG1%-13 (blue), PLA/PEG/UNG2%-13 (green) and PLA/PEG/UNG1%-26 (purple) electrospun samples. Shows the overall release profile in a sodium acetate/ acetic acid (pH=5.4) medium for the first 72 h and then in a Sörensen/ethanol mixture (30:70v/v) (a), Shows the first 7 hours release (first step) (b), and shows the release (third and fourth steps) in the Sörensen/ethanol mixture (30:70v/v) (c) (Moeini et al., 2020c)

***Scanning electron microscope (SEM) analyses and porosity test of fibers***

The fiber morphology was investigated by means of scanning electron microscopy. In the all neat fibers, PLA and PLA/PEG blends in different ratios cylindrical and defect-free fibers were obtained (**Fig. 25)**. However, the effect of PEG on morphology could be observed by its impact on the mean fiber diameter (Toncheva et al., 2016). The mean diameter of the PLA fibers was 1.576±0.206 µm, and of the PEG-containing fibers slightly decreased to 0.938±0.111 µm, 0.865±0.101 µm and 1.486±0.132 µm for PLA/PEG5, PLA/PEG13 and PLA/PEG26, respectively. It is not clear why the PLA/PEG26 fibers had

a larger diameter than the PLA/PEG5 and PLA/PEG13 fibers. The addition of the ungeremine to the PLA, PLA/PEG solutions on the other hand decreased the fiber diameter compared to the fibers in the absence of UNG **(Table 12)**. This is probably due to the increased ionic character of the spinning solution after the addition of the zwitterionic ungeremine. The addition of the ungeremine to the PLA, PLA/PEG solutions on the other hand did not have any significan effect on the fiber diameter **(Table 12)**. It appears as if the amount of PEG has little effect on the fiber diameter especially in the presence of ungeremine. It may be that the fibers with higher PEG percentage appear a little smoother and adheres to each other, indicating that the PEG is closer to the fiber surface **(Fig. 25)**. Ungeremine showed different behavior in PLA fibers in comparison PLA/PEG fibers. As it might be seen in PLA/UNG fibers, presence of beads could be explained by the immiscibility of UNG and PLA. This resulted from the ionic nature of UNG and lead agglomeration of ungeremine, also visible on the surface of PLA fiber **(Fig. 25e)**. Cylindrical and defect-free fibers were observed in other samples with ungeremine included (PLA/PEG/UNG1%-5, PLA/PEG/UNG1%-13 and PLA/PEG/UNG1%-26). In the case of the PLA/PEG/UNG2%-13, agglomeration was observed in the fibers **(Fig. 25g)**. In addition, some thinner fractions in the nano-scale (93±10 nm) were observed in the PLA/PEG/UNG2%-13 fibers that were not in PLA/PEG13, this phenomenon could be happened due to inhomogeneous distribution of the UNG in the spinning solutions. In fact, it was probably resulted from the using higher concentration of ungeremine in spinning solution of PLA/PEG/Un2%-13 **(Fig. 25g)** (Kfoury et al., 2015; Toncheva et al., 2016).

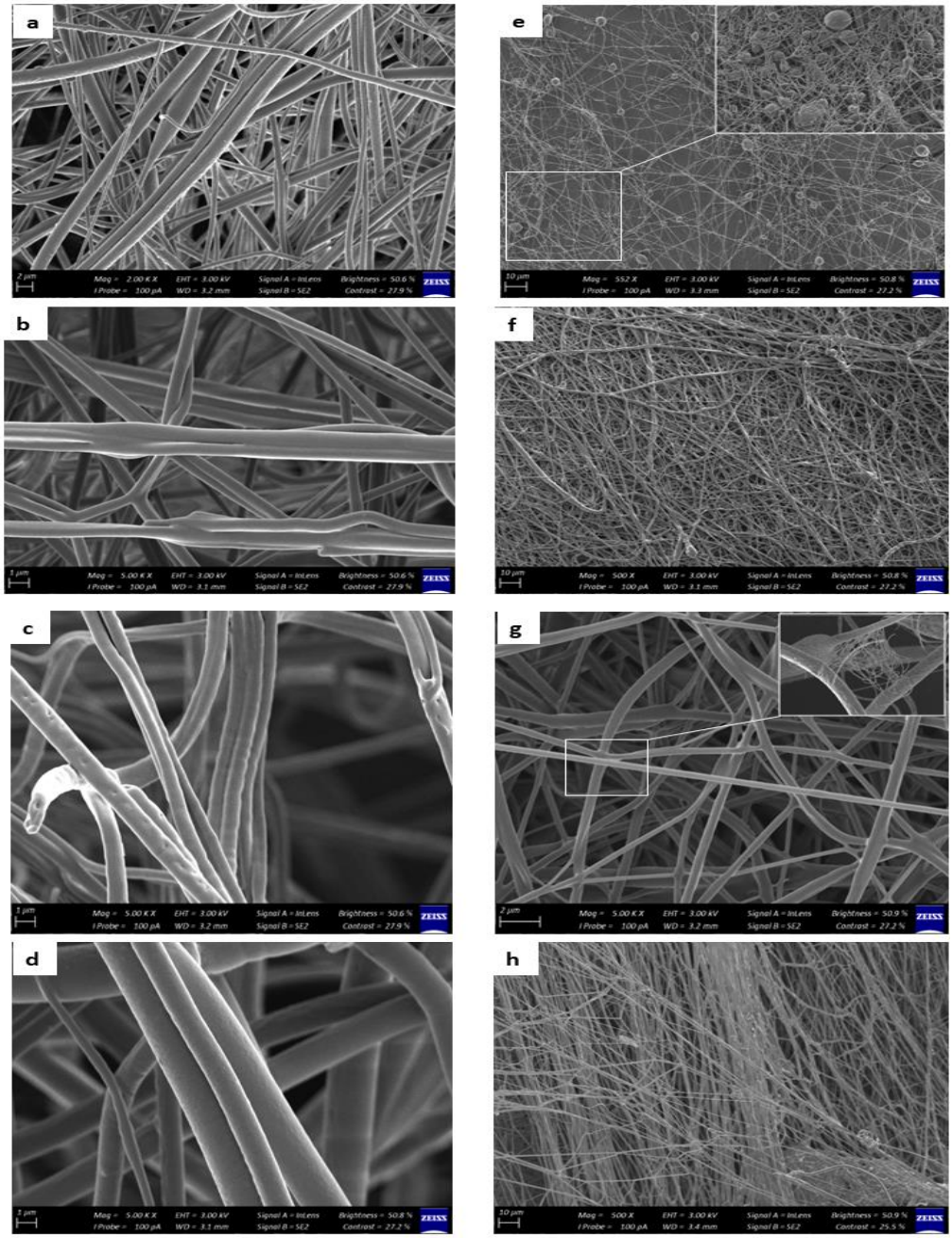


**Figure 25.** SEM micrograph of non-woven fibers prepared by electrospinning of PLA (a) PLA/PEG5 (b) PLA/PEG13 (c) PLA/PEG26 (d) PLA/UNG1% (e) PLA/PEG/UNG1%-5(f) PLA/PEG/UNG2%-13 (g) PLA/PEG/UNG1%-26 (h) (Moeini et al., 2020c)

In order to get additional information regarding the release of UNG from the fibers, SEM analyses of selected PLA/PEG/UNG fibers before and after exposure to the buffer solution were done. Results are illustrated in **(Fig. 26)**. The effect of buffer could be observed in all samples. Initially very little change in the fibers was observed. This holds with the presumption that the initial burst release of the ungeremine was due to extraction of the metabolite from the PEG-rich areas on the surface of the fibers. After 48 hours of immersion, some of the fibers appear to be stuck together; this might be an indication of PEG and UNG that has leached from the fibers. After 72 hours some of this material has disappeared; once again this might be due to PEG and UNG dissolving in the buffer medium as time progresses. These processes can be clearly seen for the PLA/PEG/UNG1%-5 fibers for example **(Fig. 26a and c)**. The same results are observed for the PLA/PEG/UNG1%-13 fibers, except that the amount of PEG released seems to be notably higher. Note that there appears to be holes/fissures formed on the fibers after day 1 (arrows in **Fig. 26d**). This trend is also seen with PLA/PEG/UNG1%-26 fibers and the fissures and holes in the fibers noticed after day 2 **(Fig. 26e)**. The results could support the premise that the UNG is present in both the PEG and PLA parts of the fiber. However, the initial release of the UNG from the fibers in the buffer is due to the PEG leaching from the fibers and then releasing the UNG as it dissolves away.

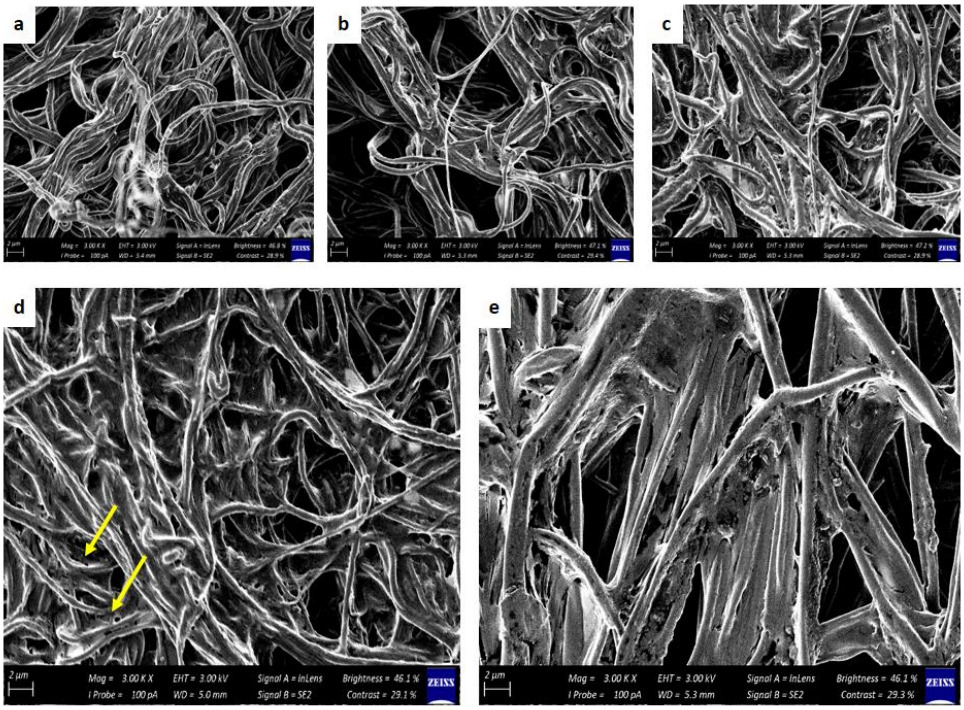


**Figure 26**. PLA/PEG/UNG1%-5 fibers after 1 (a), 2 (b) and 3 days of exposure (c), PLA/PEG/UNG1%-13 after 1 day exposure (d), and PLA/PEG/UNG1%-26 after 2 day exposure (e) (Moeini et al., 2020c)

Pores were detected in the entire fibers surface, it could be resulted from using high volatility solvent like DCM and it takes place when a rapid stage of phase separation happened during the solvent evaporation in the electrospinning process (Bognitzki et al., 2001). The porosity percentage of PLA/PEG fibrous showed slightly decrease in the porosities (from 98.68% to 95.83%) as concentration of PEG increased from 5 to 26% **(Table 12)**. Thus, in the presence of ungeremine in PLA/PEG/UNG blends fiber the further decrease in porosity volume was observed. Similar result was observed by (Serra et al., 2014).

**Table 12.** Porosity of the electrospun mats and mean fibers diameter (Moeini et al., 2020c)

| Sample name | Porosity (%) | Mean fiber diameter (µm) | Sample name | Porosity (%) | Mean fiber diameter (µm) |
|---|---|---|---|---|---|
| **PLA** | 96 | 1.576±0.206 | **PLA/UNG** | 92.02 | 0.278±0.028 |
| **PLA/PEG5** | 98.68 | 0.938±0.111 | **PLA/PEG/UNG1%-5** | 98.48 | 0.697±0.070 |
| **PLA/PEG13** | 97.55 | 0.865±0.101 | **PLA/PEG/UNG1%-13** | 96.96 | 0.802±0.093 |
| | | | **PLA/PEG/UNG2%-13** | 96.98 | 0.388±0.033 |
| **PLA/PEG26** | 95.83 | 1.486±0.132 | **PLA/PEG/UNG1%-74** | 95.15 | 1.194±0.134 |

***Wettability test***

To find out the influence of PEG on the electrophilicity of the PLA polymer matrix, the wettability of PLA, PLA/PEG5, PLA/PEG13 and PLA/PEG26 have been investigated by means of contact angle test (**Fig. 27)**. The obtained result showed the hydrophobic properties of PLA mats due to the preservation of the spherical shape of a water drop with 121° (±2.29). The hydrophilicity of the PLA/PEG electrospun blends were improved from 121° (±2.29) to 104° (±3.31) by increasing the percentage of PEG. It might be explained with the use of PEG into the polymer matrix thanks to its water solubility property. The addition of UNG into PLA and PLA/PEG blends did not have any crucial effect on the wettability of the fibers and almost similar contact angle degrees were observed 107° (±2.59) in all fibers in the presence of ungeremine. This could be explained because the deposition of UNG probably mainly occurs on the surface of the electrospun fibers.

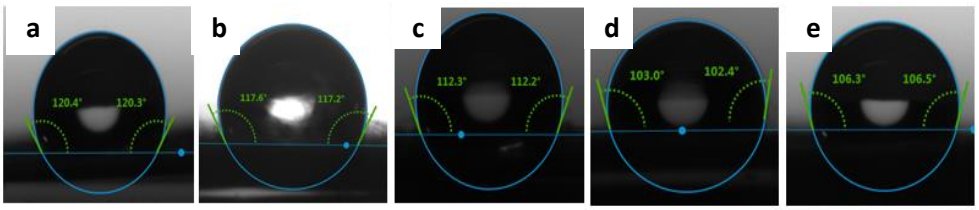


**Figure 27.** The contact angle of electrospun fibers: PLA (a), PLA/PEG-5 (b), PLA/PEG-13 (c), PLA/PEG-26 (d) and PLA/PEG/UNG1%-26 (as an example) (e) (Moeini et al., 2020c)

## 5.6. Physical-chemical characterization of PLA/α-CA films[16] (Moeini et al., 2020d)

***Structural and morphological analyses: Attenuated Total Reflection Fourier Transform Infrared Spectroscopy (FTIR-ATR), Nuclear Magnetic Resonance Spectroscopy ($^1$HNMR, Scanning Electron Microscopy (SEM) and Gel Permeation Chromatography (GPC)***

In neat PLA, peaks at 2992 and 2952 $cm^{-1}$ were related to CH asymmetric and symmetric stretching vibration, respectively. As usually occurring in semi crystalline polyesters, the stretching band of carbonyl group (-COO-) is composed of two overlapping peaks, often discernible following a deconvolution. In neat PLA, it is possible to detect a relatively broad band centered at approximately 1776 $cm^{-1}$, occurring as a shoulder of a sharper and more intense band at about 1746 $cm^{-1}$ **(Fig. 28a)**. Previous studies showed that the above mentioned peaks arise from the amorphous regions and crystalline domains of ester carbonyl groups stretching of the polymer, respectively (Dong et al., 2004; Mallardo et al., 2016; Molinaro et al., 2013; Nibler, 1978).

The $–CH_3$ bending vibration was found at 1450 $cm^{-1}$, whereas –CH symmetric and asymmetric deformations could be found at 1382 and 1359 $cm^{-1}$ (Salmieri et al., 2014). The peaks found at 1127, 1090 and 1042 $cm^{-1}$ corresponded to C-O stretching vibration (Pamula et al., 2001). Finally, in finger print region, two bands at 868 and 755 $cm^{-1}$ were related to C-C stretching vibration of, respectively, amorphous and crystalline phase of PLA, **(Fig. 28b)** (Molinaro et al., 2013).

In neat α-CA, the broad multipeaks between 2500-3000 $cm^{-1}$ were referred to both –CH and OH group stretching vibrations. The band at 1687 $cm^{-1}$ was ascribed to the stretching vibration of the carboxyl group conjugated. The peak at 1621 $cm^{-1}$ was associated to the segmental vibration of the conjugated methylene group C=C (see **Fig. 28c)**; this is

[16] This part has been done at Stellenbosch University at Department of Chemistry and Polymer Science in collaboration with CNR- IPCB- Institute for Polymers, Composites and Biomaterials and has been published in: Moeini, A.,Van Reenen,A., Van Otterlo,W., Cimmino, A., Masi, M., Lavermicocca, P., Valerio, F., Immirzi, B., Santagata, G., Malinconico, M., & Evidente, A. (2020). α-costic acid, a plant sesquiterpenoid from Dittrichia viscosa, as modifier of Poly (lactic acid) properties: a novel exploitation of the autochthone biomass metabolite for a wholly biodegradable system. Industrial Crops and Products (In press).

confirmed by the absorption bands in the range of 650-740 $cm^{-1}$ (last peaks not shown) (Bawdekar and Kalkar, 1965).

In order to consider the physical interaction occurring between PLA and α-CA, since the overlapping of most of the main functional groups peaks, the corresponding spectra comparison was not enlightening. Anyway, in order to obtain qualitative information related to their likely physical interaction, a subtraction spectrum between PLA/α-CA and PLA profiles was done and the result was reported in magnified absorbance scale. This approach, previously reported by Mallardo et al, and Santagata et al., allowed to put in evidence some peaks previously covered by more intense stretching vibration bands. In particular, the analysis of subtraction curve evidenced the appearance of a broad–OH groups peak, in the range of 3000-3500 $cm^{-1}$, likely due to hydrogen bonding occurring between the polar residues of the blend component (**Fig. 29a**, red circle) (Thirmizir et al., 2011; Mallardo et al, 2016; Santagata et al., 2017). As far as carbonyl two interesting modifications of the stretching modes were observed by spectral subtraction curve (red curve) in **(Fig. 29b),** following to PLA/α-CA interaction: the first one was related to the appearance of PLA amorphous fraction band at 1757 $cm^{-1}$, at the expense of crystalline band decreasing while the second worthy change was related to the broadening and shift of PLA/α-CA carbonyl group peaks towards higher frequency. The increasing of PLA amorphous carbonyl group suggested that, the interaction with α-CA, resulted in the prevalence of larger amorphous fraction. The enhancement of PLA amorphous region and the shift towards lower vibrational (1757 $cm^{-1}$) with respect to neat PLA (1776 $cm^{-1}$), could be due to α-CA plasticizing action; indeed, α-CA, interposing between PLA macromolecular chains, induced the free volume increasing, the heightening of macromolecular segments mobility of the amorphous region and the development of hydrogen bonding responsible of the decreasing of carbonyl stretching vibration frequency. Similar results were found by (Santagata et al., 2017).

Finalized to quantify the carbonyl content of both amorphous and crystalline regions of neat and doped PLA, a mathematical treatment, obtained by deconvolution in the Lorentzian-Gaussian function specifically was applied to the carbonyl bands at 1776 and

1746 $cm^{-1}$. The ratio between the peak areas of the carbonyl and of the reference band (–$CH_3$ bending vibration at 1450 $cm^{-1}$) was evaluated and the data reported in **Table 13.**

By the broadening of carbonyl groups and the corresponding appearance of low molecular weight functional compounds, such as ketone (1713 $cm^{-1}$) **(Fig. 29b)**, the hydrolytic degradation process induced by α-costic acid should be taken in account, as following evidenced by GPC analysis.

The $^{1}$HNMR spectra of PLA, α-CA and PLA/α-CA are shown in (**Fig. 30)**. The comparison of these spectra strongly supported the inclusion of α-CA in the film as the most significant protons $H_2$-13, H-3 and Me-14 were clearly observed in both spectra of α-CA and PLA/α-CA film.

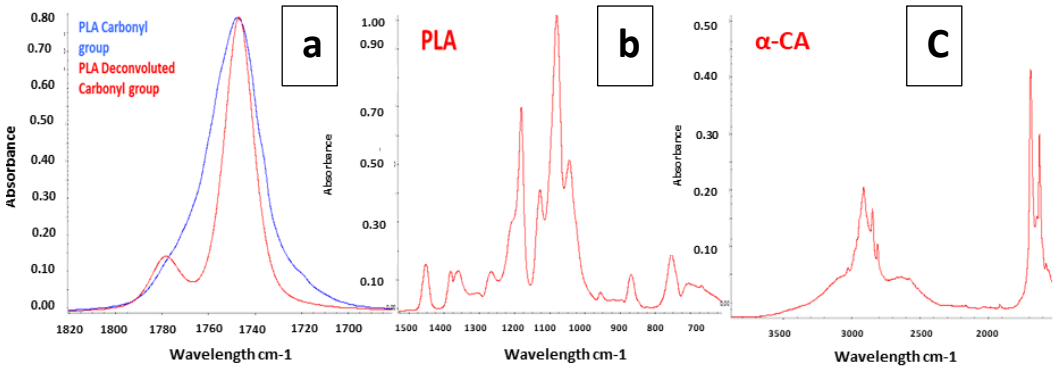


**Figure 28.** FTIR-ATR of neat PLA carbonyl group peak and its deconvolution by assuming mixed Gaussian-Lorentian function (a), neat PLA main absorption peaks (b), neat α-CA main absorption peaks (c) (Moeini et al., 2020d)

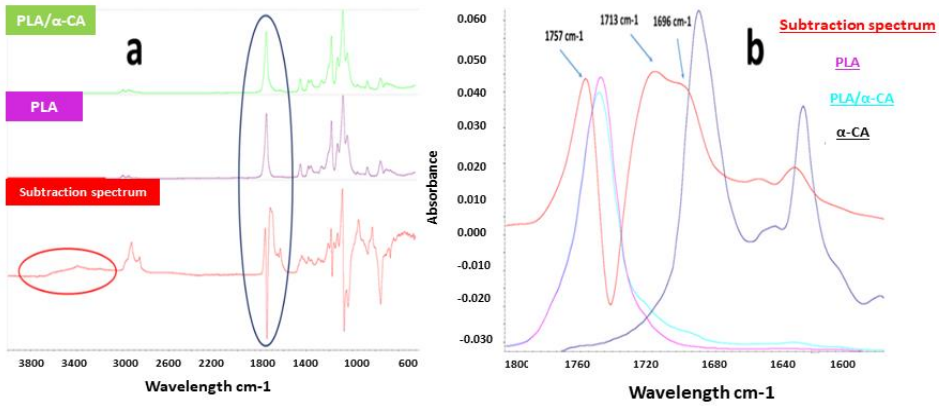


**Figure 29.** FTIR-ATR of PLA/α-CA (green curve), neat PLA (purple curve) and their spectral subtraction (a), carbonyl group of neat PLA (pink curve), neat α-CA (blue curve), PLA/α-CA (azure curve) and their spectral subtraction (red curve) in magnified absorbance scale (b). (Moeini et al., 2020d)

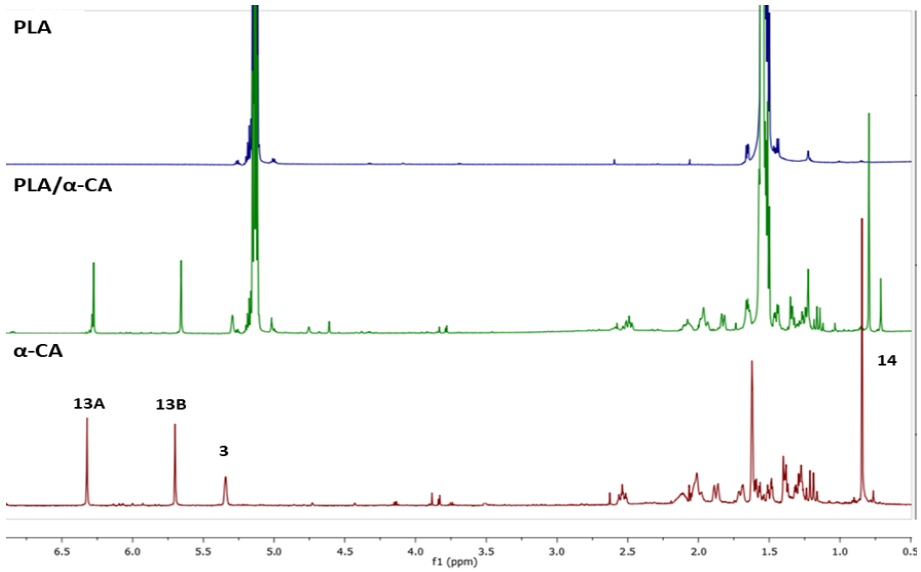


**Figure 30.** $^{1}$H NMR spectra of: poly(lactic acid) (PLA)(blue),α-costic acid (α-CA) (red) and PLA/α-CA (green) all recorded in $CDCl_3$ at 600 MHz. (Moeini et al., 2020d)

In (**Fig. 31)**, the micrographs of cryogenically fractured cross-sections of neat PLA **(Fig. 31a)** and PLA/α-CA **(Fig. 31b)** are reported. As shown in **(Fig. 31a)**, neat PLA showed an uneven and rough fracture surface, due to its brittle nature. Nevertheless, its morphology severely changed in presence of α-costic acid. In particular, from the analysis

of PLA/α-CA micrographs **(Fig. 31b)**, several discrete spherical micro-domains, distributed inside the polymeric matrix and regularly occupied by α-CA micro-particles could be evidenced. From **(Fig. 31b),** a heterogeneous surface topography was observed; indeed, the high concentration of micrometric deep coarsened interstitial cavities generally appeared as spherical polymeric microstructure domains in which α-CA particles were well implanted. The shear-yield associated with different surface fracture directions and the absence of brittle cracks, likely due to a plastic deformation occurring, evidenced a fair interfacial adhesion between the polymeric matrix and the plasticizer (green circles) ascribed to their physical interaction. Nevertheless, it was alongside possible to highlight some sporadic dark voids owed to α-CA droplets debonding phenomenon, occurring during the cryogenically film surface delamination (red circles).

The peculiar PLA/α-CA microstructure was responsible of PLA tailored performances, as following detailed. Similar results were found by (Ali et al., 2009).

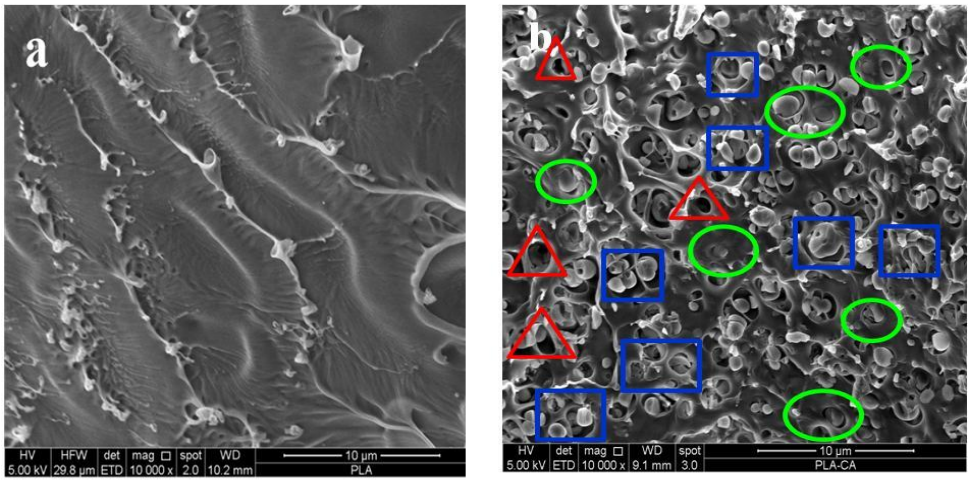


**Figure 31.** SEM micrographs of PLA(a), and PLA/α-CA (b) cross sectional surface**.** (Moeini et al., 2020d)

In **(Fig. 32)**, the chromatograms reproducing the molecular weight fraction of molecules, related to viscosity, as a function of PLA (red line) and PLA/α-CA costic acid (violet line) molecular weight are reported, whereas in **Table 13**, the average molecular weight (Mw), the number average molecular weight (Mn), the peak molecular weight (Mp), the viscosity

(η) evaluated by Mark-Houwink equation and the refractive index increment, dn/dc, are detailed. From the analysis of data related to PLA/α-CA, it is worthy to highlight a drastic decreasing of the average molecular weights and the peak molecular weight. In particular, Mn dropped to 10 kDa, the viscosity was reduced by half and the value of dn/dc pointedly changed. It is interesting to mark that in neat PLA the value of dn/dc was in good agreement with literature data (Malmgren et al., 2006), while in doped PLA a slight decreasing could be observed. It is worthy to highlight that the samples evidenced marked differences in the region of the low molecular weight fractions (**Fig. 32** and **Table 13**). Actually, it is well known that PLA is susceptible to hydrolytic degradation likely due to some water preserved into the sample during PLA processing for film preparation (Dong et al., 2013). At the same time, it is widely demonstrated that the presence of a plasticizer, by increasing the molecular mobility of the polymer, can speed up the water diffusion rate into the PLA molecules thus enhancing its hydrolytic degradation, which in turn results in a material with a somewhat lower molecular weight (Tsuji, 2010).

Hence, the physical interaction occurring between α-CA and PLA might be responsible of a random hydrolytic cleavage of ester linkages inducing a reduction of the average molecular weights (McKeen, 2012).

**Table 13.** GPC results and Carbonyl indices (CI) of amorphous and crystalline phase of PLA and PLA/α-CA samples (Moeini et al., 2020d)

| Sample | $(M_n)^-$ (Da) | Mw (Da) | Mp (Da) | η (dL/g) | CI | | dn/dc |
|---|---|---|---|---|---|---|---|
| | | | | | Crystalline (1746/1450) | Amorphous (1776/1450) | |
| **PLA** | 78408 | 100523 | 91964 | 1.67 | 2.51 | 0.28 | 0.023 |
| **PLA/α-CA** | 10046 | 77650 | 72668 | 0.82 | 2.16 | 0.36 | 0.018 |

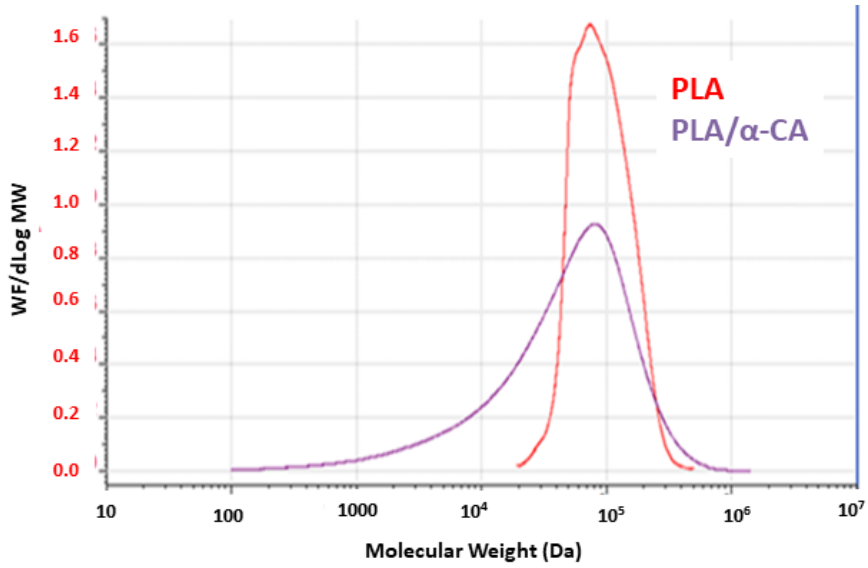


**Figure 32.** PLA (red curve) and PLA_α-CA (violet curve) macromolecular weight fraction (WF) related to viscosity (dLogMW), as a function of sample molecular weight (Moeini et al., 2020d)

***Differential Scanning Calorimetry (DSC)***

The thermal history of samples was erased by the preliminary heating cycle. The DSC thermograms recorded during fast cooling ramp and second heating of PLA and PLA/α-CA films are reported in (**Fig. 33)**, whereas the isotherm crystallization step at 110 °C followed by the second heating run are detailed in (**Fig. 34)**. All data derived from DSC analyses are reported in **Table 14**.

The glass transition temperature (Tg) is an excellent indicator of chain mobility, thus plasticizing efficiency was evaluated by measuring the decrease of Tg. From thermograms of (**Fig. 34)** and **Table 14**, it is worthy to highlight a significant dropping down of PLA glass transition temperature of about 11 °C, thus evidencing the plasticizing effect carried out by α-CA on the polymer matrix. As expected, the low molecular size of the plasticizer allowed it to engage the intermolecular spaces between polymeric chains, in this way both decreasing the inter-intra macromolecular chains hydrogen bonding, and reducing the energy needed for macromolecular motion, which in turn encouraged the free volume and the polymeric segments mobility increasing (Arias et al., 2013; Labrecque et al., 1997;

Murariu et al., 2008; Ren et al., 2006). Moreover, from **(Fig. 33)**, it is worthy to note that, in the second heating cycle, neat PLA chains gained enough mobility to disentangle from the amorphous phase rearranging in an ordered 3-D crystallites. The cold crystallization process ($T_{cc}$=127 °C) did not involve the formation of stable orthorhombic α-crystals, since, once formed, the crystallites were suddenly followed by the main melting phenomenon occurring at 148 °C (Cho and Strobl, 2006; Iannace and Nicolais, 1997). As concerning PLA/α-CA system, no melting and cooling crystallization phenomena were observed after the quenching from melt and second heating run. Probably the fast cooling hampered high melting crystallite to form, but also the cold crystallization was inhibited, thus indicating that the crystal growth of PLA chain was hindered in presence of the plasticizer. This result is, in some way, in contradiction with the results of literature data, evidencing that most of the plasticizers act like nucleating agent of PLA, able to promote its crystallization. To this aim, a high molecular scale miscibility is required to accomplish the strong enhancement of PLA chain mobility, responsible of crystalline nuclei formation (Arias et al., 2013; Dharmalingam et al., 2015; Pillin et al., 2006).

Crystallization kinetics of PLA and PLA/α-CA systems was also investigated in isothermal conditions to better understand PLA/α-CA bulk behavior. A temperature at which all the analyzed samples crystallize in a reasonable time was selected, to better compare their crystallization behavior. The isothermal crystallization at 110 °C for 30 minutes and the traces upon heating at 10 °C/min, are reported in **(Fig. 34 a,b)**, respectively. A very broad predictable crystallization peak could be observed for plain PLA (**Fig. 34a**) which occurred during all the isothermal time, followed by a sharp melting of thermally stable α-crystalline form (**Fig. 34b**). For PLA/α-CA, a very slight cold crystallization followed by two endothermic peaks associated to re-melting of the newly formed low crystallite during second heating was observed (Hwang et al., 2012; Lee and Lee, 2005; Soto-Valdez et al., 2011). Anyway, the highest melting temperature is observed for neat PLA (Tm=148 °C), thus indicating that neat sample had the highest crystallite average size, whereas plasticized PLA, forming lower crystallites, evidenced the main melting phenomena at lowest temperature (Tm≈142 °C). These outcomes could be likely

elucidated by considering that, besides working like a plasticizer, α-costic acid induced a drastic decrease of PLA molecular weight, as previously shown by GPC data, and this, in turn, could account for its noticeably different thermal behavior.

**Table 14.** Thermal properties of neat PLA, PLA/α-CA and α-CA films measured by DSC and TGA (Moeini et al., 2020d)

| Sample | $T_g$ (°C) | $\Delta H_{cc}$ (J/g) | $T_{cc}$ (°C) | $T_m$ (°C) | $\Delta H_m$ (J/g) | $\Delta H_c$ 110 °C (J/g) | $\Delta H_m$ 110 °C (J/g) | $T_{onset10\%WL}$ (°C) | $T_{peak}$ (°C) |
|---|---|---|---|---|---|---|---|---|---|
| **PLA** | 61 | 6.7 | 127 | 148 | 4.9 | 27.4 | 24 | 310 | 360 |
| **PLA in PLA/α-CA** | 52 | | 118 | 142<br>148 | | 1.9 | 0.3<br>0.1 | 300 | 350 |
| **α-CA** | - | - | - | - | - | | | 150 | 260 |
| **α-CA in PLA/α-CA** | | | | | | | | 200 | 280 |

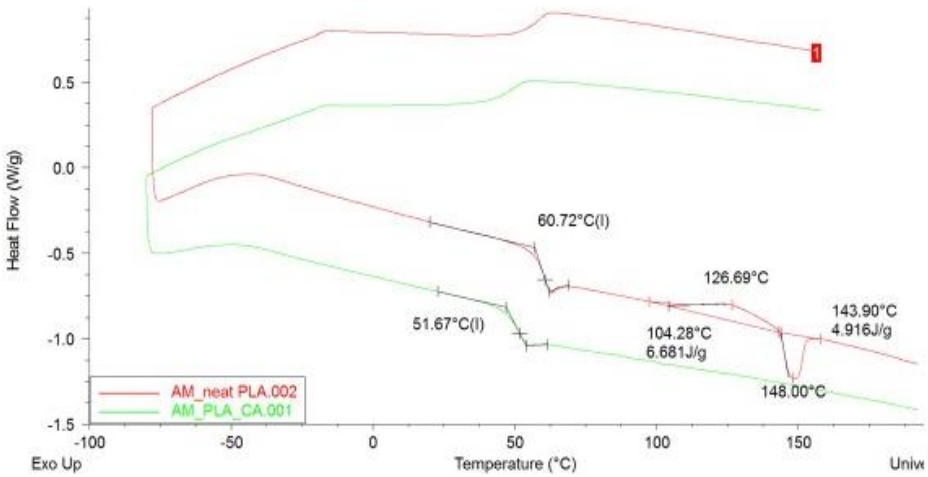


**Figure 33.** DSC thermograms of PLA and PLA/α-CA melt crystallization and second heating cycle (Moeini et al., 2020d)

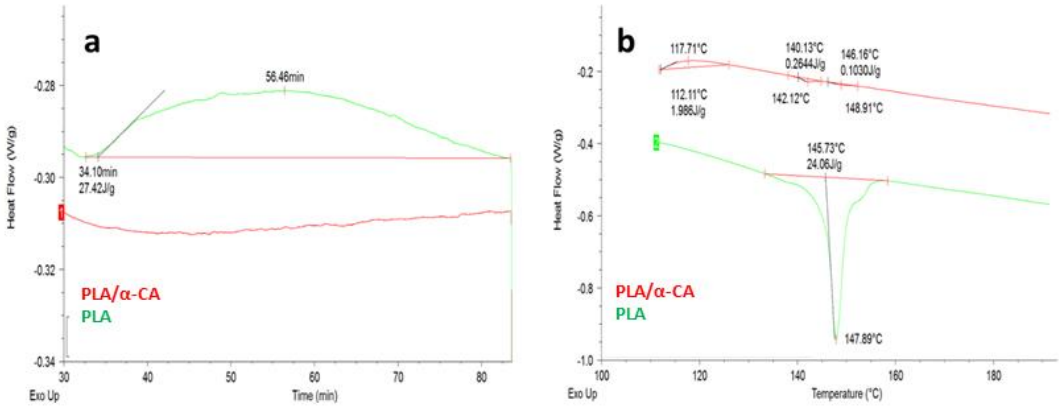


**Figure 34.** DSC thermograms of PLA and PLA/α-CA during isotherm step at 110 °C (a) and second heating cycle (b) (Moeini et al., 2020d)

***Thermogravimetric Analysis (TGA)***

TGA thermograms of α-CA, PLA and PLA/α-CA samples and their first derivatives curves (DTG) are reported in (**Fig. 35a,b).** All the curves were normalized with respect to starting sample weights and the main thermal parameter. The onset of temperature degradation ($T_{onset}$) and the temperature of maximum degradation rate ($T_{peak}$), detectable from DTG curves, are summarized in **Table 14**. From the analysis of the thermograms, it is worthy to observe that both PLA and α-CA followed a single step of thermal degradation, characterized by a harsh difference in both $T_{onset}$ and $T_{peak}$, accounting for the higher thermal stability of the neat polymer. As regarding PLA/α-CA system, the thermal behavior is markedly different from the neat both polymer and plasticizer. Indeed, it is worthy to observe that degradation kinetics profile of PLA/α-CA system (**Fig. 35b**) was characterized by only one broad thermogram, thus indicating that PLA and α-CA followed quite the same degradation profile. This outcome could point out a farly bulk miscibility between the polymer and the plasticizer, as previously found and discussed (Russo et al., 2010), according with the physical interaction occurring between the polar groups of both polymer and plasticizer. In addition, the α-costic acid was thermally stabilized, as evidenced by the shift of both $T_{onset}$ and $T_{peak}$ towards higher temperatures (see **Fig. 35** and

**Table 14**). The analysis of **(Fig. 35)** and **Table 14** showed that α-costic acid played a slight thermal pro-degrading effect on PLA. Actually, in TGA and DTG thermograms of PLA/α-CA system some bound water evolution at around 110 °C, that could trigger hydrolysis phenomena of the polymer, as previously evidenced by GPC data were highlighted (Fortunati et al., 2012; Russo et al., 2007; Silverajah et al., 2012; Wang et al., 2012).

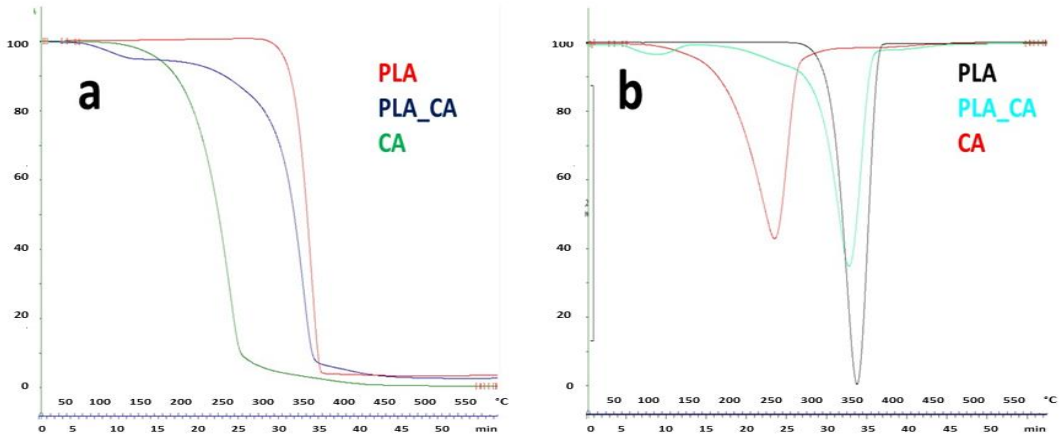


**Figure 35.** TGA (a) and DTG (b) curves of PLA, α-CA and PLA/α-CA films (Moeini et al., 2020d)

### *Tensile test*

The key goal of a plasticizer inclusion into PLA matrix is to improve its mechanical performance, by decreasing the stiffness and increasing the ductility. **Table 15** summarizes data of tensile test. As widely reported, neat PLA is a brittle polymer since it failed as soon as it passed the yield stress; so it showed a high elastic modulus and a very low elongation at break (Ljungberg and Wesslén, 2005; Wu et al., 2014). The stiffness of PLA could be explained by lack of strain-induced softening upon drawing. Usually, under force action, the polymers strain softening stimulates strain localization causing the build-up of local tri-axial stresses. If the local strain is not delocalized, this local tri-axial stresses will induce void nucleation responsible of the matrix failure; this behavior is typical of brittle polymer, like PLA (Tariq et al., 2015). The inclusion of α-CA into PLA matrix produced significant

changes in the mechanical properties of the film, by increasing both the tensile strength and the strain at break of the resulting blend. The high tensile strength could be explained by the strong interphase interaction between PLA and α-CA, which in turn reduced the stress concentration points when tensile load was applied. Indeed, the quite homogeneous distribution of α-CA molecules between the polymeric chains, allowed preserving the macromolecular entanglements upon the force action, since the applied stress was regularly delocalized along the chain orientation. The improvement of PLA toughness was responsible of a higher tenacity, furthermore supported by a significant increasing of polymer ductility.

Indeed, the addition of the plasticizer caused a progressive decreasing of the elastic modulus in favor of an enlightened rising of strain at break (Finkenstadt and Liu, 2009; Fortunati et al., 2012; Vanstrom Joseph Robert, 2012). This result was consistent with a more heightened slithering of macromolecular chains under the force action, since the homogeneous distribution of α-CA molecules among the polymeric matrix. Thus, α-CA, reducing the intermolecular forces between macromolecular chains and increasing their mobility, enhanced the flexibility and extensibility of the film, as resulted by the surge increasing of strain at break. Similar results were also found by (Wang et al., 2012).

**Table 15.**Tensile strength ($\sigma_{Max}$) and elongation at break ($\varepsilon_b$), work at maximum load and maximum load of neat PLA and PLA/α-CA (Moeini et al., 2020d)

| Sample | E (MPa) ±10% | $\sigma_{break}$ (MPa) ±5% | $\varepsilon_{break}$ (%)±10 |
|---|---|---|---|
| **PLA** | 2511 | 10.9 | 7.6 |
| **PLA/α-CA** | 1883 | 16.4 | 206 |

***Surface wettability: water contact angle (WCA) measurements***

In (**Fig. 36)** the plot of water contact angle (WCA) of neat and doped PLA is reported. The measured θ value of neat PLA film was 87.18 (±3.20)°, evidencing the high PLA both hydrophobicity and surface energy due to low polar group concentration (Aldana et al., 2014). The inclusion of α-CA in PLA matrix, an enhanced hydrophilicity was detected, as showed by the dropping down of WCA value to 77.72 (±2.58)°. This outcome, translated

in lower surface energy and higher surface contact between the substrate and the water drop, could be explained with the polar moieties increasing, due to both α-CA carboxylic groups and to polar terminal groups of PLA low molecular weight fractions, following to polymer hydrolysis (Stloukal et al., 2015).

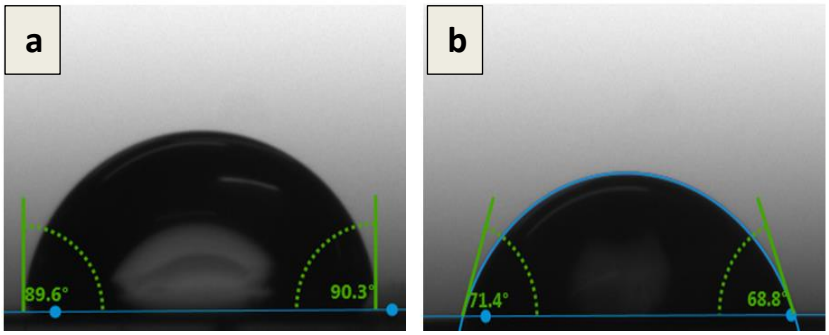


**Figure 36.** Water contact angle test neat PLA (a), and PLA/α-CA film (b) (Moeini et al., 2020d)

## 5.7. The NOVAMONT Stage[17]

### 5.7.1. Result and Discussion

The company stage started with the synthesis of ungeremine (UNG), and it synthesized by green methods through oxidation with $SeO_2$. However, the method developed to withdraw all disadvantages of the previous method, such as being time-consuming, wasting chemicals, more importantly, wasting many of the final products, especially for synthesis on a larger-scale. Indeed, in the previous method pure UNG obtained by the crystallization of basified UNG, necessitated frequently filtration followed by crystallization with the solvent that took at least three weeks for obtaining a low amount of pure crystal of UNG. In the new methods after finishing UNG synthesis, the solvent filtrated by WHATMAN(TM) MEMBRANE FILTERS, PTFE, 0.2 μm to removed Selenium (Se) trace and then pure UNG obtained by lyophilization of basified UNG solution. The UNG purity obtained in this method was almost similar to the crystal of UNG confirmed by

[17] This part has been done at Novamont Company.

HPLC. By the developed method, each gram of UNG could obtain in 5 days with 98% of efficiency[18].

The first trials before the scaling up production of CH/TPP microparticles were done according to the previous experiences, published at Carbohydrate polymers (Moeini et al., 2018). The CH/TPP microbeads manufactured in different ratios CH/TPP-1 (1:12), CH/TPP-2 (1:6), CH/TPP-3 (1:4), CH/TPP-4 (1:2) and CH/TPP-5 (1:1) to investigate and compare different chemical-physical properties of microbeads and select the most promising one for scaling up. However, thermogravimetric analysis and ATR spectra of all the samples were almost similar to the microbeads obtained by curing method (the ATR result not repeated (Moeini et al., 2018). Anyway, CH/TPP-3 was selected as the main sample because of its better antifungal properties against *P. roqueforti* according to the literature (Moeini et al., 2018).

The next step was scaling up production of CH/TPP-3 microbeads. To achieve this, various parameters such as controlling the medium pH, the amount of mother liquor (used for the curing process), and the particle size were taken into consideration. After many trials and examination of each parameter separately, the optimized condition has found in which beads productions scaled up about 800 times more than the first production in the laboratory (from 25 mg to 20 grams for each batch). Besides, all other important parameters have successfully controlled. Indeed, the final pH was 6.2, the lowest quantity of water used, and the production time kept constant (5 days for each batch).

The challenge appeared after the formulation of microbeads into Novamont polyester (NPS) polymer matrix. Indeed, brown colors and smell of bread and acetic acid of the extruded pellets could be a sign of degradation most likely due to the presence of acetic acid (AcOH) residual in the microparticles. To face this drawback, some parameters got changed for example the concentration of acetic acid was decreased to 1% (from 2%), after

[18] Based on the Novamont Company Safety policy, and protecting employees from the health issue and because ungeremine did not have a safety data sheet by the decision of Dr. Capuzzi (the project supervisor in the Company), the synthesized ungeremine during this stage did not allow using for the formulation.
**P.S.** All the ungeremine was backed to Professor Evidente's Lab.

completing swelling process mother liquor was removed, and finally, the lyophilized particles was kept into the vacuum oven at 65 °C before extruding for two weeks. The effect of decreasing AcOH in next extrusion could see by the visual observation from the extruded pellets smell and their white color. It was clear that the quantity of acetic acid significantly decreased. Although, AcOH trace could not be completely removed from the microbeads. It might be explained AcOH takes an active part in CH/TPP network structure during the swelling process. In this spite, microbeads were successfully formulated into the two MBi grades (starch-based and transparent) by film blowing methods and showed even distribution in the matrices. However, the lack of compatibility of microbeads with the polymer matrices resulted in microbeads formulated films have a rough surface.

Thanks to the wide range of properties such as being bioactive for the food packaging (Cruz-Romero et al., 2013; Kong et al., 2010; Tripathi et al., 2009) and thus, finding an alternative to solve the microbeads formulation obstacles (acetic acid, incompatibility and size). Chitosan was directly formulated in the starch-based formulation through extrusion and film blowing, to study chitosan impact on the starch-based films. The branching diagram of the entire processing steps summarized in **(Fig. 37)**.

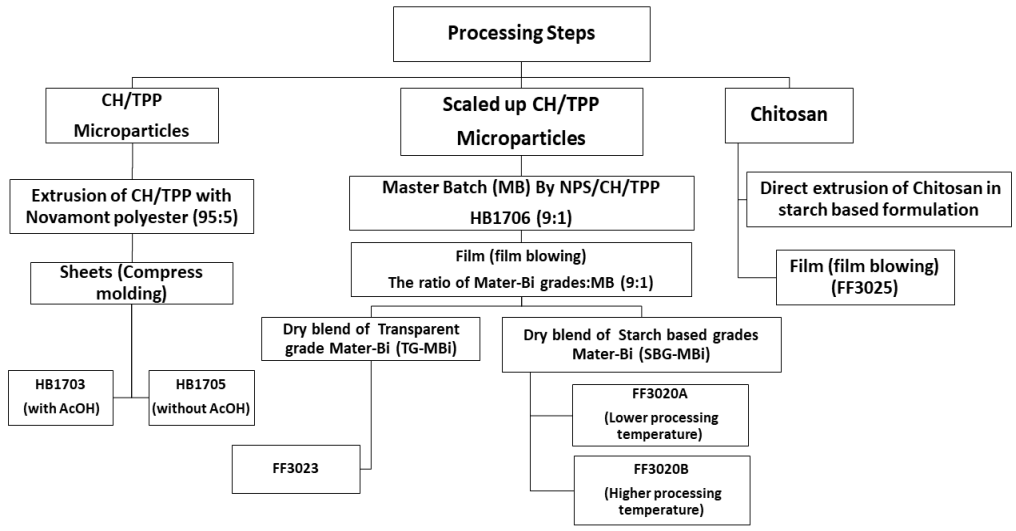


**Figure 37.** The Processing steps done in Novamont Company (Novara)

**Thermogravimetric analysis (TGA)**

***CH/TPP micro beads***

Thermogravimetric analysis represents a valid tool to evaluate the thermal degradation pattern of a polymeric system; in the specific case, it is possible to highlight the different water adsorption of the samples, as well as the physical interaction occurring between the components of the obtained biocomposites (El-hefian et al., 2012). **Table 16** reported the temperature of the main degradation steps ($T_{1onset}$°C and $T_{2onset}$ °C), and the temperature of maximum degradation rate ($T_{peak}$ °C).

As already reported in literature data and evidenced in our previous publication. CH/TPP microbeads showed three mass loss stages the first from room temperature to about 100 °C, the second between 100 °C and about 200 °C, and third at temperatures above 200 °C, attributed to the evolution of free water, freezable bound water and to the polysaccharide degradation respectively (Higuchi and Iijima, 1985; Moeini et al., 2018). The presence of water could be due to the crosslinking process of the beads occurring during the swelling in TPP water solution. Indeed, probably some water could be physically entrapped in CH/TPP three-dimensional network (Russo et al., 2007). The study on the microbeads thermograms showed that the percentage of absorbed water influenced by the amount of chitosan: The higher the concentration the higher water content (**Table 16**).

The first polysaccharides decomposition observed above 200 °C includes a random splitting of the glycosides bonds, vaporization, and elimination of volatile products (Nieto et al., 1991).

**Table 16.** Sample identification codes: Weight Loss % at 150°C ($W_L$%150°C), Onset of main temperature degradation steps ($T_{1onset}$°C), ($T_{2onset}$°C), Temperature of maximum degradation rate ($T_{peak}$°C)

| Sample | $W_{.L}$ $\%_{150}$°C | $T1_{onset}$°C | $T2_{onset}$°C | $T_{peak}$°C |
|---|---|---|---|---|
| **CH** | 7.0 | - | 250 | 316 |
| **CH/TPP (Scaled-up)** | 8.1 | 165 | 230 | 281 |
| **CH/TPP-4** | 9.2 | 169 | 240 | 281 |
| **CH/TPP-5** | 9.7 | 171 | 248 | 290 |
| **CH/TPP recovered from sheets** | 7.4 | 161 | 240 | 295 |

The observation from the degradation profile of the films (DTG curves) showed two degradation steps in CH/TPP samples, evidenced by $T1_{onset,}$ $T2_{onset}$. The first one could ascribe to the loss of the strongly bound water, as previously discussed and confirmed by literature data. In addition, the cross-linked beads induced a substantial hastening of the thermal decomposition process due to the weakening of intra-inter-molecular hydrogen bonds of CH chain pack (Kim and Lee, 1993; Neto et al., 2005; Russo et al., 2007), as a consequence of the stronger interaction occurring between chitosan and TPP. Hence, the cross-linked chitosan resulted more exposed to the bond splitting and thermal degradation than neat CH.

The effect of the extrusion and compression molding processes on the thermal properties of CH/TPP microparticles was studied by recovering the microparticles from NPS by removing polymeric matrix via its dissolution. As evidenced in **Table 16**, the microparticles preserve their thermal stability even after bearing high pressure and temperature stress. The decreasing of water content and releasing, as expected after double thermal process was observed. Therefore, it could result that cross-linked beads were stable enough to be used for the thermal formulation methods like compress molding and blow filming.

***Sheets***

In **Table 17**, the thermal parameters related to NPS based composites, are detailed. The NPS and NPS/CH/TPP (95:5) sheets have been produced by extrusion and compression molding steps. The thermograms analysis of the sheets showed that the samples roughly lost 3% of the total mass probably related to water molecules desorption at about 100 °C. It is possible to observe that the degradation pattern of NPS follows two different steps, likely related to the complex structure of the polyester. In presence of 5% w/w of CH/TPP microparticles in HB1705 formulation, all the thermal parameters underwent to a worsening likely due to the incompatibility between polymeric matrix and dispersed phase. The microparticles likely disturb the regular packing of macromolecular chains, acting as discontinuity points of polymeric structure and rendering NPS easily susceptible to thermal degradation; this outcome expected in a composite based system where no good interaction

occurs between two different phases. Consequently, $T_{onset}$, $T_{peak1}$ and $T_{peak2}$ result lowered if compared to neat NPS. Anyway, when acetic acid is still present, in HB1703 formulation, both onset, and degradation kinetics strongly improved. The sample was more stable. This worthy outcome could be ascribed to the physical interaction, occurring by hydrogen bond, between the carboxylic group of acetic acid and carbonyl group or any other polar group of the polyester fraction. Therefore, acetic acid could act as a sort of physical compatibilizer, improving the interfacial adhesion between the polymeric matrix and CH-TPP particles. Hence, the presence of AcOH improved thermal stability by delaying both the onset and rate of NPS degradation.

**Table 17.** Temperature of maximum decomposition temperatures rate ($T_{peak1}$ and $T_{peak2}$), for the sheets

| **Samples** | **$T_{onset}$** | **$T_{peak1}$ (°C)** | **$T_{peak2.}$ (°C)** |
|---|---|---|---|
| **HB1702 (NPS)** | 260 | 416 | 503 |
| **HB1705 (95:5) NPS/CH/TPP (without AcOH)** | 237 | 407 | 496 |
| **HB1703(95:5) NPS/CH/TPP (with AcOH)** | 270 | 421 | 545 |

***Films***

As far as film-based systems are concerned, the influence of CH/TPP particles on the polymer matrix was more complex **(Table 18)**. The main decomposition processes of the SBG-MBi films was observed in the range of 280-340°C, probably associated with the degradation of the starch fraction (Cerruti et al., 2011), corresponding to about 20%-30% of weight loss. The polyester segments degradation started at higher temperature, around 350 °C with about 65% mass loss (Moriana et al., 2008; Puglia et al., 2003; Ramis et al., 2004; Wang et al., 2003). In SBG-MBi system, the degradation pattern influenced by the processing temperature. In particular, at a lower temperature (FF3020A), the samples started to degrade before, likely due to the presence of some water traces inducing

degradation. Nevertheless, concerning sample FF3020B, the onset was shifted to higher temperatures. Transparent grade (TG-MBi) films look similar to NPS based sheets. The incompatibility between the two phases of biocomposites induced a slight decreasing of $T_{peak3}$. Nevertheless, generally, the effect of CH/TPP particles on the thermal behavior of films was not so marked as in the case of sheets high likely because of using just 1% of the particles into the films.

**Table 18.** Temperature of maximum decomposition temperatures rate ($T_{peak1}$ and $T_{peak2}$), for the films.

| Samples | T(onset) | $T_{peak1.}$ (°C) | $T_{peak2.}$ (°C) | $T_{peak3.}$ (°C) |
|---|---|---|---|---|
| **FF3019 ( SBG-MBi )** | 232 | 314 | 412 | 510 |
| **FF3020A SBG-MBi/MB-A (9:1)** | 221 | 320 | 416 | 518 |
| **FF3020B SBG-MBi/MB-B (9:1)** | 265 | 315 | 411 | 503 |
| **FF3022 TG-Mbi** | 278 | --- | 409 | 542 |
| **FF3023 TG-MBi/MB (9:1)** | 256 | --- | 409 | 536 |
| **FF3024** | 243 | 316 | 407 | 497 |
| **FF3025 NPS-(CH-TPS) (9:1)** | 242 | 316 | 404 | 495 |

***Scanning electron microscopy (SEM)***

SEM analyses performed on the cross-sectional fracture of all films and sheets. The micrographs of the samples are shown in (**Fig. 38)**. All formulated samples (with CH/TPP microparticles or CH) had a rough and irregular surface in comparison to the neat ones. The unevenness of sample fracture surface is probably due to the presence of microparticles randomly distributed inside the polymeric matrix. Furthermore, the particles incompatibility could be seen in quite all sheet and films. However, in some composites, it could be observed a better embedding of CH/TPP microparticles inside the polymer matrix.

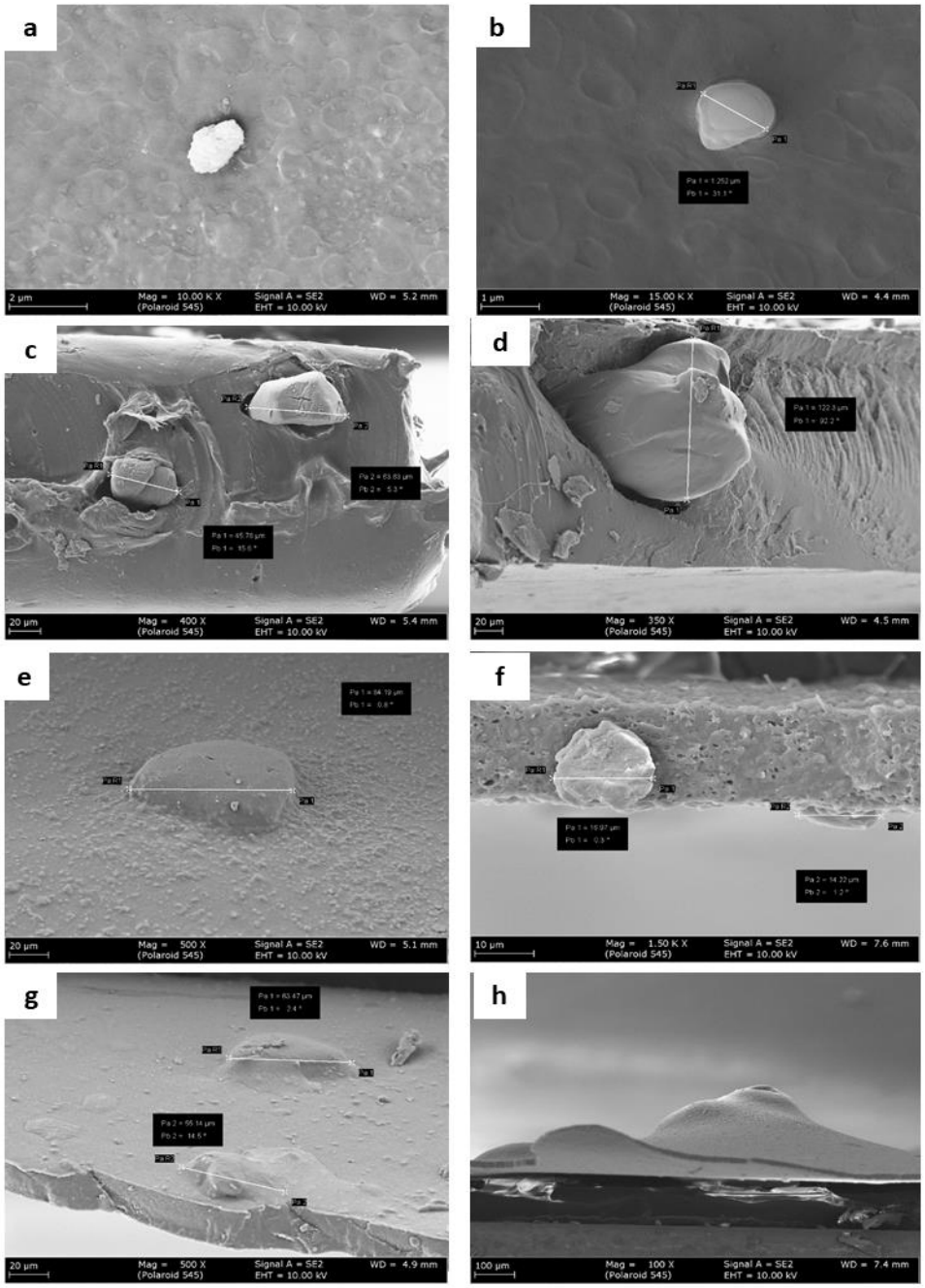


**Figure 38.** The morphograph of the sheets HB1705 (a, c and d), HB1703(b), and films FF3020B (f) FF3023(e,g) and FF3025(h)

In particular (**Fig. 38b)**, related to Sheet HB1703, (NPS)/CS-TPP (with AcOH), highlighted a good interfacial adhesion between NPS and dispersed phase, as a consequence of the presence of acetic acid; it is worthy to emphasize that there's a substantial difference between morphology of this sample and the one of Sheet HB1705 (NPS)/CH-TPP (without AcOH), reported in **(Fig. 38 a,c, and d)**. The structural properties of the compatibilized sheet confirmed the previous hypothesis related to the thermal performances of these samples. The samples FF3023 related to TG-MBi/MB (9:1) sample and reported in **(Fig. 38 e,g)**, evidence that the particles are well covered by the polymer; this outcome could be explained by considering the presence of plasticizers or additives in TG-MBi. On the contrary, the micrograph reported in (**Fig. 38f)**, does not suggest a good inclusion, as expected in a wholly separated system.

**Tensile Test**[19]

***Sheets***

Tensile tests were performed to investigate the influence of CH-TPP microparticles on mechanical performances of Novamont polyester (NPS) samples. The results are listed in **Table 19**. The analysis of data of all samples evidenced a starting elastic behavior followed by a plastic deformation up to sudden rupture of the samples. Due to the confidential information, neat sample (reference) tensile tests were considered 100% and all results have been expressed in percentage too. The mechanical properties of the biocomposites sheets were affected by the microparticles dispersion and by the physical or chemical compatibility between components of biocomposites, as widely reported in literature (Ratanakamnuan and Aht-Ong, 2006). In the specific case, the CH-TPP microparticles increased the elastic modulus of the sheet, as expected in composite based systems. It suggested that even 5% of microparticles increased the stiffness of the composites. Besides, upon tensile loading, the presence of microparticles induced a decrease in both stress and strain at break, thus evidencing that no mechanical stress transfer from matrix to dispersed phase occurred, as expected by incompatibilized systems.

[19] Because of confidential information, the Tensile Test data of the NOVAMONT reported with the percentage.

(Elfehri et al., 2015). Anyway, the sheets containing acetic acid highlighted an improvement of polymer-particles interphase reflecting on relative better tensile test properties in comparison with HB1705 sample without AcOH. This result is in accord with the TGA analysis evidencing an improved compatibility in HB1703 sheets.

**Table 19.** Young's modulus (*E*), stress at break ($\sigma_b$), Strain at break ($\varepsilon_b$), and energy at break (ASTM D1822) of the sheets

| Sample | E(%) | σ(%) | ε(%) | Energy at break |
|---|---|---|---|---|
| **HB1702 (NPS)** | 100 | 100 | 100 | 100 |
| **HB1703 (NPS)/CS-TPP sheets (with AcOH)** | 104±10 | 78±14 | 80±12 | 64±20 |
| **HB1705 (NPS)/CS-TPP sheets (without AcOH)** | 115±4 | 57±8 | 59±10 | --- |

***Films***

As shown in **Table 20**, all the films obtained by blow molding showed almost similar results expect for FF3025 which includes 1% of neat chitosan. The inclusion of microparticles and chitosan in transparent and starch-based grades of Materbi resulted in decreasing of both the tensile strength and strain at break. However, by considering the amount of additive and the results of the standard deviations of the formulated samples, the mechanical properties were almost similar to the references. The lower tensile strength could be due to the lack of interaction between microparticles and matrices, as before discussed and previously supported by TGA analysis. The effect of processing temperature could be seen by comparing FF3020A with FF3020B samples. The better mechanical properties observed in the sample FF3020B processed at higher temperatures could be explained by a better dispersion and interaction of the microparticles inside the polymeric matrix., particularly fostered at high temperature.

**Table 20.** Young's modulus (*E*), stress at break ($\sigma_b$), strain at break ($\varepsilon_b$), and energy at break (ASTM D1822) of the films

| Sample | E(%) | σ(%) | ε(%) | Energy at break | laceration resistance MD | laceration resistance TD |
|---|---|---|---|---|---|---|
| **FF3019 (SBG-MBi)** | 100 | 100 | 100 | 100 | 100 | 100 |
| **FF3020A SBG-MBi/(MB)A (9:1)** | 87±8 | 86±13 | 84±8 | 76±20 | 94±11 | 102±13 |
| **FF3020B SBG-MBi/(MB)B (9:1)** | 97±8 | 89±6 | 102±9 | 91±10 | 108±3 | 103±7 |
| **FF3022 TG-MBi** | 100 | 100 | 100 | 100 | --- | --- |
| **FF3023 TG-MBi/(MB) (9:1)** | 102±3 | 86±4 | 82±7 | 70±11 | --- | --- |
| **FF3024** | 100 | 100 | 100 | 100 | 100 | 100 |
| **FF3025 NPS-(CH-TPS) (9:1)** | 79 ± 8 | 71 ± 8 | 72 ± 9 | 54 ± 16 | 85 ± 13 | 72 ± 17 |

## 6. CONCLUSION

In this thesis, among 13 metabolites were isolated from bacterial, fungal, and plants, three of them (cavoxin, ungeremine, and α-costic acid) showed the highest inhibition against *Penicillium roqueforti* and *Aspergillus niger*, the most common mold of bakery products. The first metabolite was cavoxin, the HPLC method was developed to quantify the cavoxin. The qualitative and quantitative analysis of *Phoma cava* culture filtrates proved that cavoxin production in the stirred condition is significantly higher than the static one. The second metabolite was ungeremine (UNG), firstly encapsulated into the chitosan-tripolyphosphate (CH/TPP/UNG) microbeads and then formulated into the Mater-Bi (MBi) polymer matrix (MBi/CH/TPP/UNG) in both forms the microparticles and films showed 72 h of inhibitions against *P. roqueforti*. Additionally, ungeremine was directly formulated in poly lactic acid and polyethylene glycol (PLA/PEG/UNG) nanofibers. The releasing pattern showed an initial burst release of ungeremine presented in the PEG followed by a sustained release, indicated the ungeremine is present in both the PLA and PEG domains of nanofibers. During the Novamot stage, the synthesis of ungeremine was developed in accordance with large scale production. Besides, the CH/TPP microparticles were successfully scaled up and formulated into the starch-based, transparent and polyester-based grades of MBi by film blowing and compression molding methods. The mechanical tests of the sheets and films generally showed that microparticles increased the stiffness and decreased both stress and strain at break. Finally, α-costic acid (α-CA) was incorporated into polylactic acid (PLA). The Films did not have any antifungal activity due to the strong interaction between PLA and α-CA. Despite, α-costic acid could act as a plasticizer and improve both tensile strength and strain at break.

## 7. Acknowledgments

I gratefully acknowledge PON RI 2014-2020 Asse Prioritario I "Investimenti in Capitale Umano", Azione 1.1 "Dottorati Innovativi con caratterizzazione industriale - Dottorato in Scienze Chimiche XXXII ciclo, for supprting me. Thus, I would like kindly thank:
Professor Evidente that was always available.
Professor Van Reenen and Professor Van Otterlo from Department of Chemistry and Polymer Science, University of Stellenbosch, Stellenbosch, South Africa, who provided an environment in which I could completely focus on my project during my stage in South Africa that's why I could finish and publish three articles and one chapter during those 6 months.
Paola Lavermicocca, Francesca Valerio from Institute of Sciences of Food Production, National Research Council, Bari, Italy, who were responsible of biology part of my project.
Professor Alessio Cimmino from Department of Chemical Sciences, University of Naples "Federico II", whatever I learnt from the extraction, purification and characterization of natural products is because of him. Professor Angelina Lombardi the PhD coordinator with a great personality and always ready to help us, Professor Martino Di Serio my great examiner, Professor De Rosa and Finizia Auriemma who helped me to come in this great University.
Gianluca Anzelmo, Antonio Verdoliva Verna, Paolo Magistrali, Patrizio Salice, Ioanna Petrakou, Alessandro Montino and Giovanni Tettoni and other nice and friendly colleagues at Novamont that provided me a context to have these outcomes. I am also truly grateful to Dr. Luigi Capuzzi and Dr. Maria Dani because of supplying me such a great experience at Novamont Company.
In the end, special thanks to Professor. Mario Malinconico, Dr. Gabrialla Santagata, and Dr. Salvatore Mallardo from Institute for Polymers, Composites, and Biomaterials, National Research Council, Italy. Honestly, I was not able to finish this project without their support and motivation, particularly in the hardest time I faced during my project. Especially, Dear Dr. Gabrialla Santagata who was very compassionate and friendly like a mother, with her wise character, she was always available to help and advise me.

## 8. REFERENCES


Abou-Donia, A.H., Abib, A.A., El Din, A.S., Evidente, A., Gaber, M., and Scopa, A. (1992). Two betaine-type alkaloids from Egyptian Pancratium maritimum. Phytochemistry *31*, 2139–2141.

Aggarwal S, Pahuja S, R. (2013). Pharmaceutical relevance of crosslinked chitosan in microparticle drug delivery. International Research Journal of Pharmacy *4*, 45–51.

Ahmed, J., Varshney, S.K., Zhang, J.-X., and Ramaswamy, H.S. (2009). Effect of high pressure treatment on thermal properties of polylactides. Journal of Food Engineering *93*, 308–312.

Aldana, D., Castillo, H., Casarrubias, L., Cruz, Q., Villa, E., De Dios Hernández, M., Gallardo, S., and Sánchez, G. (2014). Barrier Properties of Polylactic Acid in Cellulose Based Packages Using Montmorillonite as Filler. Polymers *6*, 2386–2403.

Ali, F., Chang, Y., Choon Kang, S., and Yoon, J.-Y. (2009). Thermal, mechanical and rheological properties of poly (lactic acid)/epoxidized soybean oil blends. Polym. Bull. *62*, 91–98.

Alvarez, V.A., and Vázquez, A. (2006). Influence of fiber chemical modification procedure on the mechanical properties and water absorption of MaterBi-Y/sisal fiber composites. Composites Part A: Applied Science and Manufacturing *37*, 1672–1680.

Alvarez, V., A. RUSCEKAITE, R., and Vázquez, A. (2003). Mechanical Properties and Water Absorption Behavior of Composites Made from a Biodegradable Matrix and Alkaline-Treated Sisal Fibers. Journal of Composite Materials - J COMPOS MATER 37, 1575–1588.

Andolfi, A., Zermane, N., Cimmino, A., Avolio, F., Boari, A., Vurro, M., and Evidente, A. (2013). Inuloxins A-D, phytotoxic bi-and tri-cyclic sesquiterpene lactones produced by Inula viscosa: Potential for broomrapes and field dodder management. Phytochemistry *86*, 112–120.

Andolfi, A., Maddau, L., Basso, S., Linaldeddu, B.T., Cimmino, A., Scanu, B., Deidda, A., Tuzi, A., and Evidente, A. (2014). Diplopimarane, a 20-nor-ent-Pimarane Produced by the Oak Pathogen Diplodia quercivora. Journal of Natural Products *77*, 2352–2360.

Andolfi, A., Boari, A., Evidente, M., Cimmino, A., Vurro, M., Ash, G., and Evidente, A. (2015). Gulypyrones A and B and Phomentrioloxins B and C Produced by Diaporthe gulyae, a Potential Mycoherbicide for Saffron Thistle (Carthamus lanatus). Journal of Natural Products *78*, 623–629.

Angelini, S., Cerruti, P., Immirzi, B., Santagata, G., Scarinzi, G., and Malinconico, M. (2014). From biowaste to bioresource: Effect of a lignocellulosic filler on the properties of poly(3-hydroxybutyrate). International Journal of Biological Macromolecules *71*, 163–173.

Arias, V., Höglund, A., Odelius, K., and Albertsson, A.-C. (2013). Polylactides with “green” plasticizers: Influence of isomer composition. Journal of Applied Polymer Science *130*.

Atarés, L., and Chiralt, A. (2016). Essential oils as additives in biodegradable films and coatings for active food packaging. Trends in Food Science & Technology *48*, 51–62.

Auras, R., Harte, B., and Selke, S. (2004). An overview of polylactides as packaging materials. Macromolecular Bioscience *4*, 835–864.

Auras, R.A., Singh, S.P., and Singh, J.J. (2005). Evaluation of oriented poly(lactide) polymers vs. existing PET and oriented PS for fresh food service containers. Packaging Technology and Science *18*, 207–216.

Axel, C. (2015). Isolation and characterisation of antifungal compounds from lactic acid bacteria and their application in wheat and gluten-free bread.

Axel, C., Zannini, E., and Arendt, E. (2016). Mold spoilage of bread and its biopreservation: A review of current strategies for bread shelf life extension. Critical Reviews in Food Science and Nutrition *57*, 0.

Badawy, M., and Rabea, E. (2011). A Biopolymer Chitosan and Its Derivatives as Promising Antimicrobial Agents against Plant Pathogens and Their Applications in Crop Protection. Hindawi Publishing Corporation International Journal of Carbohydrate Chemistry Article ID 460381.

Baiardo, M., Frisoni, G., Scandola, M., Rimelen, M., Lips, D., Ruffieux, K., and Wintermantel, E. (2003). Thermal and mechanical properties of plasticized poly(L-lactic acid). Journal of Applied Polymer Science *90*, 1731–1738.

Barikani, M., Oliaei, E., Seddiqi, H., and Honarkar, H. (2014). Preparation and application of chitin and its derivatives: A review. Iranian Polymer Journal (English Edition) *23*, 307–326.

Barilli, E., Cimmino, A., Masi, M., Evidente, M., Rubiales, D., and Evidente, A. (2017). Inhibition of early development stages of rust fungi by the two fungal metabolites cyclopaldic acid and epi-epoformin. Pest Management Science *73*, 1161–1168.

Barilli, E., Gonzalez-Bernal, M.J., Cimmino, A., Agudo-Jurado, F.J., Masi, M., Rubiales, D., and Evidente, A. (2019). Impact of fungal and plant metabolites application on early development stages of pea powdery mildew. Pest Management Science.

Bastioli, C. (1998). Properties and applications of Mater-Bi starch-based materials. Polymer Degradation and Stability 59, 263–272.

Bawdekar, A.S., and Kalkar, G.R. (1965). Terpenoids—LXVIII: Structure and absolute configuration of costic acid—a new sesquiterpenic acid from costus root oil. Tetrahedron *21*, 1521–1528.

Belhassen, R., Boufi, S., Vilaseca, F., Lopez, J., Méndez, J., Franco, E., Pèlach, M.À., and Mutjé, P. (2008). Biocomposites based on Alfa fibers and starch-based biopolymer. Polymers for Advanced Technologies 20, 1068–1075.

Bhumkar, D.R., and Pokharkar, V.B. (2006). Studies on effect of pH on cross-linking of chitosan with sodium tripolyphosphate: A technical note. AAPS PharmSciTech *7*, E138–E143.

Bogaert, J.-C., and Coszach, P. (2000). Poly(lactic acids): a potential solution to plastic waste dilemma. Macromolecular Symposia *153*, 287–303.

Boua-In, K., Chaiyut, N., and Ksapabutr, B. (2010). Preparation of polylactide by ring-opening polymerisation of lactide. Optoelectronics and Advanced Materials: Rapid Communications 4, 1404–1407.

Bognitzki, M., Czado, W., Frese, T., Schaper, A., Hellwig, M., Steinhart, M., Greiner, A., and Wendorff, J.H. (2001). Nanostructured Fibers via Electrospinning. Advanced Materials 13, 70–72.

Bundela, H., and Bajpai, A.K. (2008). Designing of hydroxyapatite-gelatin based porous matrix as bone substitute: Correlation with biocompatibility aspects. Express Polymer Letters *2*, 201–213.

Cakmakci, S., Gurses, M., Hayaloglu, A.A., Cetin, B., Sekerci, P., and Dagdemir, E. (2015). Mycotoxin production capability of Penicillium roqueforti in strains isolated from mould-ripened traditional Turkish civil cheese. Food Additives and Contaminants - Part A Chemistry, Analysis, Control, Exposure and Risk Assessment *32*, 245–249.

Carey, F.A., and Sundberg, R.J. (2008). Advanced organic chemistry Part B: Reactions and Synthesis.

Casu, L., Cottiglia, F., Leonti, M., De Logu, A., Agus, E., Tse-Dinh, Y.-C., Lombardo, V., and Sissi, C. (2011). Ungeremine effectively targets mammalian as well as bacterial type I and type II topoisomerases. Bioorganic & Medicinal Chemistry Letters *21*, 7041–7044.

Cerruti, P., Santagata, G., Gomez, G., Ambrogi, V., Carfagna, C., Malinconico, M., and Persico, P. (2011). Effect of a natural polyphenolic extract on the properties of a biodegradable starch-based polymer. Polymer Degradation and Stability *96*, 839–846.

Chase, M.W., Reveal, J.L., and Fay, M.F. (2009). A subfamilial classification for the expanded asparagalean families Amaryllidaceae, Asparagaceae and Xanthorrhoeaceae. Botanical Journal of the Linnean Society *161*, 132–136.

Chen, T., Li, W., Gong, T., Fu, Y., Ding, R., Gong, T., and Zhang, Z. (2017). Analysis of lycobetaine in rat plasma by LC-ESI-MS/MS. Journal of Chromatographic Science *55*, 301–308.

Cho, T.-Y., and Strobl, G. (2006). Temperature dependent variations in the lamellar structure of poly(l-lactide). Polymer *47*, 1036–1043.

Chung, H.J., and Park, T.G. (2007). Surface engineered and drug releasing pre-fabricated scaffolds for tissue engineering. Advanced Drug Delivery Reviews *59*, 249–262.

Cimmino, A., Andolfi, A., Avolio, F., Ali, A., Tabanca, N., Khan Ikhlas, A., and Evidente, A. (2013). Cyclopaldic Acid, Seiridin, and Sphaeropsidin A as Fungal Phytotoxins, and Larvicidal and Biting Deterrents against Aedes aegypti (Diptera: Culicidae): Structure Activity Relationships. Chemistry & Biodiversity *10*, 1239–1251.

Cimmino, A., Andolfi, A., and Evidente, A. (2014). Phytotoxic Terpenes Produced by Phytopathogenic Fungi and Allelopathic Plants. Natural Product Communications *9*, 401–408.

Cimmino, A., Masi, M., Evidente, M., Superchi, S., and Evidente, A. (2015a). Fungal phytotoxins with potential herbicidal activity: chemical and biological characterization. Natural Product Reports *32*, 1629–1653.

Cimmino, A., Masi, M., Evidente, M., and Evidente, A. (2015b). Fungal Phytotoxins with Potential Herbicidal Activity to Control Chenopodium album. Natural Product Communications 10, 1119–1126.

Cimmino, A., Masi, M., Evidente, M., Superchi, S., and Evidente, A. (2017). Amaryllidaceae alkaloids: Absolute configuration and biological activity. Chirality *29*, 486–499.

Conn, R.E., Kolstad, J.J., Borzelleca, J.F., Dixler, D.S., Filer, L.J.J., LaDu, B.N.J., and Pariza, M.W. (1995). Safety assessment of polylactide (PLA) for use as a food-contact polymer. Food and Chemical Toxicology : An International Journal Published for the British Industrial Biological Research Association *33*, 273–283.

Courgneau, C., Domenek, S., Guinault, A., Avérous, L., and Ducruet, V. (2011). Analysis of the Structure-Properties Relationships of Different Multiphase Systems Based on Plasticized Poly(Lactic Acid). Journal of Polymers and the Environment 1–10.

Crispin, X., Marciniak, S., Osikowicz, W., Zotti, G., van der Gon, A.W.D., Louwet, F., Fahlman, M., Groenendaal, L., De Schryver, F., and Salaneck, W.R. (2003). Conductivity, morphology, interfacial chemistry, and stability of poly(3,4-ethylene dioxythiophene)–poly(styrene sulfonate): A photoelectron spectroscopy study. Journal of Polymer Science Part B: Polymer Physics *41*, 2561–2583.

Cruz-Romero, M.C., Murphy, T., Morris, M., Cummins, E., and Kerry, J.P. (2013). Antimicrobial activity of chitosan, organic acids and nano-sized solubilisates for potential use in smart antimicrobially-active packaging for potential food applications. Food Control *34*, 393–397.

Dae-Hyun, K., Seong-Ki, N., and Jong-Shin, P. (2003). Preparation and characterization of modified starch-based plastic film reinforced with short pulp fiber. I. Structural properties. Journal of Applied Polymer Science *88*, 2100–2107.

Dash, M., Chiellini, F., Ottenbrite, R.M., and Chiellini, E. (2011). Chitosan - A versatile semi-synthetic polymer in biomedical applications. Progress in Polymer Science (Oxford) *36*, 981–1014.

Datta, R., Tsai, S.-P., Bonsignore, P., Moon, S.-H., and Frank, J.R. (1995). Technological and economic potential of poly(lactic acid) and lactic acid derivatives. FEMS Microbiology Reviews *16*, 221–231.

Dharmalingam, S., G. Hayes, D., C. Wadsworth, L., N. Dunlap, R., DeBruyn, J., Lee, J., and L. Wszelaki, A. (2015). Soil Degradation of Polylactic Acid/Polyhydroxyalkanoate-Based Nonwoven Mulches. Journal of Polymers and the Environment *23*.

Di Biase, M., Lavermicocca, P., Lonigro, S., and Valerio, F. (2014). Lactobacillus brevis-based bioingredient inhibits Aspergillus niger growth on pan bread. Italian Journal of Agronomy 9, 146–151.

Dini, E., Alexandridou, S., and Kiparissides, C. (2003). Synthesis and characterization of cross-linked chitosan microspheres for drug delivery applications. Journal of Microencapsulation 20, 375–385.

Dong, T., He, Y., Shin, K., and Inoue, Y. (2004). Formation and Characterization of Inclusion Complexes of Poly(butylene succinate) with a- andc-Cyclodextrins. Macromolecular Bioscience *4*, 1084–1091.

Dong, W., Zou, B., Yan, Y., Ma, P., and Chen, M. (2013). Effect of Chain-Extenders on the

Properties and Hydrolytic Degradation Behavior of the Poly(lactide)/ Poly(butylene adipate-co-terephthalate) Blends. International Journal of Molecular Sciences *14*.

Dorgan, J.R., Lehermeier, H.J., Palade, L.-I., and Cicero, J. (2001). Polylactides: properties and prospects of an environmentally benign plastic from renewable resources. Macromolecular Symposia *175*, 55–66.

Drumright, R.E., Gruber, P.R., and Henton, D.E. (2000). Polylactic Acid Technology. Advanced Materials *12*, 1841–1846.

El-hefian, E.A., Nasef, M.M., and Hamid, A. (2012). Preparation and Characterization of Chitosan/Agar Blended Films: Part 2. Thermal, Mechanical, and Surface Properties. E-Journal of Chemistry *9*, 510–516.

Elfehri Borchani, K., Carrot, C., and Jaziri, M. (2015). Biocomposites of Alfa fibers dispersed in the Mater-Bi® type bioplastic: Morphology, mechanical and thermal properties. Composites Part A: Applied Science and Manufacturing 78, 371–379.

European Commission (2004). Commission Regulation (EC) No 1935/2004 of 27 October 2004 on materials and articles intended to come into contact with food and repealing Directives 80/590/EEC and 89/109/EEC. Official Journal of European Union, OJ L 338 4–17.

European Commission (2015). Closing the loop - An EU action plan for the Circular Economy COM/2015/0614 final.

Evidente, A., and Randazzo, G. (1985). Structure of Cavoxin, a New Phytotoxin from Phoma cava and Cavoxone, Its Related Chroman-4-One. Journal of Natural Products *48*, 916–923.

Evidente, A., Iasiello, I., and Randazzo, G. (1984a). Isolation of Sternbergine, a New Alkaloid From Bulbs of Sternbergia lutea. Journal of Natural Products *47*, 1003–1008.

Evidente, A., Iasiello, I., and Randazzo, G. (1984b). An improved method for the large-scale preparation of. lycorine. Chem Ind 27, 348–349.

Evidente, A., Randazzo, G., Surico, G., Lavermicocca, P., and Arrigoni, O. (1985). Degradation of Lycorine by Pseudomonas Species Strain ITM 311. Journal of Natural Products *48*, 564–570.

Evidente, A., Iacobellis, N.S., Scopa, A., and Surico, G. (1990). Isolation of β-phenyllactic acid related compounds from Pseudomonas syringae. Phytochemistry *29*, 1491–1497.

Evidente, A., Sparapano, L., Fierro, O., Bruno, G., Giordano, F., and Motta, A. (1997). Sphaeropsidins B and C, Phytotoxic Pimarane Diterpenes from Sphaeropsis sapinea F. Sp. cupressi and Diplodia mutila. Phytochemistry 45, 705–713.

Evidente, A., Cabras, A., Maddau, L., Marras, F., Andolfi, A., Melck, D., and Motta, A. (2006). Viridenepoxydiol, a New Pentasubstituted Oxiranyldecene Produced by Trichoderma viride. Journal of Agricultural and Food Chemistry *54*, 6588–6592.

Evidente, A., Venturi, V., Masi, M., Degrassi, G., Cimmino, A., Maddau, L., and Andolfi, A. (2011). In Vitro Antibacterial Activity of Sphaeropsidins and Chemical Derivatives toward

Xanthomonas oryzae pv. oryzae, the Causal Agent of Rice Bacterial Blight. Journal of Natural Products *74*, 2520–2525.

Evidente, A., Kornienko, A., Cimmino, A., Andolfi, A., Lefranc, F., Mathieu, V., and Kiss, R. (2014). Fungal metabolites with anticancer activity. Natural Product Reports *31*, 617–627.

Fahnestock, K., S. Austero, M., and Schauer, C. (2011). Natural Polysaccharides: From Membranes to Active Food Packaging.

Fales, H.M., Warnhoff, E.W., and Wildman, W.C. (1955). Alkaloids of the Amaryllidaceae. VI. The Action of Oxidizing Agents on Lycorine and Caraninel. J. Am. Chem. Soc. *77*, 5885–5890.

Filtenborg, O., Frisvad, J.C., and Thrane, U. (1996). Moulds in food spoilage. International Journal of Food Microbiology *33*, 85–102.

Forni, F., Vandelli, M.A., and Cameroni, R. (1992). Influence of drug loading level on drug release and dynamic swelling of crosslinked gelatin microspheres. Journal of Microencapsulation *9*, 29–39.

Fortunati, E., Armentano, I., Zhou, Q., Iannoni, A., Saino, E., Visai, L., Berglund, L., and Kenny, J. (2012). Multifunctional bionanocomposite films of poly(lactic acid), cellulose nanocrystals and silver nanoparticles. Carbohydrate Polymers *87*.

di Franco, C.R., Cyras, V.P., Busalmen, J.P., Ruseckaite, R.A., and Vázquez, A. (2004). Degradation of polycaprolactone/starch blends and composites with sisal fibre. Polymer Degradation and Stability *86*, 95–103.

Frisvad, J., and Samson, R. (1991). Mycotoxins produced by species of Penicillium and Aspergillus occurring in cereals. Dev Food Sci 26, 441–476.

Frisvad, J., Larsen, T.O., Thrane, U., Meijer, M., Varga, J., Samson, R., and Nielsen, K. (2011). Fumonisin and Ochratoxin Production in Industrial Aspergillus niger Strains. PloS One 6, e23496.

Fwu-Long, M.I., Shyu, S.S., Lee, S.T., and Wong, T.B.I. (1999). Kinetic study of chitosan-tripolyphosphate complex reaction and acid-resistive properties of the chitosan-tripolyphosphate gel beads prepared by in-liquid curing method. Journal of Polymer Science, Part B: Polymer Physics *37*, 1551–1564.

Gan, Q., and Wang, T. (2007). Chitosan nanoparticle as protein delivery carrier-Systematic examination of fabrication conditions for efficient loading and release. Colloids and Surfaces B: Biointerfaces *59*, 24–34.

Garcia-Valdez, O., Champagne, P., and Cunningham, M.F. (2018). Graft modification of natural polysaccharides via reversible deactivation radical polymerization. Progress in Polymer Science 76, 151–173.

Ghaani, M., Cozzolino, C.A., Castelli, G., and Farris, S. (2016). An overview of the intelligent packaging technologies in the food sector. Trends in Food Science & Technology *51*, 1–11.

Graniti, A., Sparapano, L., and Evidente, A. (1992). Cyclopaldic acid, a major phytotoxic metabolite of Seiridium cupressi, the pathogen of a canker disease of cypress. Plant Pathology *41*,

563–568.

Groot, W., van Krieken, J., Sliekersl, O., and de Vos, S. (2010). Production and Purification of Lactic Acid and Lactide. Poly(Lactic Acid).

Harris, R., Lecumberri, E., Mateos-Aparicio, I., Mengíbar, M., and Heras, A. (2011). Chitosan nanoparticles and microspheres for the encapsulation of natural antioxidants extracted from Ilex paraguariensis. Carbohydrate Polymers *84*, 803–806.

Hayes, R., Ahmed, A., Edge, T., and Zhang, H. (2014). Core–shell particles: Preparation, fundamentals and applications in high performance liquid chromatography. Journal of Chromatography A *1357*, 36–52.

Hernández, V., Máñez, S., Recio, M.C., Giner, R.M., and Ríos, J.L. (2005). Anti-inflammatory profile of dehydrocostic acid, a novel sesquiterpene acid with a pharmacophoric conjugated diene. European Journal of Pharmaceutical Sciences *26*, 162–169.

Higuchi, A., and Iijima, T. (1985). DSC investigation of the states of water in poly (vinyl alcohol) membranes. Polymer *26*, 1207–1211.

Higuera-Ciapara, I., Felix-Valenzuela, L., Goycoolea, F.M., and Argüelles-Monal, W. (2004). Microencapsulation of astaxanthin in a chitosan matrix. Carbohydrate Polymers *56*, 41–45.

Homklin, R., and Hongsriphan, N. (2013). Mechanical and Thermal Properties of PLA/PBS Co-continuous Blends Adding Nucleating Agent. Energy Procedia *34*, 871–879.

Hui, Y.H., Culbertson, J.D., Duncan, S.E., Legarreta, I.G., Li-Chan, E.C.Y., Ma, C.Y., Manley, C., McMeekin, T., Nip, W.-K., Nollet, L., et al. (2005). Handbook of food science, technology, and engineering.

Hwang, S.W., Shim, J.K., Selke, S.E., Soto-Valdez, H., Matuana, L., Rubino, M., and Auras, R. (2012). Poly(L-lactic acid) with added α-tocopherol and resveratrol: Optical, physical, thermal and mechanical properties. Polymer International *61*, 418–425.

Iannace, S., and Nicolais, L. (1997). Isothermal crystallization and chain mobility of poly(L-lactide). Journal of Applied Polymer Science *64*, 911–919.

Iannace, S., Ali, R., and Nicolais, L. (2001). Effect of processing conditions on dimensions of sisal fibers in thermoplastic biodegradable composites. Journal of Applied Polymer Science *79*, 1084–1091.

Ingrao, C., Tricase, C., Cholewa-Wójcik, A., Kawecka, A., Rana, R., and Siracusa, V. (2015). Polylactic acid trays for fresh-food packaging: A Carbon Footprint assessment. Science of The Total Environment *537*, 385–398.

Introzzi, L., Fuentes-Alventosa, J.M., Cozzolino, C.A., Trabattoni, S., Tavazzi, S., Bianchi, C.L., Schiraldi, A., Piergiovanni, L., and Farris, S. (2012). "Wetting enhancer" pullulan coating for antifog packaging applications. ACS Applied Materials and Interfaces *4*, 3692–3700.

Jandas, P.J., Mohanty, S., Nayak, S.K., and Srivastava, H. (2011). Effect of surface treatments of

banana fiber on mechanical, thermal, and biodegradability properties of PLA/banana fiber biocomposites. Polymer Composites *32*, 1689–1700.

Jia-hui, Y., Yu-min, D., and Hua, Z. (1999). Blend films of chitosan-gelatin. Wuhan University Journal of Natural Sciences *4*, 476.

Johnson, J.L., Raghavan, V., Cimmino, A., Moeini, A., Petrovic, A.G., Santoro, E., Superchi, S., Berova, N., Evidente, A., and Polavarapu, P.L. (2018). Absolute configurations of chiral molecules with multiple stereogenic centers without prior knowledge of the relative configurations: A case study of inuloxin C. Chirality *30*.

Kalia, S., and Avérous, L. (2011). Biopolymers: Biomedical and Environmental Applications (Wiley).

Ke, T., and Sun, X. (2003). Melting behavior and crystallization kinetics of starch and poly(lactic acid) composites. Journal of Applied Polymer Science *89*, 1203–1210.

Kfoury, G., Raquez, J.-M., Hassouna, F., Leclère, P., Toniazzo, V., Ruch, D., and Dubois, P. (2015). Toughening of poly(lactide) using polyethylene glycol methyl ether acrylate: Reactive versus physical blending. Polymer Engineering & Science *55*, 1408–1419.

Khan, T.A., Peh, K.K., and Ch'ng, H.S. (2002). Reporting degree of deacetylation values of chitosan: the influence of analytical methods. Journal of Pharmacy & Pharmaceutical Sciences : A Publication of the Canadian Society for Pharmaceutical Sciences, Societe Canadienne Des Sciences Pharmaceutiques *5*, 205–212.

Kim, J.H., and Lee, Y.M. (1993). Synthesis and properties of diethylaminoethyl chitosan. Polymer *34*, 1952–1957.

Ko, J.., Park, H.., Hwang, S.., Park, J.., and Lee, J.. (2002). Preparation and characterization of chitosan microparticles intended for controlled drug delivery. International Journal of Pharmaceutics *249*, 165–174.

Kong, M., Guang Chen, X., Xing, K., and Jin Park, H. (2010). Antimicrobial properties of chitosan and mode of action: A state of the art review. International Journal of Food Microbiology 144, 51–63.

Kornienko, A., and Evidente, A. (2008). Chemistry, biology, and medicinal potential of narciclasine and its congeners. Chemical Reviews *108*, 1982–2014.

Kumar, S., Prakash, N., and Datta, D. (2011). Biopolymers Based on Carboxylic Acids Derived from Renewable Resources. In Biopolymers: Biomedical and Environmental Applications, pp. 167–182.

Labrecque, L. V, Kumar, R.A., Davé, V., Gross, R.A., and McCarthy, S.P. (1997). Citrate esters as plasticizers for poly(lactic acid). Journal of Applied Polymer Science *66*, 1507–1513.

Lamoral-Theys, D., Decaestecker, C., Mathieu, V., Dubois, J., Kornienko, A., Kiss, R., and Pottier, A.E. and L. (2010). Lycorine and its Derivatives for Anticancer Drug Design. Mini-Reviews in Medicinal Chemistry *10*, 41–50.

Lavermicocca, P., Valerio, F., Evidente, A., Lazzaroni, S., Corsetti, A., and Gobbetti, M. (2000). Purification and Characterization of Novel Antifungal Compounds from the Sourdough <em>Lactobacillus plantarum</em> Strain 21B. Applied and Environmental Microbiology 66, 4084 LP – 4090.

Lawrie, G., Keen, I., Drew, B., Chandler-Temple, A., Rintoul, L., Fredericks, P., and Grøndahl, L. (2007). Interactions between alginate and chitosan biopolymers characterized using FTIR and XPS. Biomacromolecules *8*, 2533–2541.

Lee, S., and Lee, J.W. (2005). Characterization and processing of Biodegradable polymer blends of poly(lactic acid) with poly(butylene succinate adipate). Korea Australia Rheology Journal *17*, 71–77.

Lee, P.S., Han, J.Y., Song, T.W., Sung, J.H., Kwon, O.S., Song, S., and Chung, Y.B. (2006). Physicochemical characteristics and bioavailability of a novel intestinal metabolite of ginseng saponin (IH901) complexed with β-cyclodextrin. International Journal of Pharmaceutics *316*, 29–36.

Liu, H., and Zhang, J. (2011). Research progress in toughening modification of poly(lactic acid). Journal of Polymer Science Part B: Polymer Physics *49*, 1051–1083.

Liu, L., Jin, T., Finkenstadt, V., Liu, C.-K., Cooke, P., Coffin, D., Hicks, K., and Samer, C. (2009). Antimicrobial Packaging Materials from Poly(Lactic Acid) Incorporated with Pectin-Nisaplin® Microparticles. CHEMISTRY & CHEMICAL TECHNOLOGY *3*, 221–230.

Ljungberg, N., and Wesslén, B. (2005). Preparation and Properties of Plasticized Poly(lactic acid) Films. Biomacromolecules *6*, 1789–1796.

Llorens, E., del Valle, L.J., Ferrán, R., Rodríguez-Galán, A., and Puiggalí, J. (2014). Scaffolds with tuneable hydrophilicity from electrospun microfibers of polylactide and poly(ethylene glycol) mixtures: morphology, drug release behavior, and biocompatibility. Journal of Polymer Research *21*, 360.

Luo, C.J., Nangrejo, M., and Edirisinghe, M. (2010). A novel method of selecting solvents for polymer electrospinning. Polymer *51*, 1654–1662.

Luzi, F., Torre, L., Kenny, J.M., and Puglia, D. (2019). Bio- and Fossil-Based Polymeric Blends and Nanocomposites for Packaging: Structure¯Property Relationship. Materials (Basel, Switzerland) *12*, 471.

Madanat, H., Al Antary, T., and Abu Zarqa, M. (2016). Toxicity of six ethanol plant extracts against the green peach aphid Myzus persicae Sulzer (Homoptera: Aphididae).

Madhavan Nampoothiri, K., Nair, N.R., and John, R.P. (2010). An overview of the recent developments in polylactide (PLA) research. Bioresource Technology *101*, 8493–8501.

Mahmoodi, A., Ghodrati, S., and Khorasani, M. (2019). High-Strength, Low-Permeable, and Light-Protective Nanocomposite Films Based on a Hybrid Nanopigment and Biodegradable PLA for Food Packaging Applications. ACS Omega *4*, 14947–14954.

Mallardo, S., De Vito, V., Malinconico, M., Volpe, M.G., Santagata, G., and Di Lorenzo, M.L. (2016). Poly(butylene succinate)-based composites containing β-cyclodextrin/d-limonene inclusion complex. European Polymer Journal *79*, 82–96.

Malmgren, T., Mays, J., and Pyda, M. (2006). Characterizationof poly(lactic acid) by size exclusion chromatography, differential refractometry,light scattering and thermal analysis. Journal of Thermal Analysis and Calorimetry *83*, 35–40.

Maoz, M., and Neeman, I. (2000). Effect of Inula viscosa extract on chitin synthesis in dermatophytes and Candida albicans. Journal of Ethnopharmacology *71*, 479–482.

Masi, M., Andolfi, A., Mathieu, V., Boari, A., Cimmino, A., Moreno Y Banuls, L., Vurro, M., Kornienko, A., Kiss, R., and Evidente, A. (2013). Fischerindoline, a pyrroloindole sesquiterpenoid isolated from Neosartorya pseudofischeri, with in vitro growth inhibitory activity in human cancer cell lines. Tetrahedron *69*, 7466–7470.

Masi, M., Maddau, L., Linaldeddu, B.T., Cimmino, A., D'Amico, W., Scanu, B., Evidente, M., Tuzi, A., and Evidente, A. (2016). Bioactive Secondary Metabolites Produced by the Oak Pathogen Diplodia corticola. Journal of Agricultural and Food Chemistry *64*, 217–225.

Masi, M., Moeini, S.A., Boari, A., Cimmino, A., Vurro, M., and Evidente, A. (2017a). Development of a rapid and sensitive HPLC method for the identification and quantification of cavoxin and cavoxone in Phoma cava culture filtrates. Natural Product Research *6419*, 1–5.

Masi, M., Cimmino, A., Boari, A., Tuzi, A., Zonno, M.C., Baroncelli, R., Vurro, M., and Evidente, A. (2017b). Colletochlorins E and F, New Phytotoxic Tetrasubstituted Pyran-2-one and Dihydrobenzofuran, Isolated from Colletotrichum higginsianum with Potential Herbicidal Activity. Journal of Agricultural and Food Chemistry *65*, 1124–1130.

Mathieu, V., Chantome, A., Lefranc, F., Cimmino, A., Miklos, W., Paulitschke, V., Mohr, T., Maddau, L., Kornienko, A., Berger, W., et al. (2015). Sphaeropsidin A shows promising activity against drug-resistant cancer cells by targeting regulatory volume increase. Cellular and Molecular Life Sciences : CMLS 72.

McKeen, L.W. (2012). Renewable Resource and Biodegradable Polymers. Plastics Design Library 353–378.

Milovanovic, S., Stamenic, M., Markovic, D., Ivanovic, J., and Zizovic, I. (2015). Supercritical impregnation of cellulose acetate with thymol. Journal of Supercritical Fluids *97*, 107–115.

Mitrus, M., Wójtowicz, A., and Moscicki, L. (2010). Biodegradable Polymers and Their Practical Utility. In Thermoplastic Starch, pp. 1–33.

Moeini, A., Cimmino, A., Dal Poggetto, G., Di Biase, M., Evidente, A., Masi, M., Lavermicocca, P., Valerio, F., Leone, A., Santagata, G., et al. (2018). Effect of pH and TPP concentration on chemico-physical properties, release kinetics and antifungal activity of Chitosan-TPP-Ungeremine microbeads. Carbohydrate Polymers *195*, 631–641.

Moeini, A., Masi, M., Zonno, M.C., Boari, A., Cimmino, A., Tarallo, O., Vurro, M., and Evidente, A. (2019). Encapsulation of inuloxin A, a plant germacrane sesquiterpene with potential herbicidal

activity, in β-cyclodextrins. Organic & Biomolecular Chemistry *17*, 2508–2515.

Moeini, A., Pedram, P., Makvandi, P., Malinconico, M., and Gomez d'Ayala, G. (2020a). Wound healing and Antimicrobial effect of active Secondary Metabolites in Chitosan-based Wound dressings: A review. Carbohydrate Polymers 115839.

Moeini, A., Mallardo, S., Cimmino, A., Dal Poggetto, G., Masi, M., Di Biase, M., van Reenen, A., Lavermicocca, P., Valerio, F., Evidente, A., et al. (2020b). Thermoplastic starch and bioactive chitosan sub-microparticle biocomposites: Antifungal and chemico-physical properties of the films. Carbohydrate Polymers *230*, 115627.

Moeini, A., Cimmino, A., Masi, M., Evidente, A., and Van Reenen, A. (2020c). The incorporation and release of ungeremine, an antifungal Amaryllidaceae alkaloid, in poly(lactic acid)/poly(ethylene glycol) nanofibers. Journal of Applied Polymer Science *n/a*, 49098.

Moeini, A., van Reenen, A., Van Otterlo, W., Cimmino, A., Masi, M., Lavermicocca, P., Valerio, F., Immirzi, B., Santagata, G., Malinconico, M., et al. (2020d). α-costic acid, a plant sesquiterpenoid from Dittrichia viscosa, as modifier of Poly (lactic acid) properties: a novel exploitation of the autochthone biomass metabolite for a wholly biodegradable system. Industrial Crops and Products *146*, 112134.

Molinaro, S., Cruz Romero, M., Boaro, M., Sensidoni, A., Lagazio, C., Morris, M., and Kerry, J. (2013). Effect of nanoclay-type and PLA optical purity on the characteristics of PLA-based nanocomposite films. Journal of Food Engineering *117*, 113–123.

Monde, K., Satoh, H., Nakamura, M., Tamura, M., and Takasugi, M. (1998). Organochlorine Compounds from a Terrestrial Higher Plant: Structures and Origin of Chlorinated Orcinol Derivatives from Diseased Bulbs of Lilium maximowiczii. Journal of Natural Products *61*, 913–921.

Morganti, P., and Coltelli, M. (2019). A New Carrier for Advanced Cosmeceuticals. Cosmetics 6, 10.

Moriana, R., Contat-Rodrigo, L., Santonja-Blasco, L., and Amparo, R. (2008). Thermal characterisation of photo-oxidized HDPE/Mater-Bi and LDPE/Mater-Bi blends buried in soil. Journal of Applied Polymer Science 109, 1177–1188.

Morreale, M., Scaffaro, R., Maio, A., and La Mantia, F.P. (2008). Effect of adding wood flour to the physical properties of a biodegradable polymer. Composites Part A: Applied Science and Manufacturing *39*, 503–513.

Mueller-Riebau, F., Berger, B., and Yegen, O. (1995). Chemical Composition and Fungitoxic Properties to Phytopathogenic Fungi of Essential Oils of Selected Aromatic Plants Growing Wild in Turkey. Journal of Agricultural and Food Chemistry - J AGR FOOD CHEM 43.

Murariu, M., Da Silva Ferreira, A., Alexandre, M., and Dubois, P. (2008). Polylactide (PLA) designed with desired end-use properties: 1. PLA compositions with low molecular weight ester-like plasticizers and related performances. Polymers for Advanced Technologies *19*, 636–646.

Muriel-Galet, V., Talbert, J.N., Hernandez-Munoz, P., Gavara, R., and Goddard, J.M. (2013).

Covalent Immobilization of Lysozyme on Ethylene Vinyl Alcohol Films for Nonmigrating Antimicrobial Packaging Applications. Journal of Agricultural and Food Chemistry *61*, 6720–6727.

Murray, A.P., Faraoni, M.B., Castro, M.J., and Cavallaro, N.P.A. and V. (2013). Natural AChE Inhibitors from Plants and their Contribution to Alzheimer's Disease Therapy. Current Neuropharmacology *11*, 388–413.

Mutsuga, M., Kawamura, Y., and Tanamoto, K. (2008). Migration of lactic acid, lactide and oligomers from polylactide food-contact materials. Food Additives & Contaminants: Part A *25*, 1283–1290.

Nair, J.J., and van Staden, J. (2013). Pharmacological and toxicological insights to the South African Amaryllidaceae. Food and Chemical Toxicology *62*, 262–275.

Neto, C.G.T., Giacometti, J.A., Job, A.E., Ferreira, F.C., Fonseca, J.L.C., and Pereira, M.R. (2005). Thermal Analysis of Chitosan Based Networks. Carbohydrate Polymers *62*, 97–103.

Nguyen Van Long, N., Joly, C., and Dantigny, P. (2016). Active packaging with antifungal activities. International Journal of Food Microbiology *220*, 73–90.

Nibler, J.W. (1978). Infrared absorption spectroscopy. Second edition (Nakanishi, Koji). Journal of Chemical Education *55*, A316.

Nieto, J.M., Peniche-Covas, C., and Padro´n, G. (1991). Characterization of chitosan by pyrolysis-mass spectrometry, thermal analysis and differential scanning calorimetry. Thermochimica Acta *176*, 63–68.

Oka, T., Toyomura, T., Honjo, K., Wada, Y., and Futai, M. (2001). Four subunit a isoforms of Caenorhabditis elegans vacuolar H+-ATPase. The Journal of Biological Chemistry *276*, 33079–33085.

Omezzine, F., Daami-Remadi, M., Rinez, A., Ladhari, A., and Haouala, R. (2011). In vitro assessment of Inula spp. organic extracts for their antifungal activity against some pathogenic and antagonistic fungi. African Journal of Microbiology Research *5*, 3527–3531.

Ortega-Toro, R., Santagata, G., Gomez d'Ayala, G., Cerruti, P., Talens Oliag, P., Chiralt Boix, M.A., and Malinconico, M. (2016). Enhancement of interfacial adhesion between starch and grafted poly(ε-caprolactone). Carbohydrate Polymers *147*, 16–27.

Osbourn, A.E., and Lanzotti, V. (2009). Plant-derived natural products: Synthesis, function, and application (Springer).

Pamuła, E., Błażewicz, M., Paluszkiewicz, C., and Dobrzyński, P. (2001). FTIR study of degradation products of aliphatic polyesters carbon fibres composites. Journal of Molecular Structure 596, 69–75.

Persico, P., Ambrogi, V., Carfagna, C., Cerruti, P., Ferrocino, I., and Mauriello, G. (2009). Nanocomposite polymer films containing carvacrol for antimicrobial active packaging. Polymer Engineering & Science *49*, 1447–1455.

Pieróg, M., Ostrowska-Czubenko, J., and Gierszewska-Druzyńska, M. (2012). Thermal degradation of double crosslinked hydrogel chitosan membranes. Progress on Chemistry and Application of Chitin and Its Derivatives *2012*, 67–74.

Pilla, S., Kim, S.G., Auer, G.K., Gong, S., and Park, C.B. (2009). Microcellular extrusion-foaming of polylactide with chain-extender. Polymer Engineering & Science *49*, 1653–1660.

Pillin, I., Montrelay, N., and Grohens, Y. (2006). Thermo-mechanical characterization of plasticized PLA: Is the miscibility the only significant factor? Polymer *47*, 4676–4682.

PlasticsEurope (2018). Plastics – the Facts 2018. Brussels, Belgium: PlasticsEurope, Association of Plastics Manufacturers.

Puglia, D., Tomassucci, A., and Kenny, J. (2003). Processing, properties and stability of biodegradable composites based on Mater-Bi-(R) and cellulose fibres. Polymers for Advanced Technologies 14, 749–756.

Puopolo, G., Cimmino, A., Palmieri, M.C., Giovannini, O., Evidente, A., and Pertot, I. (2014). Lysobacter capsici AZ78 produces cyclo(l-Pro-l-Tyr), a 2,5-diketopiperazine with toxic activity against sporangia of Phytophthora infestans and Plasmopara viticola. Journal of Applied Microbiology *117*, 1168–1180.

Qin, Y., Liu, D., Wu, Y., Yuan, M., Li, L., and Yang, J. (2015). Effect of PLA/PCL/cinnamaldehyde antimicrobial packaging on physicochemical and microbial quality of button mushroom (Agaricus bisporus). Postharvest Biology and Technology *99*, 73–79.

Rafael, A., Bruce, H., and Susan, S. (2004). An Overview of Polylactides as Packaging Materials. Macromolecular Bioscience *4*, 835–864.

Raghavan, D., and Emekalam, A. (2001). Characterization of starch/polyethylene and starch/polyethylene/poly(lactic acid) composites. Polymer Degradation and Stability *72*, 509–517.

Ramis, X., Cadenato, A., Salla, J., Morancho, J.M., Vallés, A., Contat, L., and Amparo, R. (2004). Thermal Degradation of Polypropylene/starch-based materials with enhanced biodegradability.

Ratanakamnuan, U., and Aht-Ong, D. (2006). Preparation and characterization of low-density polyethylene/banana starch films containing compatibilizer and photosensitizer. Journal of Applied Polymer Science *100*, 2717–2724.

Ren, Z., Dong, L., and Yang, Y. (2006). Dynamic mechanical and thermal properties of plasticized poly(lactic acid). Journal of Applied Polymer Science *101*, 1583–1590.

Riggi, E., Santagata, G., and Malinconico, M. (2011). Bio-based and biodegradable plastics for use in crop production. Recent Patents on Food, Nutrition & Agriculture *3*, 49–63.

Risch, S.J. (2009). Food packaging history and innovations. Journal of Agricultural and Food Chemistry *57*, 8089–8092.

Robertson, G. (2009). Food Packaging and Shelf Life. In Taylor & Francis, pp. 1–16.

Roller, S., and Covill, N. (1999). The antifungal properties of chitosan in laboratory media and apple Juice. International Journal of Food Microbiology 47, 67–77.

Rozenblat, S., Grossman, S., Bergman, M., Gottlieb, H., Cohen, Y., and Dovrat, S. (2008). Induction of G2/M arrest and apoptosis by sesquiterpene lactones in human melanoma cell lines. Biochemical Pharmacology *75*, 369–382.

Russo, R., Malinconico, M., and Santagata, G. (2007). Effect of cross-linking with calcium ions on the physical properties of alginate films. Biomacromolecules *8*, 3193–3197.

Russo, R., Abbate, M., Malinconico, M., and Santagata, G. (2010). Effect of polyglycerol and the crosslinking on the physical properties of a blend alginate-hydroxyethylcellulose. Carbohydrate Polymers *82*, 1061–1067.

Salmieri, S., Islam, F., Khan, R.A., Hossain, F.M., Ibrahim, H.M.M., Miao, C., Hamad, W.Y., and Lacroix, M. (2014). Antimicrobial nanocomposite films made of poly(lactic acid)–cellulose nanocrystals (PLA–CNC) in food applications—part B: effect of oregano essential oil release on the inactivation of Listeria monocytogenes in mixed vegetables. Cellulose *21*, 4271–4285.

Santagata, G., Valerio, F., Cimmino, A., Dal Poggetto, G., Masi, M., Di Biase, M., Malinconico, M., Lavermicocca, P., and Evidente, A. (2017). Chemico-physical and antifungal properties of poly(butylene succinate)/cavoxin blend: Study of a novel bioactive polymeric based system. European Polymer Journal *94*, 230–247.

Sarasua, J.-R., Prud'homme, R.E., Wisniewski, M., Le Borgne, A., and Spassky, N. (1998). Crystallization and Melting Behavior of Polylactides. Macromolecules *31*, 3895–3905.

Schettini, E., Santagata, G., Malinconico, M., Immirzi, B., Scarascia Mugnozza, G., and Vox, G. (2013). Recycled wastes of tomato and hemp fibres for biodegradable pots: Physico-chemical characterization and field performance. Resources, Conservation and Recycling *70*, 9–19.

Schinella, G.R., Tournier, H.A., Prieto, J.M., de Buschiazzo, P.M., and Ríos, J.L. (2002). Antioxidant activity of anti-inflammatory plant extracts. Life Sciences *70*, 1023–1033.

Schrader, K.K., Andolfi, A., Cantrell, C.L., Cimmino, A., Duke, S.O., Osbrink, W., Wedge, D.E., and Evidente, A. (2010). A Survey of Phytotoxic Microbial and Plant Metabolites as Potential Natural Products for Pest Management. Chemistry & Biodiversity *7*, 2261–2280.

Schrader, K.K., Avolio, F., Andolfi, A., Cimmino, A., and Evidente, A. (2013). Ungeremine and its hemisynthesized analogues as bactericides against flavobacterium columnare. Journal of Agricultural and Food Chemistry *61*, 1179–1183.

Schwarzböck, T., Van Eygen, E., Rechberger, H., and Fellner, J. (2016). Determining the amount of waste plastics in the feed of Austrian waste-to-energy facilities. Waste Management & Research *35*, 207–216.

Seo, D.J., Nguyen, D.M.C., Park, R.D., and Jung, W.J. (2014). Chitosan-cinnamon beads enhance suppressive activity against Rhizoctonia solani and Meloidogyne incognita invitro. Microbial Pathogenesis *66*, 44–47.

Serra, T., Ortiz-Hernandez, M., Engel, E., Planell, J.A., and Navarro, M. (2014). Relevance of PEG in PLA-based blends for tissue engineering 3D-printed scaffolds. Materials Science and Engineering C *38*, 55–62.

Shtacher, G., and Kashman, Y. (1970). 12-carboxyeudesma-3,11(13)-diene. A novel sesquiterpenic acid with a narrow antifungal spectrum. Journal of Medicinal Chemistry *13*, 1221–1223.

Shu, X.Z., and Zhu, K.J. (2000). A novel approach to prepare tripolyphosphate/chitosan complex beads for controlled release drug delivery. International Journal of Pharmaceutics *201*, 51–58.

Shu, X.Z., and Zhu, K.J. (2001). Chitosan/gelatin microspheres prepared by modified emulsification and ionotropic gelation. Journal of Microencapsulation *18*, 237–245.

Silverajah, V.S.G., Ibrahim, N., Zainuddin, N., Yunus, W., and Hassan, H. (2012). Mechanical, Thermal and Morphological Properties of Poly(lactic acid)/Epoxidized Palm Olein Blend. Molecules (Basel, Switzerland) *17*, 11729–11747.

Singhvi, M., and Gokhale, D. (2013). Biomass to biodegradable polymer (PLA). RSC Advances *3*, 13558–13568.

Siracusa, V., and Ingrao, C. (2016). The Use of Polylactic Acid in Food Packaging. In Reference Module in Food Science

Siracusa, V., Rocculi, P., Romani, S., and Rosa, M.D. (2008). Biodegradable polymers for food. Trends in Food Science and Technology *19*, 634–643.

Smitha, B., Sridhar, S., and Khan, A.A. (2005). Chitosan-sodium alginate polyion complexes as fuel cell membranes. European Polymer Journal *41*, 1859–1866.

Soto-Valdez, H., Auras, R., and Peralta, E. (2011). Fabrication of poly(lactic acid) films with resveratrol and the diffusion of resveratrol into ethanol. Journal of Applied Polymer Science *121*, 970–978.

Soundararajan, A. (2015). Recent Research in the Applications of Chitin, Chitosan and Oligosaccharides. pp. 303–333.

Souza, N.L.G.D., Salles, T.F., Brandão, H.M., Edwards, H.G.M., and De Oliveira, L.F.C. (2015). Synthesis, Vibrational Spectroscopic and Thermal Properties of Oxocarbon Cross-Linked Chitosan. Article J. Braz. Chem. Soc *26*, 1247–1256.

Soykeabkaew, N., Supaphol, P., and Rujiravanit, R. (2004). Preparation and Characterization of Jute- and Flax-Reinforced Starch-Based Composite Foams. Carbohydrate Polymers 58, 53–63.

Srinatha, A., Pandit, J.K., and Singh, S. (2008). Ionic Cross-linked Chitosan Beads for Extended Release of Ciprofloxacin: In vitro Characterization. Indian Journal of Pharmaceutical Sciences *70*, 16–21.

Stavrianakou, Sotiria, Liakopoulos, Georgios , Miltiadou, Despoina, Markoglou, Anastasios , Ziogas, Basil , Karabourniotis, G. (2010). Antifungal and Antibacterial Capacity of Extracted Material from non-Glandular and Glandular Leaf Hairs Applied at Physiological Concentrations.

Plant Stress *4*, 25–30.

Stloukal, P., Kalendova, A., Mattausch, H., Laske, S., Holzer, C., and Koutny, M. (2015). The influence of a hydrolysis-inhibiting additive on the degradation and biodegradation of PLA and its nanocomposites. Polymer Testing *41*, 124–132.

Suhr, K.I., and Nielsen, P. V (2005). Inhibition of Fungal Growth on Wheat and Rye Bread by Modified Atmosphere Packaging and Active Packaging Using Volatile Mustard Essential Oil. Journal of Food Science *70*, M37–M44.

Suyatma, N., Copinet, A., Tighzert, L., and Coma, V. (2004). Mechanical and Barrier Properties of Biodegradable Films Made from Chitosan and Poly (Lactic Acid) Blends.

Syad, A.N., Shunmugiah, K.P., and Kasi, P.D. (2013). Antioxidant and anti-cholinesterase activity of Sargassum wightii. Pharmaceutical Biology *51*, 1401–1410.

Tariq, F., Noori, M., and Ali, N.A. (2015). Study of Mechanical , Thermal and Barrier Properties of Biodegradable Polylactic acid-Polyethylene Glycol- Alumina Nanocomposite. *56*, 1689–1698.

Tawakkal, I.S.M.A., Cran, M.J., Miltz, J., and Bigger, S.W. (2014). A review of poly(lactic acid)-based materials for antimicrobial packaging. Journal of Food Science *79*.

Thirmizir, M.Z.A., Ishak, Z.A.M., Taib, R.M., Rahim, S., and Jani, S.M. (2011). Natural Weathering of Kenaf Bast Fibre-Filled Poly(Butylene Succinate) Composites: Effect of Fibre Loading and Compatibiliser Addition. Journal of Polymers and the Environment *19*, 263–273.

Tolaimate, A., Desbrières, J., Rhazi, M., Alagui, A., Vincendon, M., and Vottero, P. (2000). On the influence of deacetylation process on the physicochemical characteristics of chitosan from squid chitin. Polymer *41*, 2463–2469.

Toncheva, A., Spasova, M., Paneva, D., Manolova, N., and Rashkov, I. (2011). Drug-loaded electrospun polylactide bundles. Journal of Bioactive and Compatible Polymers *26*, 161–172.

Toncheva, A., Paneva, D., Maximova, V., Manolova, N., and Rashkov, I. (2012). Antibacterial fluoroquinolone antibiotic-containing fibrous materials from poly(l-lactide-co-d,l-lactide) prepared by electrospinning. European Journal of Pharmaceutical Sciences *47*, 642–651.

Toncheva, A., Mincheva, R., Kancheva, M., Manolova, N., Rashkov, I., Dubois, P., and Markova, N. (2016). Antibacterial PLA/PEG electrospun fibers: Comparative study between grafting and blending PEG. European Polymer Journal *75*, 223–233.

Tringali, C. (2001). Bioactive compounds from natural sources: isolation, characterization and biological properties.

Tripathi, S., Mehrotra, G.K., and Dutta, P.K. (2009). Physicochemical and bioactivity of cross-linked chitosan–PVA film for food packaging applications. International Journal of Biological Macromolecules *45*, 372–376.

Tsui, H. (2002). Polyesters III - Applications and commercial products.

Tsuji, H. (2010). Poly(Lactic Acid): Synthesis, Structures, Properties, Processing, and Applications. In Poly(Lactic Acid): Synthesis, Structures, Properties, Processing, and Applications, pp. 343–381.

Tsuji, H., Mizuno, A., and Ikada, Y. (2000). Properties and morphology of poly(L-lactide). III. Effects of initial crystallinity on long-term in vitro hydrolysis of high molecular weight poly(L-lactide) film in phosphate-buffered solution. Journal of Applied Polymer Science *77*, 1452–1464.

Turco, Ortega-Toro, R., Tesser, Mallardo, Collazo-Bigliardi, S., Boix, Malinconico, Rippa, Serio, and Santagata (2019). Poly (Lactic Acid)/Thermoplastic Starch Films: Effect of Cardoon Seed Epoxidized Oil on Their Chemicophysical, Mechanical, and Barrier Properties. Coatings *9*, 574.

Turner, W.B., and Aldridge, D.C. (1983). Fungal metabolites, vol II. Paris: Academic 257–259.

Valerio, F., Di Biase, M., Huchet, V., Desriac, N., Lonigro, S.L., Lavermicocca, P., Sohier, D., and Postollec, F. (2015). Comparison of three Bacillus amyloliquefaciens strains growth behaviour and evaluation of the spoilage risk during bread shelf-life. Food Microbiology *45*, 2–9.

Valerio, F., Masi, M., Cimmino, A., Moeini, S.A., Lavermicocca, P., and Evidente, A. (2017). Antimould microbial and plant metabolites with potential use in intelligent food packaging. Natural Product Research *6419*, 1–6.

Vanstrom Joseph Robert (2012). Mechanical Characterization of Commercial Ciodegradable Plastic Films.

Vurro, M., Boari, A., Evidente, A., Andolfi, A., and Nadjia, Z. (2009). Natural metabolites for parasitic weed management. Pest Management Science *65*, 566–571.

Vyazovkin, S., Chrissafis, K., Di Lorenzo, M.L., Koga, N., Pijolat, M., Roduit, B., Sbirrazzuoli, N., and Suñol, J.J. (2014). ICTAC Kinetics Committee recommendations for collecting experimental thermal analysis data for kinetic computations. Thermochimica Acta *590*, 1–23.

Wang, J., Zhai, W., and Zheng, W.-G. (2012). Poly(Ethylene Glycol) Grafted Starch Introducing a Novel Interphase in Poly(Lactic Acid)/Poly(Ethylene Glycol)/Starch Ternary Composites. Journal of Polymers and the Environment 20.

Wang, W., Ben-Daniel, B.H., and Cohen, Y. (2004). Control of Plant Diseases by Extracts of Inula viscosa. Phytopathology *94*, 1042–1047.

Wang, X.-L., Yang, K.-K., Wang, Y.-Z., Wu, B., Liu, Y., and Yang, B. (2003). Thermogravimetric analysis of the decomposition of poly(1,4-dioxan-2-one)/starch blends. Polymer Degradation and Stability 81, 415–421.

Wu, Y., Qin, Y., Yuan, M., Li, L., Chen, H., Cao, J., and Yang, J. (2014). Characterization of an antimicrobial poly(lactic acid) film prepared with poly(ε-caprolactone) and thymol for active packaging. Polymers for Advanced Technologies *25*, 948–954.

Xu, Y., and Du, Y. (2003). Effect of molecular structure of chitosan on protein delivery properties of chitosan nanoparticles. International Journal of Pharmaceutics *250*, 215–226.

Yee Bond, T., A. Talib, R., Abdan, K., Chin, N., Kadir, R., and Yunos, K. (2016). Comparative

Study of Chemical, Mechanical, Thermal, and Barrier Properties of Poly(Lactic Acid) Plasticized with Epoxidized Soybean Oil and Epoxidized Palm Oil. Bioresources *11*, 1518–1540.

Yuniarto, K., Purwanto, Y.A., Purwanto, S., Welt, B.A., Purwadaria, H.K., and Sunarti, T.C. (2016). Infrared and Raman studies on polylactide acid and polyethylene glycol-400 blend. AIP Conference Proceedings 1725, 20101.

Zermane, N., Vurro, M., Boari, A., Avolio, F. (2011). Towards broomrape and field dodder management using natural metabolites from plants. (Martina Franca, Italy), p. 82

Zhang, R.Y., and Ma, P.X. (1999). Poly(alpha-hydroxyl acids) hydroxyapatite porous composites for bone-tissue engineering. I. Preparation and morphology. Journal of Biomedical Materials Research *44*, 446–455.

Zurita, R., Puiggalí, J., and Rodríguez-Galán, A. (2005). Triclosan Release from Coated Polyglycolide Threads. Macromolecular Bioscience *6*, 58–69.

La borsa di dottorato è stata cofinanziata con risorse del
Programma Operativo Nazionale Ricerca e Innovazione 2014-2020 (CCI 2014IT16M2OP005),
Fondo Sociale Europeo, Azione I.1 "Dottorati Innovativi con caratterizzazione Industriale"

UNIONE EUROPEA
Fondo Sociale Europeo


**Arash Moeini, a PhD student at Naples Federico II, he worked on the isolating of natural metabolites to find their biological activity, as well as the formulating of the active metabolites into the suitable biopolymers or macromolecules for different purposes (Food packaging, Herbicide, and Drug formulation). He could successfully publish 13 articles, chapters, and reviews in the quiet good and high IF journals, attend in 3 international conferences, and a "start cup" during his PhD period.**

## Highlight

- **Among 13 active metabolites three of them were selected as the most active compounds aganist *P. roqueforti* and *A. Niger.***
- **Cavoxin quantification and qualification analysis were done by HPLC. The results were proved the amount of cavoxin produced in the stirred condition is significantly higher than the static state.**
- **Ungeremine was encapsulated into CH/TPP microparticles, and then submicron particles were formulated in MBi by the compression molding method. The bioassay result showed three days of inhibition against *P. Roqueforti* in the activated films.**
- **Uugeremine was also formulated in PLA/PEG nanofibers by electrospinning method. The released rate of the UNG was proved the existence of UNG in both polymer matrices.**
- **α-Costic acid was formulated into PLA and acted as a plasticizer.**
- **In Novamont Company, the UNG synthesis method was developed. The sub-micron particles were successfully scaled up and formulated into Novamont polyester sheets, starch-based, and transparent grades of Mater-Bi by both compression molding and film blowing.**